SYNTHESIS OF ZEOLITE 4A AND ZEOLITE 13X FROM LOCALLY
AVAILABLE RAW MATERIALS BY THERMAL ACTIVATION METHODS

A THESIS SUBMITTED TO
THE GRADUATE SCHOOL OF NATURAL AND APPLIED SCIENCES
OF
MIDDLE EAST TECHNICAL UNIVERSITY

BY

SALİH KAAN KİRDECİLER

IN PARTIAL FULFILLMENT OF THE REQUIREMENTS
FOR
THE DEGREE OF DOCTOR OF PHILOSOPHY
IN
MICRO AND NANOTECHNOLOGY

JANUARY 2022

Approval of the thesis:

SYNTHESIS OF ZEOLITE 4A AND ZEOLITE 13X FROM LOCALLY AVAILABLE RAW MATERIALS BY THERMAL ACTIVATION METHODS

submitted by **SALİH KAAN KİRDECİLER** in partial fulfillment of the requirements for the degree of **Doctor of Philosophy** in **Micro and Nanotechnology, Middle East Technical University** by,

Prof. Dr. Halil Kalıpçılar
Dean, Graduate School of **Natural and Applied Sciences**   _____

Prof. Dr. Deniz Üner
Head of the Department, **Micro and Nanotechnology**   _____

Prof. Dr. Burcu Akata Kurç
Supervisor, **Micro and Nanotechnology, METU**   _____

Prof. Dr. Hayrettin Yücel
Co-Supervisor, **Chemical Engineering, METU**   _____

Examining Committee Members:

Prof. Dr. Görkem Külah
Chemical Engineering, METU   _____

Prof. Dr. Burcu Akata Kurç
Micro and Nanotechnology, METU   _____

Assoc. Prof. Dr. Fatma Toksoy Köksal
Geological Engineering, METU.   _____

Prof. Dr. Eda Ayşe Aksoy
Basic Pharmaceutical Sciences, Hacettepe University   _____

Prof. Dr. Selahattin Yılmaz
Chemical Engineering, Izmir Institute of Tech.   _____

Date: 26.01.2022

I hereby declare that all information in this document has been obtained and presented in accordance with academic rules and ethical conduct. I also declare that, as required by these rules and conduct, I have fully cited and referenced all material and results that are not original to this work.

Name Last name : Salih Kaan Kirdeciler

Signature :

ABSTRACT

SYNTHESIS OF ZEOLITE 4A AND ZEOLITE 13X FROM LOCALLY AVAILABLE RAW MATERIALS BY THERMAL ACTIVATION METHODS

Kirdeciler, Salih Kaan
Doctor of Philosophy, Micro and Nanotechnology
Supervisor : Prof. Dr. Burcu Akata Kurç
Co-Supervisor: Prof. Dr. Hayrettin Yücel

Synthesis of zeolites from laboratory-grade chemicals is an expensive way to produce these unique particles. Zeolite 3A, 4A, 5A among Linde Type A (LTA) zeolites, and zeolite 13X among the Faujasite (FAU) type are highly valuable commercial products for various application fields, such as catalysis, water sorption, and detergent industries as water softeners. There is still great interest in finding alternative synthesis routes that will reduce the production cost of these materials in high demand. Due to these facts, using locally available raw materials as starting chemicals for zeolite synthesis has been of significant importance. Accordingly, the main focus of this thesis was using national Turkish local sources to obtain a synthetic material of high demand in Turkey, which is being fully imported from abroad. During zeolite conversion using locally available minerals, the challenge in the process is the impurities existing in the raw materials such as quartz. The aim is to investigate the synthesis of high purity zeolite 4A and zeolite 13X from Turkish raw kaolin and feldspar sources with a cost-effective approach and minimum impurity in the final products.

For this purpose, meta-kaolinization, alkali fusion, and one-pot fusion methods for kaolin; alkali fusion and one-pot fusion methods for sodium feldspar were optimized for locally available raw materials, followed by hydrothermal synthesis. These processes opened up the possibility of obtaining zeolitic materials from locally available minerals, particularly sodium feldspar, which Turkey possesses highest amount of reserve in the world. Another aspect of this thesis was to use sodium carbonate as an alkali fusion agent to synthesize desired zeolites as an environmentally friendly alternative to sodium hydroxide. The third highlight of this thesis was to adapt one-pot fusion method to synthesize zeolite 3A and zeolite 5A directly, which eliminates the traditionally used ion-exchange procedures for the first time. Lastly, the whole process was scaled-up, allowing one to produce higher amount of products and thus testing the products in real industrial applications. In this way, the locally produced zeolitic materials were tested in various industrial areas to see whether their quality specifications were met. In conclusion, high purity industrial grade zeolites were successfully synthesized from Turkey's various kaolin and sodium feldspar sources. The one-pot fusion method was found to be adaptable to different alkali fusible aluminosilicate raw materials.

Keywords: Zeolite 4A, Zeolite 13X, one-pot fusion, pilot-scale zeolite production

ÖZ

ZEOLİT 4A VE ZEOLİT 13X'İN YEREL VE DOĞAL KAYNAKLARDAN TERMAL AKTİVASYON YÖNTEMLERİ İLE SENTEZLENMESİ

Kirdeciler, Salih Kaan
Doktora, Mikro ve Nanoteknoloji
Tez Yöneticisi: Prof. Dr. Burcu Akata Kurç
Ortak Tez Yöneticisi: Prof. Dr. Hayrettin Yücel

Ocak 2022, 184 sayfa

Zeolitlerin laboratuvar seviyesi kimyasallar kullanılarak sentezlenmesi, bu özgün parçacıklar için pahalı bir yöntemdir. Linde Tipi A (LTA) zeolitlerinden zeolit 3A, zeolit 4A, zeolit 5A ve Faujasite (FAU) zeolitlerinden zeolit 13X; katalizör, nem tutucu, su yumuşatıcıları gibi bir çok uygulamada kullanılmaları nedeniyle oldukça önemli malzemelerdir. Alternatif sentez yöntemlerinin geliştirilmesi, bahsi geçen ve kendilerine yüksek talep bulunan bu malzemelerin üretim maliyetlerinin düşürülmesi açısından yoğun araştırma konusu olmaktadır. Dolayısıyla, yerli hammaddelerin başlangıç ana maddesi olarak kullanılmasıyla zeolit sentezlenmesi uzun zamandır önemli bir araştırma alanıdır. Bu tezin odak noktası, ülkemizde sıklıkla kullanılan ve tamamı ithal olan zeolitlerin yerli kaynaklar kullanarak üretilmesidir. Yerli doğal kaynakların zeolite dönüştürülmesindeki zorlayıcı kısım, kaynakların içerisinde bulunan quartz benzeri safsızlıklardır. Bu çalışmanın amacı, yüksek saflıkta zeolit 4A ve zeolit 13X'in yerli doğal kaynaklardan olan kaolin ve sodyum feldspat kullanılarak, maliyet efektif bir yaklaşımla, en az ikincil fazları barındıracak şekilde sentezlenmesidir. Bu amaçla, kaolin kaynağı için meta-kaolinizasyon, alkali füzyon ve tek-kap füzyon metotları, sodium feldspat için ise alkali füzyon ve tek-kap füzyon metotları sonrası hidrotermal sentez yöntemi

uygulanmıştır. Bu prosesler, yerli hammaddelerin, özellikle dünyadaki en yüksek miktarda rezervi ülkemizde bulunan sodyum feldspat'ın zeolite dönüştürülmesinin yolunu açmıştır. Bu tezin bir başka boyutu ise, sodyum karbonatın, sodyum hidroksite alternatif olarak çevreci bir yaklaşımla kullanılmasıdır. Üçüncü vurgulanacak kısım ise, zeolit 3A ve zeolit 5A'nın, iyon-değişim prosedürü kullanılmadan, doğrudan bu yöntemle ilk kez üretilmesidir. Son olarak, bu çalışmada tüm proses, pilot ölçekte tekrarlanmış, daha yüksek miktarlarda üretim gerçekleştirmiş, ve böylece gerçek endüstriyel uygulamaların spesifikasyonların sağlanması konusunda denemeler gerçekleştirilmiştir. Bu şekilde, yerli malzemeler kullanılarak üretilen zeolitlerin, ticari ürünlerle karşılaştırmaları yapılabilmiştir. Sonuç olarak, yüksek saflıkta, endüstriyel ürünler ile rekabet edebilecek olan zeolitler, ülkemizin yerli kaolin ve sodyum feldspat kaynakları kullanılarak üretilmiştir. Tek-kap füzyon yöntemi, alkali füzyon'a uygun diğer alüminosilikat kaynakları için de kullanılabilir olarak değerlendirilmektedir.

Anahtar Kelimeler: Zeolit 4A, zeolite 13X, tek-kap füzyonu, pilot ölçek zeolit üretimi

To my lovely family…

ACKNOWLEDGMENTS

TABLE OF CONTENTS

LIST OF TABLES

LIST OF FIGURES

FIGURES

xxii

LIST OF ABBREVIATIONS

ABBREVIATIONS

LTA   Linde Type A

FAU   Faujasite

PBU   Primary Building Unit

SBU   Secondary Building Unit

WMA   Warm Mix Asphalt

HMA   Hot Mix Asphalt

ZSM   Zeolite Socony Mobil

STPP   Sodium Tripolyphosphate

TGA   Thermogravimetric Analysis

MOF   Metal-Organic Framework

XRD   X-Ray Diffraction

MOR   Mordenite

CLI   Clinoptilolite

ANA   Analcime

HEM   Hematite

MAG   Magnetite

XRF   X-Ray Fluorescence

SEM   Scanning Electron Microscope

EDX   Energy Dispersive X-Ray

CHAPTER 1

INTRODUCTION

Zeolites are crystalline; porous aluminosilicates that are used widely in the industry due to their different properties, such as water softeners in detergents, desiccants in insulating windows, catalysts in the petrochemical industry, or warm mix asphalt additives as a volume expander. The most famous zeolite family is Linde Type A (LTA) due to their Si/Al ratio being close to 1, leading them to be the highest ion carriers among all zeolite types. The most common zeolite type is zeolite 4A, with 4-angstrom pores and sodium cations as charge balancing ions. These properties carry zeolite 4A to the most used zeolite with the highest ion exchange capacity among all. Zeolite 3A and zeolite 5A are the other LTA members, which can be produced via ion exchange of zeolite 4A with calcium and potassium, respectively. These zeolites are also of interest due to the highly ordered pore structures and well-defined 3-angstrom and 5-angstrom pores for gas separation or moisture adsorption applications. Zeolite 13X is another well-known zeolite type with 8-angstrom pores from the faujasite (FAU) family of zeolites. It is also famous for its water adsorption capability of absorbing up to 25% of its original weight.

These zeolites are usually synthesized using the bottom-up approach with the hydrothermal synthesis method. Typically, precursor chemicals need to be placed in a vessel with desired conditions for the particles' nucleation and growth in the liquid medium, called hydrothermal synthesis. There is a great effort to minimize the total cost of the synthesis by finding alternative resources to be used as starting chemicals, including natural raw materials, or modifying the synthesis conditions. This chapter will explain the history of zeolites, zeolite types, their importance, synthesis methods, alternatives, and the aims of this thesis.

1.1 History of Zeolites

Zeolites are crystalline, hydrated aluminosilicates. Zeolite term was first used by a Swedish scientist, Axel Fredrik Cronstedt, in 1756. He discovered that when he heats a natural stone called "stilbite," it visibly loses its water content in the vapor phase. Based on this basic experiment, he used the words "zeo" and "lithos", which means "to boil" and "stone", respectively. Natural zeolites were of interest for a long time with discoveries of Stilbite (1756), Chabazite (1722), Faujasite (1842), Clinoptilolite, and Erionite (1890), Mazzite (1972), and many others for hundreds of years[1,2].

At the beginning of the 1940s, research on zeolites focused on investigating natural zeolites by mineralogists about stability over other minerals. Later on, it was evolved into the synthesis of these materials in laboratories more from the chemical point of view. Union Carbide Corporation is one of the pioneers of the synthetic zeolite manufacturing business, which initiated the research on adsorption, purification, separation, and catalysis in 1948. The company had made patent applications on zeolite A, Zeolite X, Zeolite Y, published structures of these zeolites and succeeded in granting the patents until 1964[2–4].

The first publication of synthetic zeolites was made on zeolite 4A by Breck et al.[3], who had worked for Union Carbide Corporation in 1956. The framework type was named Linde Type A (LTA), and the most common form is zeolite 4A, which consists of sodium as charge balancing cations in the pores and has an average of 4-angstrom pore diameter. Later on, Union Carbide researchers continued to work on discoveries on the faujasite (FAU) type framework and discovered zeolite X in 1959 [5] and zeolite Y in 1964 [4]. These new types of zeolites have bigger pore diameters with respect to the LTA structure (8-angstroms), leading to higher water adsorption capacity and molecular sieving property for larger gas molecules. Zeolites are of interest since different crystal structures lead to unique surface properties, and these crystals can be tailored for needed applications. This property places these crystals in an indispensable position for industrial applications.

2

1.2 Zeolite Structure, Properties, Formation, and Classifications

Zeolites are crystalline materials that can be considered to be consisting of two systems. These are covalently bonded, negatively charged aluminosilicate framework structures and ionically bonded charge balancing cations such as sodium, potassium, and calcium [6][7]. The international zeolite association classified over 200 different framework types and over a thousand different zeolite types until this day [8]. In the framework of zeolites, indefinitely extending silica and alumina octahedra are placed by sharing their oxygens which are mainly formulated by $M_{2/n}O.Al_2O_3.x\ SiO_2.\ y\ H_2O,$ where M is the charge balancing cation. Schematic representations of LTA and FAU structures are given in Figure 1.1.
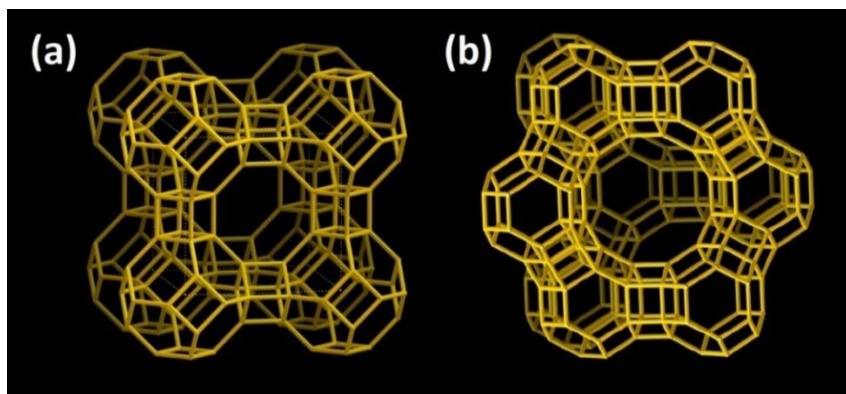
Figure 1.1. Schematic representations of basic building units of (a) LTA and (b) FAU structures [9].

Primary building units (PBUs) and secondary building units (SBUs) are the main subunits in a zeolite structure. Primary building units are the 4+ charged silicon oxide tetrahedra and 5+ charged aluminum oxide tetrahedra. The oxygen sharing geometry of these silica and alumina forms a unique geometric form called secondary building unit. These secondary building units (SBUs) can be in various geometries such as single/double rings, polyhedral, etc. The repetition of these SBUs results in various unique pore structures, channels, and cages. At present, 23 different types of SBUs are known to exist [10].

1.3   Main Applications of Zeolites

Zeolites have been widely used in industry for a long time with their superior properties in modifiable surface area, pore size, pore diameter, acidity, particle size, net charge, etc. Over a few decades, zeolites were widely studied due to their unique ordered pore structures with adjustable properties such as pore size and diameter, acidity, hydrophilicity, net charge, etc. in various application fields such as cation exchangers [11,12], selective catalysis [13–15], membrane systems [16–18], detergents [19][19–21], etc.

Zeolite 4A, the first synthetic zeolite, was engineered N_2 generation from the air as a molecular sieve by Breck and coworkers [3], as explained before. Zeolite 4A is one of the most essential zeolite types of all since it has the highest cation exchange capacity since its Si/Al ratio is 1. This unique property is widely used in the detergent industry as a water softener to enhance the washing capability of detergents.

The molecular sieving property of zeolites was highly used in the petroleum industry as driers with potassium exchanged form of zeolite 4A, which is called zeolite 3A, while weakly polar molecule remover & normal/iso-paraffin separator as calcium exchanged form of the same zeolite, now called zeolite 5A. The water sorption capability of zeolites increases the application fields of the zeolites to desiccants in insulating windows [22–24]. This is another major application field, and just in Turkey, approximately ten tons of zeolite 3A are imported annually. Zeolite beads are prepared from these imported zeolites and placed in insulating windows [25]. Also, the benefit of ordered pore structures can be used in gas separation processes, such as liquid nitrogen production from the air, CO_2, and H_2S [17,26–28]. Another primary application of zeolites is catalysis due to their active Bronsted and Lewis acid sites and high surface areas [13,29,30]. Also, due to the ordered pore structures, selective catalysis on desired molecules can be performed [31,32].

Zeolite 13X is another important zeolite type with a faujasite structure with larger pore openings; with respect to zeolite 4A has the highest adsorption capacity among

all zeolites. It is widely used in high purity oxygen generators and adsorbents for bigger molecules than N_2. Zeolite Y is widely used in catalytic applications since it has a higher Si/Al ratio than zeolite 13X, which is in the same faujasite family[33].

The porous structure of the zeolites can be utilized in odor control systems since the pore sizes and properties can be engineered for the desired molecule to be captured [34–36]. Also, fragrance molecules can be adsorbed inside the pores of zeolites to be able to increase the mechanical and thermal stability of these fragrances [37–39].

The heat of adsorption is another crucial phenomenon for the zeolites since zeolite 13X can adsorb 25% of water vapor in its pores while zeolite 4A can adsorb almost 22% of water vapor by its weight. This high adsorption capacity is used in heat pump cycles in several commercial applications, such as the patented "zeolite drying technology" of BSH [40] or the "ZeoTherm" heat pump system by Vaillant [41]. Vaillant reported that the heat pump's efficiency increased 35% with respect to state-of-the-art, high-end heat pumps in the market.

Every application requires an engineered product with superior capabilities on this particular application, even the known name of the zeolite is the same. Zeolite 3A, a potassium exchanged version of zeolite 4A, is used as a desiccant in insulating windows. Even in the literature, there is not much further information about the product type, but within the meetings with the desiccant producers, the importance of the ion exchange level was revealed. In technical data sheets of the producers, it can be seen that 30%, 40%, and 50% (Ion exchange, K_2O/Al_2O_3, [%mol/mol]) are suitable for desiccant production [42]. These exceptionally engineered zeolites were used in insulating windows over other desiccant types such as calcium oxides, clay, or calcium sulfides due to the high adsorption capacity in low relative humidity environments and fast adsorption-desorption behaviors shown in Figure 1.2.
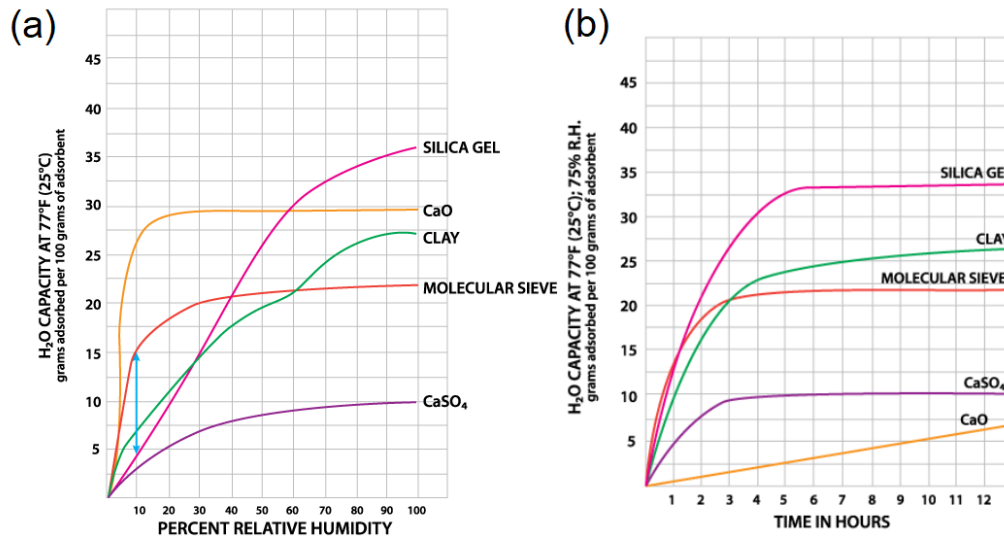
Figure 1.2. The water adsorption capacity of several desiccant materials with respect to relative humidity level (a) and time (b) [43]

Another engineering over the zeolite 4A shall be required to apply detergent builders. Zeolite 4A is a well-known cubic crystal with sharp edges, which is a drawback in detergents since they can be knotted in textile fibers and damage them. In contrast, cubes with rounded corners and edges tend to decrease the incrustation of textile materials [44]. Also, particles smaller than 1 mm in average diameter may be retained in the textile fiber and damage it, while particles over 10 mm in size cause an unacceptable deposition on textile materials, fabric, and machine parts [45]. These requirements shall be satisfied with the tailor-made zeolite 4A crystals. Gel formulation and reaction condition optimizations were performed by several groups for chamfered/non-sharp edged zeolite 4A synthesis [46,47]. Also, another major zeolite producer, PQ Corp., defined their product as detergent grade zeolite "Doucil ® 4A" as round edged zeolite 4A [48]. Also, detergent-grade zeolites shall satisfy the requirement of color and iron impurity levels due to the minimization of the coloring and defect formation in the fabric.

Warm mix asphalt additive is the same type of zeolite, zeolite 4A from the Linde Type A family. This time the basic requirement is the water sorption capacity of the zeolite. The same zeolite 4A is used as a WMA additive but in a dehydrated form,

unlike desiccant application [49,50]. Due to the kinetics of the moisture adsorption/desorption mechanism variation with the particle size itself, smaller particles were desired for this application field [51].

Recently zeolite crystals have been widely used in sensor applications as modifiers of the electrodes. The zeolites' high surface area and flexible structures are attractive materials as electrode modifiers to increase the sensitivity, response amplitude, and linear range with a lower detection limit. The use of zeolites is another means to modify electrodes for superior responses [52–55]. These applications are usually in the liquid medium, while recently, there has been more research on gas-phase applications such as formaldehyde sensors [56], gas sensors [57], and humidity sensors [58,59].

1.4   Zeolite Market and Most Commonly Used Zeolites

The market of zeolites/molecular sieves was around $27.1 billion worldwide in 2020, while estimated to be $32.7 billion in 2027 [60]. The highest share in volume is at zeolite A (Linde Type A), which acts as an ion exchanger in detergents, while zeolite X and Y (FAU family zeolites) are popular in the catalyst industry [61].

The market growth is steady, and this growth is due to the demand from the petrochemical refining, gas separation, and wastewater filtration end-use industries. Zeolite A is the most widely used zeolite in industries for separation and purification applications. Zeolite 4A, the highest market volume zeolite, is used as a water softener. After the European Union (EU) ban on the use of Sodium Tripolyphosphate (STPP) in detergents to control the increasing level of soluble phosphorus in municipal wastewater, Zeolite 4A was considered an ideal substitute to STPP and witnessed a substantial increase in demand. Several commercial detergents contain synthetic zeolites, which help increase their washing efficiency [62,63]. Even zeolites are not recently discovered crystals, and this research field has been investigated for decades, the publication numbers are getting higher every year, as

shown in Figure 1.3. Metal-organic frameworks (MOFs) have been of interest in recent years, developed with the know-how built with zeolite research over the years [64].
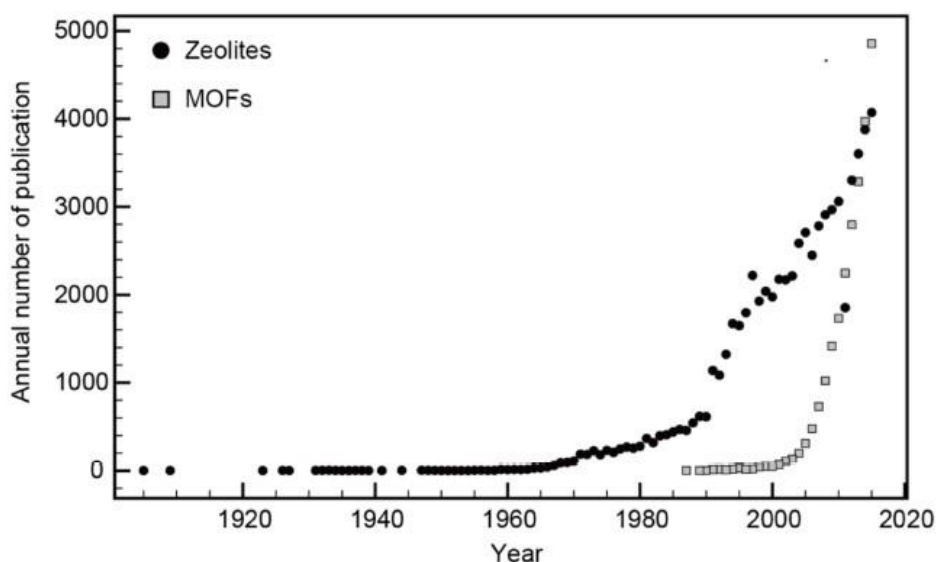
Figure 1.3. The number of publications on zeolites (black circles) and MOFs (grey squares) annually [64].

1.4.1 Zeolite 4A and Zeolite 13X

Zeolite 4A is the sodium form of the Linde Type A (LTA) family, with the highest ion exchange capacity since the Si/Al ratio has a limit value of 1 [65,66]. This highest ion-exchange property makes this type of zeolite widely used in detergents as a water softener [65]. These zeolite types are mentioned as low silica zeolites, and they were synthesized from similar gels. An increase in the silicon to aluminum ratio results in zeolite 13X formation instead of zeolite 4A, as shown in Figure 2.7[67].

Zeolite 4A and Zeolite 13X are built from the same structure of sodalite. Sodalite cages came together in a different orientation to form either zeolite 4A or zeolite 13X [68], as shown in Figure 1.4.
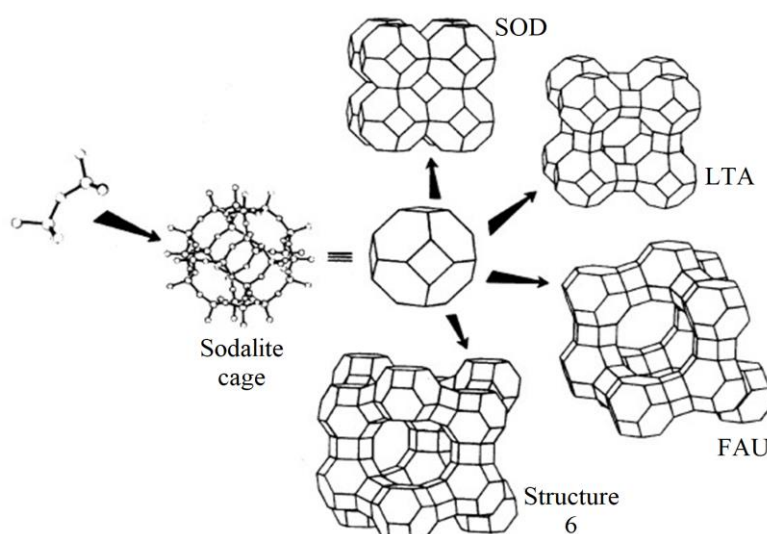
Figure 1.4. Formation of Zeolite 4A "LTA" and Zeolite 13X "FAU" from basic building unit of Sodalite cage [68].

Zeolite 13X has bigger pore openings (8 angstroms) with respect to zeolite 4A (4 angstroms), which increases is favorable for fragrance carrier applications [37,38,69].

1.4.2   Zeolite 3A and Zeolite 5A

Zeolite 3A and zeolite 5A are the ion-exchanged forms of zeolite 4A with potassium and calcium, respectively. Since the hydrodynamic diameter of these ions varies, and the structure of the zeolite A is the same, the opening of the zeolite cavity varies with the ion filling the pores. Since potassium is a bigger ion in size, it forms a 3 angstroms opening named zeolite 3A, and a smaller sized ion, calcium, exchanged version has an opening of 5 angstroms called zeolite 5A [35,70–72]. Schematic representation of pore openings of LTA zeolites was shown in Figure 1.5.
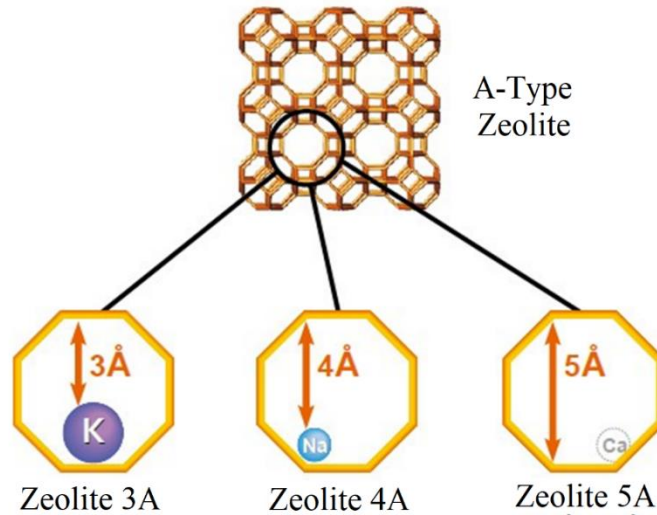
Figure 1.5. Schematic representation of zeolite A family with different pore diameters with different ions

Ion Exchange is the route to change the exchangeable cation in the zeolite framework, usually sodium, with the desired cation in a liquid medium with continuous agitation. The researchers have investigated and reported this phenomenon for decades, and its properties are well known, such as equilibriums, the affinity of some ions, kinetics, and free energy of exchange [65,73,74]. With the help of this well-known ion exchange procedure, as-synthesized zeolite 4A can be converted into zeolite 3A and zeolite 5A [72,75].

1.5   Goals and Objectives

Turkey is importing different types of zeolites from abroad for about fifty thousand tons per year as a builder for detergents, ten thousand tons per year as desiccant for insulating windows, and approximately five thousand tons annually as a catalyst in petrochemical industrial uses. The local zeolite production does not exist mainly due to the production cost based on foreign raw materials. The main goal of this thesis is to synthesize zeolite 4A and zeolite 13X from locally available raw materials in Turkey, which show variations with respect to their international counterparts. For this purpose, kaolin and sodium feldspar were the main raw minerals chosen and

obtained from various local resources. Optimization of all synthesis parameters from each source was conducted to obtain zeolites of differing types and qualities. In this research, several objectives were set and achieved, which can be listed as follows;

- Synthesis of zeolite 4A and zeolite 13X from high-quality kaolin sources
- Synthesis of zeolite 4A from low-quality kaolin sources
- Synthesis of zeolite 4A and zeolite 13X from various sodium feldspar sources
- Direct synthesis of zeolite 3A and zeolite 5A without ion-exchange
- Scaling up the synthesis system for industrial application trials
- Industrial application results

CHAPTER 2

LITERATURE REVIEW

There has been excellent progress in zeolite synthesis and its applications since the first natural zeolite "stabite" by a Swedish mineralogist, Cronstedt, in 1756. In the first decade of research, the research focused on the adsorption properties, dehydroxylation of zeolites, and reversible cation exchange properties [2,76,77]. In the 19th century, the first hydrothermal synthesis of a zeolite, "levynite" was proposed, and structures of dehydrated zeolites were reported [77]. In the mid 20th century, the definition of molecular sieves was first proposed, and numerous synthetic zeolites were proposed, such as zeolite A, X, and Y by Minton and Breck [2,7]. International Zeolite Association announced that 255 zeolite frameworks had been discovered until now [78].

2.1 Zeolite Synthesis

Zeolite synthesis is a way of producing unique structures with different ion exchange and molecular sieving capabilities via crystallization of aqueous solutions of silicate and aluminate anions in an alkaline medium. Zeolites are usually synthesized with the hydrothermal synthesis method with some exceptions, such as solvothermal or ionothermal methods [79]. Hydrothermal synthesis methods involve dissolving an aluminum source (source of $[AlO_4]^{-5}$) in an alkali medium, a silica source (source of $[SiO_4]^{-4}$) in a different alkali medium, and a template or seed crystals if necessary. These solutions were added into each other to form a slurry and stirred until the initial homogenous gel forms [77,80,81]. The starting material properties are crucial for the final product purity and quality. Industrial-grade chemicals commonly synthesize these zeolites to fulfill industrial requirements such as low impurity, high crystallinity, and homogeneity [2,3,82].

It is accepted that zeolite formation mainly involves two mechanistic steps (1) the formation of aluminosilicate gel or reaction mixture and (2) the nucleation and growth of zeolite crystals from the reaction [76]. The first schematic representation of zeolite formation was given by Breck, where the zeolite formation is composed of depolymerization of gel structure, rearrangement of the aluminosilicate and silicate anions, and regrouping of the tetrahedra about hydrated sodium ions to form the basic polyhedral units. Upon the linkage of these units, the ordered crystal structure of zeolite is formed, as shown in Figure 2.1.
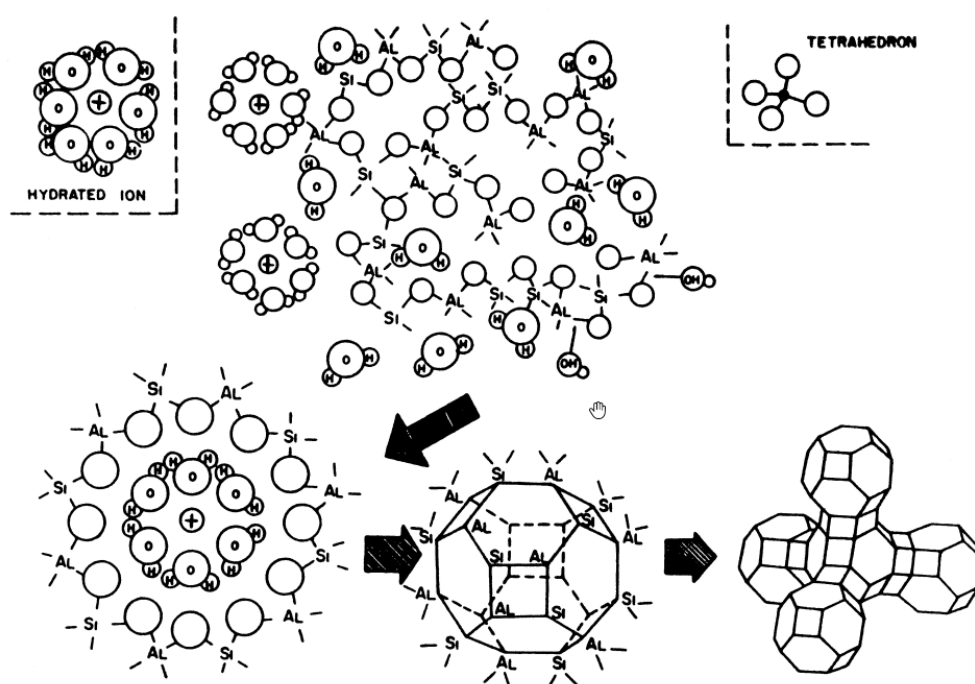
Figure 2.1 The first depiction of zeolite synthesis [83].

It was concluded that the zeolitic product is formed by the reaction of the soluble species with nuclei or zeolite crystals according to the following simple mechanism where the rate-determining step was controversial [76].

Amorphous solid → Soluble species (S)

(S) + Nuceli (or zeolite crystal) → Zeolite A
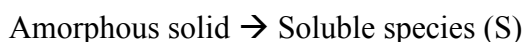
Zeolites are traditionally produced with the hydrothermal synthesis method from reactive gels in alkaline media at temperatures between about 80-200°C. The control of the synthesis process and crystallization with desired parameters need an understanding of the crystallization process and the influence of numerous variables. The factors controlling the synthesis of zeolites are nicely summarized in two groups by Mintova et al. as chemical and physical parameters in Figure 2.2.
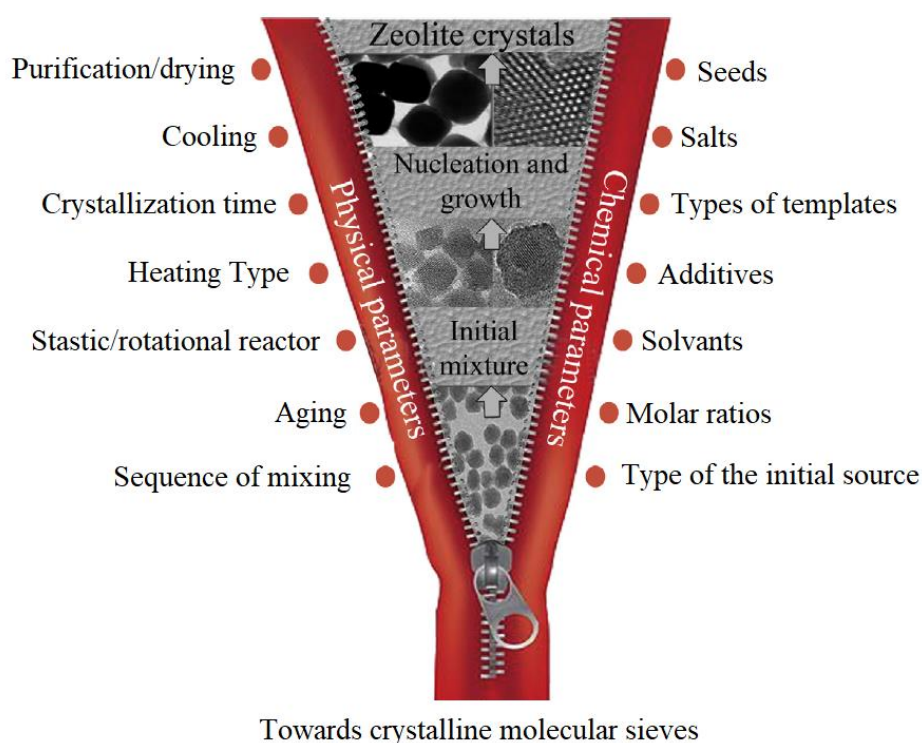
Figure 2.2. Main parameters governing zeolite synthesis [84].

For the zeolite formation, a typical hydrothermal zeolite synthesis can be described in the following steps:

1. Reactants containing silica and alumina sources are mixed in a basic medium with a cation source.

2. The aqueous reaction mixture is heated in an appropriate reaction vessel and kept at that particular temperature where the reactants remain amorphous.

3. After the "induction period" mentioned above, zeolite crystals can be observed.

4. After all amorphous material is replaced by zeolite crystals, washing, filtration, and drying steps are pursued.

These steps are illustrated in Figure 2.1; the amorphous precursors contain Si-O and Al-O bonds from which, in the presence of a mineralizing agent, the crystalline product (e.g., Zeolite A) contains Si-O-Al linkages are created during the hydrothermal reaction.
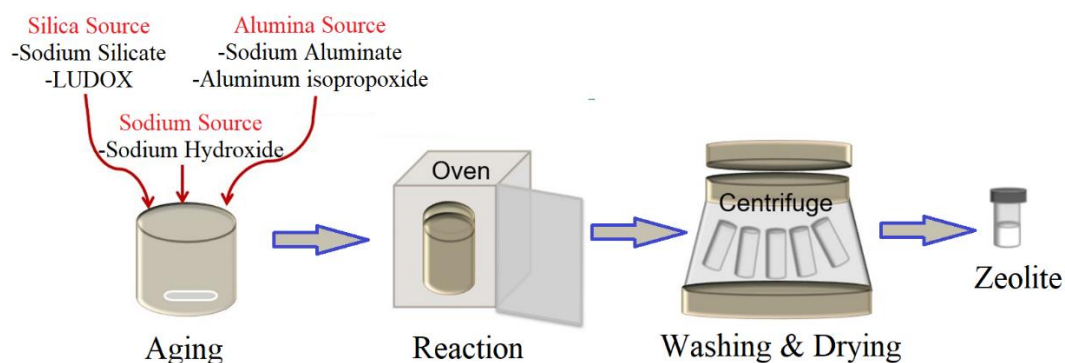
Figure 2.3. Schematic representation of a standard hydrothermal synthesis procedure of zeolites.

The commercial production of zeolites, such as zeolite A, is mainly conducted using raw chemical compounds such as sodium silicate, Ludox, fumed silica, as silica source and sodium aluminate, aluminum isopropoxide, and aluminum wire as alumina source. As shown in Figure 2.3, required chemicals are mixed in an aqueous media in an appropriate vessel with a proper amount of sodium and potassium sources to generate the alkaline medium for nucleation and growth of zeolite crystals. Usually, these chemicals shall be prepared in different vessels for complete control

over the synthesis. These chemicals are mixed and aged for nuclei formation. Aged gels are placed in a previously heated oven for an appropriate time for the reaction to occur. The suspension formed is washed with distilled water followed by filtration and drying. The final powder product is highly dependent on several synthesis parameters such as composition, alkalinity, templates, seeds, aging time and temperature, and reaction time and temperature [7,79]. Since the final product's purity is an important parameter, the quality of the starting material should also be high. For those reasons, industrial-grade chemicals are still in use for large-scale production. Nowadays, laboratory-grade fumed silica costs around $200/kg, while sodium aluminate costs nearly $40/kg, making fumed silica hardly appropriate for mass production design. There is tremendous interest in lowering these costs by changing these chemicals with natural raw materials [44,85–88]. These studies mainly focus on using natural materials such as kaolin [89–91], diatomite [92,93], and montmorillonite [82] or waste materials like waste porcelain or by-products such as fly ashes [94–96]. Additional pre-treatments were highly recommended to achieve high-quality final products, such as acid wash of raw materials [72] or liquid extraction of silica or alumina sources [97,98]. Zeolite synthesis parameters such as aging and reaction conditions such as agitation, temperature, and durations are highly effective on the final product quality [77,99]. Another critical parameter affecting the final zeolite quality is activation conditions of the natural raw materials since amorphous phase or water-soluble aluminosilicates are necessary for zeolite formation [77,100].

Composition is one of the most crucial parameters since it highly affects the final product type and quality. Several different zeolites can be synthesized with similar compositional reaction gels. Reaction composition diagrams for low silica zeolites are shown in Figure 2.4 [81].

17
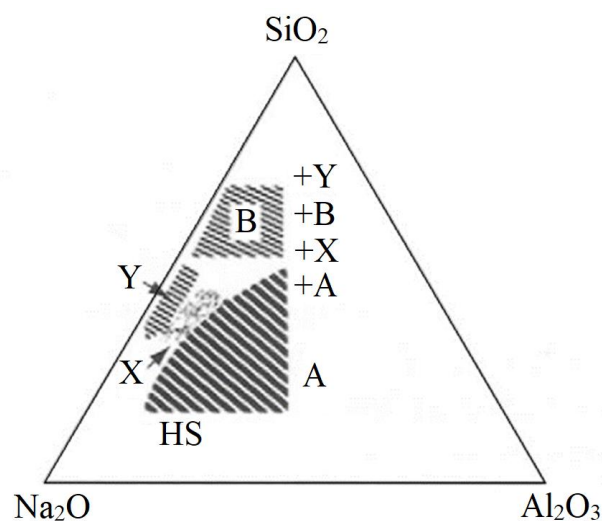
Figure 2.4. Reaction Composition Diagrams for Several Zeolite Types (HS: Sodalite, A: Zeolite 4A, Y: Zeolite Y, X: Zeolite 13X, B: Analcime) [81].

Reaction compositions can be altered by changing the amount and type of chemicals used as starting materials. Widely used starting chemicals of silica and alumina for zeolite synthesis are sodium silicate, sodium aluminate, or fumed silica, which is relatively costly, but with very little impurity content. Reducing the cost of the chemicals used as starting materials is of enormous interest due to the high demand for zeolites in industrial applications.

2.1.1 Synthesis Parameters

Zeolite synthesis is commonly explained by the gel preparation and hydrothermal synthesis parts. The gel is mainly the deterministic characteristic parameter on the formation of zeolite type. For example, low Si/Al zeolites such as the LTA family should be synthesized with gels Si/Al ratios of 0.8 to 2. Higher Si/Al ratio gels usually end up with higher silica zeolites such as analcime, zeolite X, or zeolite Y. However, in between these boundary areas of zeolite A and zeolite X, adjustments in the synthesis conditions are necessary to obtain the desired product other than the temperature and pressure applied during the hydrothermal process. These can be

summarized as batch composition, reactant sources, Si/Al ratio, alkalinity, inorganic cations, aging, stirring, organic templates, solvents, water content, temperature, and seeding. [101–104]. Controlling all these parameters leads to total control on the final zeolite type, average particle size, particle morphology, and synthesis yield. The type and quality of the final product are directly related to the main application area, which shows a range of variations upon their usage purpose. One of the primary purposes of zeolite research, as well as this thesis, is to meet the exact criteria expected from different application areas.

2.1.2 Activation of Raw Materials

Raw materials such as kaolin, a layered crystal clay type, can be activated via a thermal activation route, specifically called metakaolinization. This procedure dehydrates the structure of kaolin and converts raw material into amorphous metakaolin [19,105,106]. Also, alkaline digestion is proposed to extract silicates and aluminates in an alkali medium and high pressure [98,107]. This technique is beneficial since it prepares dissolved silicates and aluminates from solid form aluminosilicates while getting rid of the impurities such as mica, quartz, and iron is possible with additional filtration step [100,108]. Nevertheless, this technique requires an extra filtration step, which adds complexity to the overall system. Another popular activation method of raw materials is alkali fusion, a solid-solid reaction; an alkali source diffuses and reacts with the secondary material and forms a water-soluble alkali powder product. In this technique, an alkali agent such as sodium hydroxide or sodium carbonate is mixed with the raw material, which has a higher melting temperature with respect to the alkali agent. Mixture heated up to the melting temperatures of alkali agent which were used. This molten alkali agent diffuses through the raw material and forms soluble forms of alkali in the solid form [20,109,110]. The overall aim is to produce semi-products that can be converted into zeolites by hydrothermal synthesis.

Metakaolinization is the process of dehydroxylation of kaolin source, which terminates the structural layers of kaolin and eventually forms an activated state that is unstable and amorphous to X-ray [111]. In literature, there are numerous studies suggesting various temperatures and durations for the metakaolinization step [19,89,105,112–114]. Chandrasekhar and Pramada [89] reported that the final product is strongly influenced by the metakaolinization temperature for zeolite 13X, which was suggested to be performed above 700°C. Also, the same group reported that the metakaolin decomposition occurs after 950°C [112]. Contrary to the reports of Chandrasekhar and co-workers, Murat et al. reported stated that the content of the iron ions in the synthesis solution is the determining step for the kinetics of the synthesis other than the structural disorganization state of the metakaolin [115]. Also, there is no agreement on the metakaolinization duration. Kovo et al. [116] reported that 50 minutes at 600°C is sufficient for metakaolinization and decreased the duration to 10 minutes in another study [117], while Otieno et al. [114] used a metakaolinization procedure at 750°C for 8 h. These temperatures and durations have to be optimized depending on the quality of the raw material in every particular application.[118]. The quality, which means the content of the raw material source other than kaolin clay, is highly dependent on the mining site [105]. As shown in Figure 2.9, kaolin crystal is in the pseudohexagonal phase, but it could also exist in other phases like triclinic, pseudo-monoclinic, and polymorphs. Kaolin minerals usually contain secondary impurities such as quartz, feldspars, micas, iron, and titanium oxides, depending on the mining site. Montmorillonite, illite, and aluminum hydrated oxides can be found in kaolin reserves [105,119]. These impurities have a strong influence on the final zeolite to be synthesized. Due to this phenomenon, several treatments on low-quality kaolin sources such as acid washing were proposed to synthesize pure zeolites out of these clays [105,106,120].

2.1.3 Gel Formula

Gel formula consists of two critical parameters, which are SiO_2/Al_2O_3 ratio and alkalinity at the same time. The formula is generally shown as x SiO_2: y Al_2O_3: z Na_2O: w H_2O, where x/y represents SiO_2/Al_2O_3, and z/w represents alkalinity. This formulation is the deterministic step of the synthesis about the zeolite type eventually will form [66,77]. Instead of kaolin as silica and alumina source, additional sodium silicate might increase the Si/Al of the gel results with zeolite Y and zeolite 13X with similar synthesis conditions with zeolite 4A [107,116]. Various zeolites can be synthesized from Si/Al ratios of 1 (zeolite 4A) to 100 (ZSM-5 and zeolite Beta) by proper adjustment of the SiO_2/Al_2O_3 ratio of the gel [77].

Alkalinity is the second important part of the gel formulation. Higher alkalinity leads to the higher solubility of the silica and alumina sources and speeds the polymerization reaction of the polysilicate and aluminate ions [81]. Further, increasing the NaOH concentrations in the medium results in higher hydroxy sodalite (HS) formation than desired zeolite 4A formation in various reports [121,122]. Also, the alkalinity should be optimized for each synthesis since hydroxy sodalite is not the only secondary phase since Lapides et al. [121] reported zeolite 4A and zeolite 13X could be produced with the same gel after 120 h of reaction with 2.2 M NaOH concentration. Liu et al. reported that the higher the alkalinity, the better the particle size distribution with smaller average particle sizes [101].

2.1.4 Aging Conditions

Aging is the time when the aluminosilicate gel forms and nuclei formation in this gel occurs. Under well-designed synthesis conditions, the aging of zeolite synthesis increases the degree of crystallization in the final products [123]. Also, Jihong et al. [81] reported that the aging duration directly affects the nucleation and crystal growth of the zeolites. In a study by Kovo and Holmes [116], aging with continuos

agitation was performed for 48 h, and it increased the total surface area and crystallinity of the zeolite Y. The same zeolite can be synthesized with different recipes. For example, Feng et al. [124] synthesized ZSM-5 with 2 h of continuous agitation aging. In comparison, Wang et al. [125] synthesized the same zeolite type with 8 h of continuous agitation followed by 12 h of static aging. Di Renzo et al. [126] reported that stirring decreases the final product's particle size by accelerating the mass transfer rate. Fan et al. reported an increase in the aging duration from 0 to 192 h, increasing the FAU ratio with respect to LTA due to the aging requirement for the six-membered ring of FAU crystals [102].

2.1.5   Reaction Conditions

Reaction conditions such as agitation, temperature, and duration strongly influence the desired zeolite phase. Ciric et al. [127] reported that temperature strongly affects nucleation rates, while Zhdanov and Samulevich reported that the reaction temperature increase results in higher nucleation and growth rates [128]. Due to the metastable nature of the synthesized zeolites, reaction durations are important since the dissolution of the phases such as zeolite 4A can occur in longer durations of reaction, and the formation of sodalite as a competing phase can be observed [102,129]. Bayati et al. reported that increasing reaction temperature dramatically increased the average particle size of the zeolite 4A, while reaction duration did not significantly affect the final zeolite crystallinity [104]. Liu et al. reported that increasing reaction temperature with the same gel composition increased zeolite 4A crystallinity up to 90°C. In contrast, a further increase in the temperature resulted in the formation of zeolite 13X as a competing phase. Liu et al. also reported that the initial precipitation of zeolite 4A starts at around 1 h, and crystallinity increases up to 4 h. However, after a further increase in the reaction duration, zeolite 13X crystals were started to be observed [101].

2.2   Raw Material Dependency of Zeolite Types

Even with the laboratory-grade very pure chemicals, depending on the nature of the dissolution rate differentiations, two different compositional regions were proposed by Breck and Flanigen [4,130] for zeolite Y synthesis with sodium silicate and colloidal silica as the silicon source. These regions in the ternary diagram are shown in Figure 2.5.
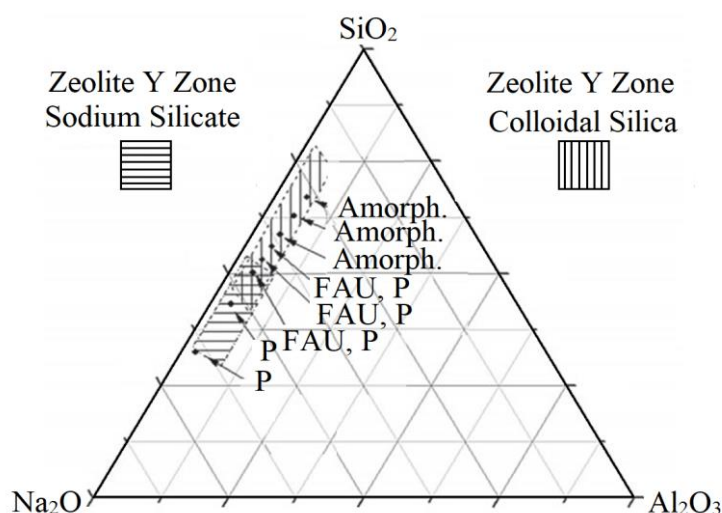
Figure 2.5. Ternary diagram zones for zeolite Y synthesized from different silica sources [92].

Christidis and Papantoni reported that some of the silica sources, such as volcanic glasses, are unfavorable for zeolite Y nucleation due to the Si-O linkages in the glass. This phenomenon corresponds to the starting gel formulation change as an experimental constrain. On the other hand, direct dissolution of perlite as a silica and alumina source favors resulting zeolite P, zeolite V and sodalite [131]. Aly et al. reported that the change of the alumina source (sodium aluminate, aluminum nitrate, and aluminum chloride) results in different crystallinity of ZSM-5 with respect to each other due to the dissolution rate variances of these chemicals [132].

Breck and Flanigen were the pioneers of ternary phase diagram users in zeolite synthesis gels to illustrate the possible regions of pure zeolite phase formation. These

ternary diagrams refer to the approximate regions where different frameworks were formed based on the solution's molar fractions of silicon dioxide, aluminum oxide, and sodium oxide. Oleksiak and Rimmer et al. adapted two ternary phase diagrams of Breck and Flannigen to demonstrate the differentiation of the regions for two different silica sources [133]. Synthesis with silica source as sodium silicate is (a) and colloidal silica as silica source is (b) in Figure 2.6.
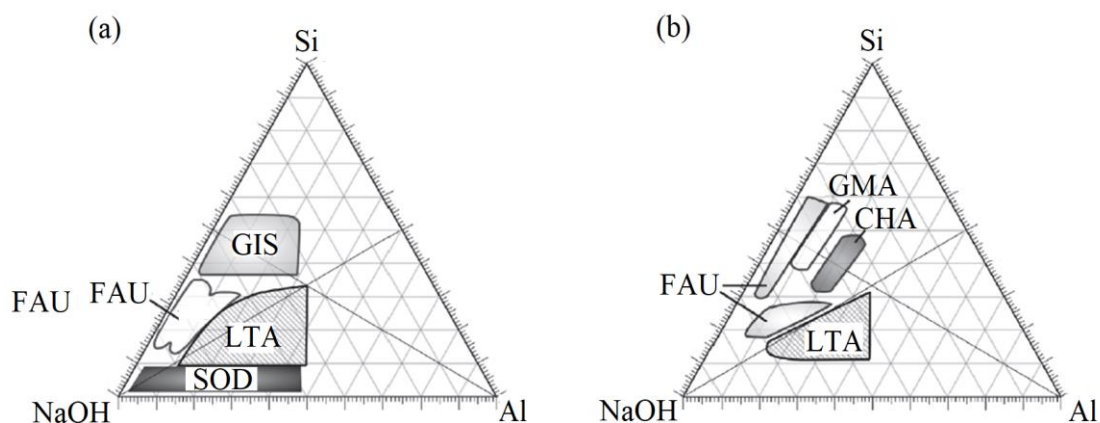
Figure 2.6. Ternary phase diagrams adapted from Breck and Flanigen (1968) with the following silica sources: (a) sodium silicate and (b) colloidal silica [133].

As shown in Figure 2.2, the designated area for LTA and FAU is differentiated from the silica source. As Oleksiak and Rimmer et al. mentioned, zeolite synthesis is a complex mechanism that can not be easily explained by changing one parameter at a time due to the synergetic effects of the changed parameters [133].

Maldonado et al. reported that the gel molar fractions of LTA crystals and FAU crystals, given in Figure 2.7, while the effect of water content in the gel formula is given in Figure 2.8. It was shown that the one component change in all reaction parameters, such as alkalinity, Si/Al ratio, synthesis duration, reaction temperature, etc., has numerous effects on zeolite to be formed [67].
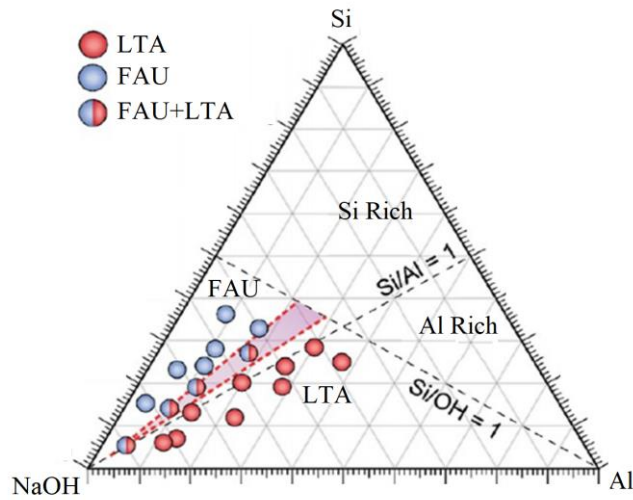
Figure 2.7. Kinetic ternary phase diagrams of zeolite structures showing single- and multi-phase (shaded) regions at increasing temperature: (A) LTA and FAU (65 °C, 7 days)[67].
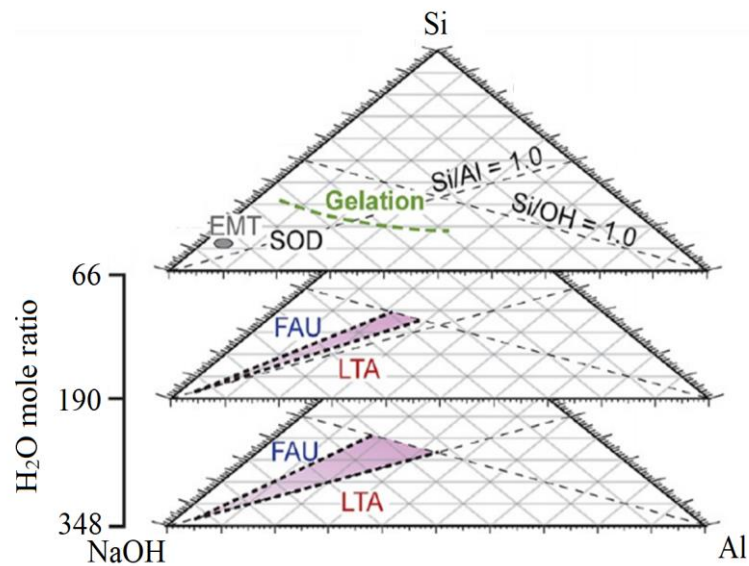
Figure 2.8. Kinetic phase diagrams for zeolite growth solutions at varying water content heated for seven days at 65 °C [67].

According to the literature review, even one synthesis parameter such as water content or initial chemicals to be used in the synthesis affects zeolite to be formed.

Based on these findings, systematic studies for zeolite synthesis with different sources and synthesis conditions shall be reported independently.

2.2.1 Synthesis of zeolites from natural raw materials

There are over two hundred different types of zeolites at present that are based on their silica-to-alumina ratio. There is paramount attention in seeking cheap raw materials to replace high-cost pure chemical materials to synthesize zeolites concerning energy consumption and production cost. Natural raw materials have been of interest since the early days of synthetic zeolite inventions [3]. Cost effectivity is the primary motivation of using similar chemical content, crude or semi-processed natural raw material by transforming it into value-added zeolite [3,130]. For that purpose, clay minerals are the most well-known alternative for synthesizing zeolite A due to their suitable silica-to-alumina ratio as starting material. The most suitable starting materials for zeolite synthesis can be given as natural silicates, aluminates, or aluminosilicates such as bauxite [134,135], kaolin [91,107], and natural zeolites [136,137].

2.2.1.1   Kaolin

Kaolin is the general name of the rocks which are rich in kaolinite. Kaolin is a well-known type of clay that is a natural material, which can be classified in industrial minerals, with a chemical composition of $Al_2Si_2O_5(OH)_4$.
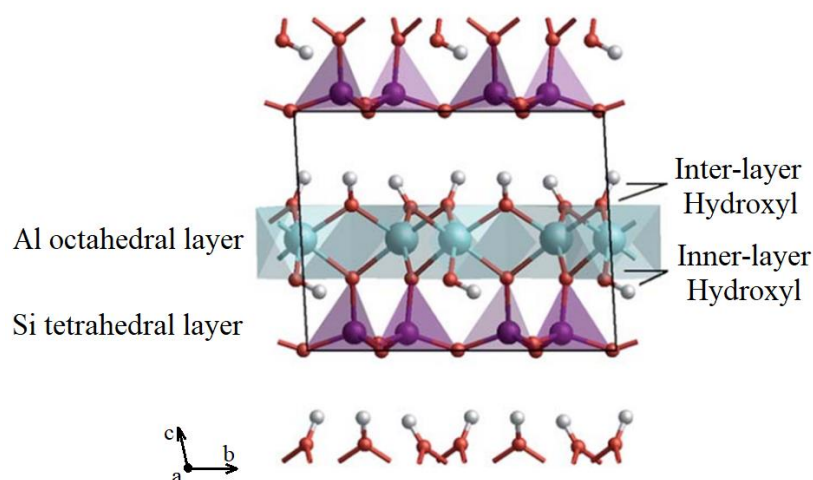
Figure 2.9. The ideal layered structure of kaolin unit cell. [9].

As shown in Figure 2.9, the framework structure of kaolin is composed of a sheet of vertex sharing SiO4 tetrahedra forming six-membered silicates. These silicates are linked by shared oxygen atoms parallel to the c-axis to a sheet of edge-sharing AlO6 octahedra forming four-membered aluminates. Strong ionic/covalent bonds bind together the silicate and aluminate layers via apical oxygen atoms. However, these layers are connected by much weaker hydrogen bonds. These definitions are defined for an idealized structure, while disorders are common in kaolin minerals [9]. The chemical and crystallographic properties of kaolin depend on its origin, making it an ongoing research topic even today for zeolite synthesis.

The usage of kaolin as a source of alumina and silica for zeolite synthesis has been known since the 1980s [138]. It needs calcination at a temperature between 600 °C to 1000 °C to produce metakaolin, which is a process of dehydroxylation with the following reaction:

$$Si_2Al_2O_5(OH)_4 \xrightarrow{Heat} Al_2O_3 . 2SiO_2$$
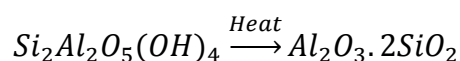
Kaolin has been used to synthesize various types of zeolites such as zeolite 4A [21,112,139], zeolite X [89,107,140], zeolite Y [117,141] and ZSM-5 [117,142].

2.2.1.2   Feldspar

Feldspar is one of the most abundant minerals in the earth's crust, forming about 60% of terrestrial rocks [143]. The term feldspar encompasses a whole range of materials. Most deposits offer sodium feldspar as well as potassium feldspar and mixed feldspars. They are primarily used in industrial applications for their alumina and alkali content.   There are several application fields of feldspars, such as glass production, fiberglass production, floor tile, and tableware production.

Feldspar minerals are essential components in igneous, metamorphic, and sedimentary rocks to such an extent that the classification of several rocks is based upon feldspar content. The mineralogical composition of most feldspars can be expressed in terms of the ternary system Potassium Feldspars ($KAlSi_3O_8$), Sodium Feldspars ($NaAlSi_3O_8$), and Calcium Feldspars ($CaAl_2Si_2O_8$).   Chemically, the feldspars are silicates of aluminum-containing sodium, potassium, iron, calcium, or barium or combinations of these elements. Silicon and aluminum atoms in feldspars form tetrahedra by bonding to four oxygen atoms. In Figure 2.10, SiO_4 and AlO_4 tetrahedra shown in grey color create a three-dimensional framework by sharing common vertices [144,145]. Aluminum atoms occupy half of the tetrahedral sites in anorthite ($CaSi_2Al_2O_8$) and a quarter of the sites in albite ($NaAlSi_3O8$) and microcline ($KAlSi_3O_8$). [146].
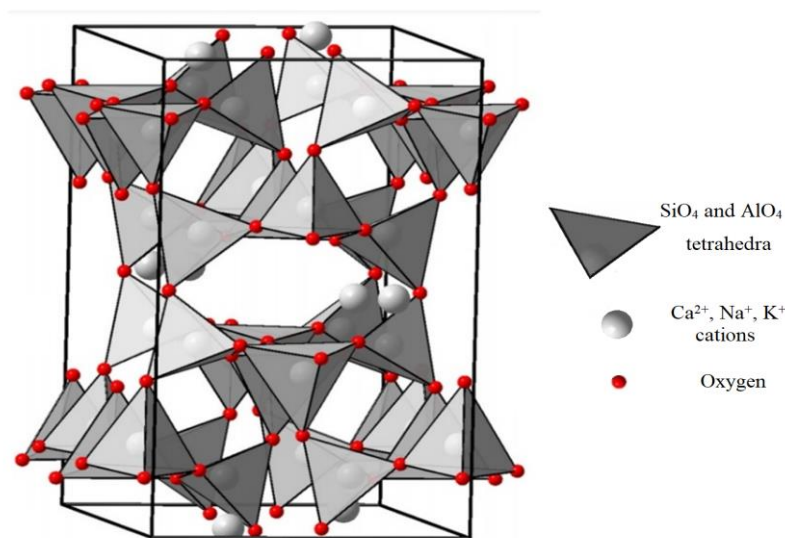
Figure 2.10. The ideal structure of feldspar showing the constructed unit cell. [146].

There is not a great interest in using feldspar as a source of zeolite synthesis, even the benefit of extra cations in its structure with respect to kaolin or halloysite. Also, the advantage in the existence of more silica (approximately Si/Al ratio of 5) in its natural structure makes these raw materials a suitable candidate for moderate Si/Al ratio zeolites such as zeolite X, zeolite Y, and ZSM-5. However, the studies over the usage of feldspar for zeolite synthesis are limited due to its crystalline structure, which is not possible to dehydrate the structure as it was proposed in the metakaolinization process. There are some studies focused on the acidic or basic medium, high temperature, and high-pressure extraction studies, such as Lothenbach et al. reported HCl extraction and formation of zeolite 13X from the extracted liquid [147]. Meng et al. reported KOH extraction followed by hydrothermal reaction to obtain zeolite W as the final product [148]. Su et al. reported the synthesis of zeolite 4A from potassium feldspar with KOH extraction followed by acid dissolution and hydrothermal synthesis [129]. Also, generating zeolite-like structures such as geopolymers or silica nanoparticles was proposed with alkali fusion of the raw material with sodium hydroxide and sodium carbonate [149,150]. The solid phase

alkali fusion reactions of respectively sodium feldspar with sodium hydroxide and sodium carbonate are given below;

$$NaAlSi_3O_8 + 4NaOH \rightarrow NaAlSiO_4 + 2Na_2SiO_3 + 2H_2O$$

$$NaAlSi_3O_8 + 2Na_2CO_3 \rightarrow NaAlSiO_4 + 2Na_2SiO_3 + 2CO_2$$
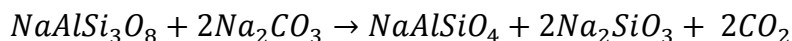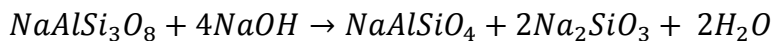
The total feldspar reserves of the world are estimated to be $1,7 \times 10^9$ tons, while Turkey has 14% of total reserves with $2,4 \times 10^8$ tons of reserves. Turkey has the largest reserves of sodium feldspar type [11], which increases the importance of utilizing the valuable raw material by converting this raw material into zeolites as a value-added product.

2.2.1.3   Other Natural Sources

Several different natural sources are proposed for the raw material for zeolite synthesis, such as bauxite [134,135], clinoliptolite [136,137], and pyrophyllite [151]. The most common property of these materials is the abundance of silica and alumina in their natural structure.

Bauxite is a rock composed mainly of aluminum-iron and aluminum hydroxide minerals (boehmite, gibbsite, diaspore). Bauxite is formed from aluminum silicate rocks which are filtrated and watered in tropical areas as second concretion conditions. The colors differ in green, brown, red, and white. Bauxite is an important raw material in world trading since it is one of the primary raw materials of aluminum. It is also commonly used as an abrasive in the cement and iron-steel industry. The world's bauxite reserve is 25 billion tons, where 23 billion tons are minable. Australia has 24% percent of world bauxite reserves, where Brazil has 12%, Guinea has 24%. Turkey has an estimated amount of 97 million tons with 45 million tons of visible reserve.

Bauxites are usually considered to be of two significant types; "lateritic" and "karst" bauxites. The different mineral compositions of these two main bauxite types have

influenced the way they are processed. In general, lateritic bauxites are easier to digest than karst bauxites and are treated by Bayer process variations using less severe conditions of caustic concentration, temperature, and durations. The difference in the "processibility" of these two bauxite types will also influence the strategies for developing viable processes for treating high silica versions of these ores [10].

Clinoptilolite, one of the most commonly used natural zeolites with mainly aluminosilicate structure, is applied as a chemical sieve, feed, and food additive, as well as gas and odor absorber. It has a relatively large amount of pore spaces with respect to the other natural zeolites, high resistance to elevated temperatures, and a neutral chemical structure. Clinoptilolite can easily absorb ammonia and other toxic gases from air and water. Thus, they can be used in filters for health reasons and odor removal in industrial applications. Also, these natural zeolites are widely used in agriculture as water absorbers and ammonia absorbers in cat litters [11,152].

Pyrophyllite [$Al_2Si_4O_{10}(OH)_2$] is an essential aluminosilicate with a Si/Al ratio of 2 used in various industries such as metallurgy, construction additives, petroleum, and chemical industries with its superior physical and mechanical properties. It is a type of hydrous aluminosilicate mineral with a continuous layered structure. Usually, water is located between two tetrahedral silica layers linked with aluminum and forms an "aluminum hydroxide" layer [151,153].

These materials are widely used in various industries. Simultaneously, the common property containing silica and alumina in their structures leads these materials to possible candidates for zeolite synthesis starting materials.

CHAPTER 3

EXPERIMENTAL

3.1   Materials

Various kaolin sources were used throughout the work. High-quality kaolin was purchased from Kaolin Endüstriyel Mineraller San. ve Tic. A.Ş. was named as Kaolin B0 Extra, mined from Bulgaria. The rest of the kaolin sources, defined as low-quality kaolin sources in this particular study, were obtained from various mining sites of Aydın, Turkey. Various sodium feldspar minerals were obtained from several mining sites in the region of Aydın/Muğla; Turkey operated by Polat Maden A.Ş. and Esan A.Ş. Sodium carbonate was used in this study was supplied from Kazan Soda Elektrik; Aluminum hydroxide used in this study was purchased from Eti Aluminyum, while Sodium hydroxide was supplied from Koruma Klor Alkali in a dry flake form. All the sources were used as received; no purification and grinding were performed before activation of the raw materials. The raw materials' technical data sheets (TDS) are given in appendices. No laboratory-grade chemicals were used throughout the thesis study. All these chemicals were industry-grade and used for mass production purposes. Double distilled water (DDW) with < 18 was Ω used in this study. The laboratory-grade chemicals used in this study were sodium aluminate powder branded as Riedel de Haen, and calcium carbonate and potassium carbonate from Merck for proof of concept studies.

3.2   Sample Preparation and Characterizations

The chemical composition of the materials used in the thesis study was characterized via X-Ray Fluorescence (XRF) spectroscopy technique. The results are listed in Table 3.1.

Table 3.1 Chemical Content of the Starting Materials

Source	Source Type	Code	Content (wt. %)						
			SiO$_2$	Al$_2$O$_3$	Na$_2$O	K$_2$O	CaO	TiO$_2$	Fe$_2$O$_3$
		B0 Extra	54.2	37.8	0.13	2.16	0.53	1.88	2.5
		K1	51.8	46.2	0.2	0.6	0.8	0.7	0.33
		K2	52.4	46.9	0.09	0.2	0.33	0.81	0.34
Si&Al	Kaolin	K3	52.2	44.1	0.01	0.19	0.16	1.1	0.29
		K4	62.8	33.5	0.2	0.6	0.42	0.56	1.32
		K5	61.2	35.9	0.25	0.2	0.15	0.51	0.48
		K6	61	36.4	0.15	0.24	0.09	0.79	0.3
		Esan 5 Mic	70	18.5	10.5	0.3	0.7	0.02	0.02
Si,Al&Na	Sodium Feldspar	Polat Oğlankayası	67	19	10	0.6	0.2	0.35	0.22
		Polat Gökbel	65,0	21,0	9.5	0.5	0.15	0.35	0.15
Al	Sodium Aluminate*	-	0	53	41	0	0	0	0
	Aluminum Hydroxide*	-	0	65.36	0	0	0	0	0
Na	Sodium Hydroxide*	-	0	0	77.48	0	0	0	0
	Sodium Carbonate*	-	0	0	58.48	0	0	0	0
Ca	Calcium Carbonate*	-	0	0	0	0	56.03	0	0
K	Potassium Carbonate*	-	0	0	0	68.16	0	0	0

* Calculated from the Technical Data Sheets of these materials, rest of the results were obtained from XRF analysis

Kaolin mineral should ideally have a Si/Al ratio of 1, while according to Table 3.1, the higher silica content in kaolin samples was observed. This excess silica in the structure refers to the quartz impurity in the structure. Also, titanium and iron complexes with minor amounts of calcium, sodium, and potassium were observed in the kaolin sources as impurities. It is possible to eliminate these impurities from the raw materials, but all the raw materials were used as-received in this study. As observed in kaolin sources, feldspars also showed minor amounts of titanium and iron complexes in the raw materials, while sodium complexes are in the structure of the feldspar. Minor amounts of calcium and potassium oxides were observed, which might be the forms of calcium feldspar and potassium feldspar.

Activation of kaolin samples was conducted in three different ways. Metakaolinization is the first method, high-temperature treatment of the raw kaolin without any additives, which is well known in the industry. Alkali fusion is the second way, which source was mixed with a proper amount of alkali sources such as sodium hydroxide or sodium carbonate in this study. High-temperature treatment generates sodium aluminosilicates out from the kaolin source. The third method was one pot fusion which introduced the aluminum source into the fusion mixture to arrange the desired gel formula. In this way, no additional chemicals were used to obtain desired zeolites in the hydrothermal synthesis procedure.

Activation of sodium feldspar samples was conducted in two different methods. Due to the feldspar mineral's nature, there is no way to generate an amorphous output by simple heat treatment methods such as metakaolinization. Alkali fusion and one-pot fusion methods were applied to generate desired products from sodium feldspar samples.

3.2.1   Raw Kaolin Preparation

Characterization of the kaolin as starting raw material is the critical point of the calculation. X-Ray Fluorescence (XRF) Spectrometry results in the distribution of elements in weight fractions and these results should be converted into molar concentrations in 100 grams of raw material. A sample calculation is given below;

Table 3.2 Chemical Analysis of Raw Kaolin Source

wt.%	SiO_2	Al_2O_3	Na_2O	K_2O	Fe_2O_3	TiO_2	CaO
B0 Extra	54.22	37.77	0.13	2.16	2.5	1.88	0.53

These results are weight percentages, so the moles of these compounds shall be calculated according to 100 grams of raw material basis;

$$n_{SiO_2} = W_{SiO_2}/MW_{SiO_2}$$

$$n_{SiO_2} = 54.22\ g/60.08\ \frac{g}{mol}$$

$$n_{SiO_2} = 0.903\ moles$$

Same calculations shall be performed for Al_2O_3;

$$n_{Al_2O_3} = W_{Al_2O_3}/MW_{Al_2O_3}$$

$$n_{Al_2O_3} = 37.77\ g/101.96\ \frac{g}{mol}$$

$$n_{Al_2O_3} = 0.370\ moles$$

The rest of the moles were calculated accordingly, and the results of these calculations were given below;

$$n_{Na_2O} = 0.002\ moles,\ n_{K_2O} = 0.023\ moles,\ n_{Fe_2O_3} = 0.0016\ moles,$$

$$n_{TiO_3} = 0.024\ moles,\ n_{CaO} = 0.009\ moles$$

These moles correspond to the 100 g basis of the kaolin source. If this source is scaled according to 1 mole of Al$_2$O$_3$, a scale factor of $1/n_{Al_2O_3} = 1/0.370 = 2.699497$

When all the sources were multiplied with the scale factor, including the formula weight, the formula which will be used in further calculations will be obtained.

$$2.44 \, SiO_2 : 1 \, Al_2O_3 : 0,006 \, Na_2O, FW = 269,95 \, ^g/_{mol}$$
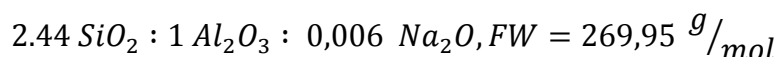
Note [1]: The rest of the components were not given in the above formula since they are impurities and will not affect zeolite synthesis calculations.

Note [2]: The loss on ignition of the kaolin source was 12.4 wt%. The water content in the raw material is not added to the source calculations since all the water content is lost during the heat treatment processes.

3.2.1.1 Metakaolinization Route

Metakaolinization procedure performed in a high-temperature calcination oven with the temperature ramp of 3°C/min up to 850°C with a dwell time of 1.5 h followed by a natural cool-down step. The resulting solid particles grounded with the help of a mortar and fine powder of metakaolin are stored in a closed cap vessel. This form of the kaolin is called "metakaolin".

3.2.1.2 Alkali Fusion Route

Alkali Fusion procedure performed in a high-temperature calcination oven with the temperature ramp of 3°C/min up to 850°C with a dwell time of 1.5 h followed by a natural cool-down step with a proper mixture of kaolin and sodium hydroxide. The resulting solid particles grounded with the help of a mortar and fine powder of alkali fusion product are stored in a closed cap vessel.

3.2.1.3 One-Pot Fusion Route

One-Pot Fusion procedure performed in a high-temperature calcination oven with the temperature ramp of 3°C/min up to 850°C with a dwell time of 1.5 h followed by a natural cool-down step with a proper mixture of kaolin, aluminum hydroxide, and sodium hydroxide. The resulting solid particles grounded with the help of a mortar and fine powder of one-pot fusion product are stored in a closed cap vessel.

3.2.2 Raw Sodium Feldspar Preparation

Sodium feldspar is another crucial mineral for industrial usages such as ceramics, glass, and paint productions. This raw material varies from kaolin in the use of zeolite production since it is impossible to dehydroxylate the structure in relatively mild temperatures such as 850°C. However, fusion with an alkali source forms soluble aluminosilicate, which can be converted into zeolites with hydrothermal synthesis methods. Characterization of the kaolin as starting raw material is the critical point of the calculation. X-Ray Fluorescence (XRF) Spectrometry results in the distribution of elements in weight fractions and these results should be converted into molar concentrations in 100 grams of raw material. A sample calculation is given below;

Table 3.3 Chemical Analysis of Raw Sodium Feldspar Source

wt.%	SiO_2	Al_2O_3	Na_2O	K_2O	Fe_2O_3	TiO_2	CaO
Sodium Feldspar	63.5	22.4	10.5	0.243	0.15	0.4	-

These results are weight percentages, so the moles of these compounds shall be calculated according to 100 grams of raw material basis;

$$n_{SiO_2} = W_{SiO_2}/MW_{SiO_2}$$

$$n_{SiO_2} = 63.5\ g/60.08\ \frac{g}{mol}$$

$$n_{SiO_2} = 1.0569\ moles$$

Same calculations shall be performed for Al₂O₃;

$$n_{Al_2O_3} = W_{Al_2O_3}/MW_{Al_2O_3}$$

$$n_{Al_2O_3} = 22.4\ g/101.96\ \frac{g}{mol}$$

$$n_{Al_2O_3} = 0.2197\ moles$$

Same calculations shall be performed for Na₂O;

$$n_{Na_2O} = W_{Na_2O}/MW_{Na_2O}$$

$$n_{Na_2O} = 10.5\ g/61.9789\ \frac{g}{mol}$$

$$n_{Na_2O} = 0.1694\ moles$$

The rest of the moles were calculated accordingly, and the results of these calculations were given below;

$$n_{K_2O} = 0.0026\ moles,\ n_{Fe_2O_3} = 0.00094\ moles,$$

$$n_{TiO_3} = 0.005\ moles$$

These moles corresponds to the 100 g basis of the kaolin source; if this source is scaled according to 1 mole of Al₂O₃, a scale factor of $1/n_{Al_2O_3} = 1/\ 0.2197 =$ 4.551786

When all the sources were multiplied with the scale factor, including the formula weight, the formula which will be used in further calculations will be obtained.

$$4.81\ SiO_2 : 1\ Al_2O_3 :\ 0.77\ Na_2O, FW = 455.1786\ ^g/_{mol}$$

Note: The rest of the components were not given in the above formula since they are impurities and will not affect zeolite synthesis calculations.

For the fusion processes, two alkaline sources were used as sodium source, sodium hydroxide and sodium carbonate, as explained below;

3.2.2.1   Alkali Fusion Route

Alkaline fusion of sodium feldspar and sodium hydroxide/sodium carbonate was performed in a high-temperature calcination oven with a temperature ramp of 3°C/min up to 850°C with a dwell time of 1.5 h followed by a natural cool-down step. The resulting solid particles grounded with the help of a mortar and fine powder of fusion product were stored in a closed cap vessel.

3.2.2.2   One-Pot Fusion Route

One-Pot Fusion of sodium feldspar, aluminum hydroxide, and sodium hydroxide/sodium carbonate was performed in a high-temperature calcination oven with a temperature ramp of 3°C/min up to 850°C with a dwell time of 1.5 h followed by a natural cool-down step. The resulting solid particles grounded with the help of a mortar and fine powder of one-pot fusion product were stored in a closed cap vessel.

3.3   Zeolite Synthesis

Zeolites were synthesized with the hydrothermal synthesis method. The desired gel was obtained by mixing prepared raw materials, distilled water, and additional chemicals if necessary. The mixture was hydrothermally treated in HDPE bottles and aged at 25°C or in the hot water bath with continuous agitation. After the proper duration (varies in the optimization studies), the HDPE bottle is transferred in a previously heated oven at 100 °C for proper time (varies in the optimization studies). HDPE bottles were placed in 25°C water baths, and caps were opened right after the

reaction. The resulting suspension was centrifuged and washed 4 times with distilled water directly after synthesis, followed by air drying at 60 °C overnight.

3.4   Material Characterizations

There are four main characterization techniques for zeolites to evaluate the quality of the final product, which are X-Ray Diffraction (XRD), Scanning Electron Microscopy (SEM), X-Ray Fluorescence Spectrometry (XRF), and Thermal Gravimetric Analysis (TGA), which explains details about the synthesis products. These characterization techniques are explained below. All characterizations were performed using the facilities at Middle East Technical University, Central Laboratory.

3.4.1   X-Ray Diffraction

X-Ray Diffraction analysis gives detailed information about the crystal phases in the product. Schematic representation of the XRD technique is shown in Figure 3.1. The impurities and crystallinity of the sample can be analyzed with respect to a reference zeolite.
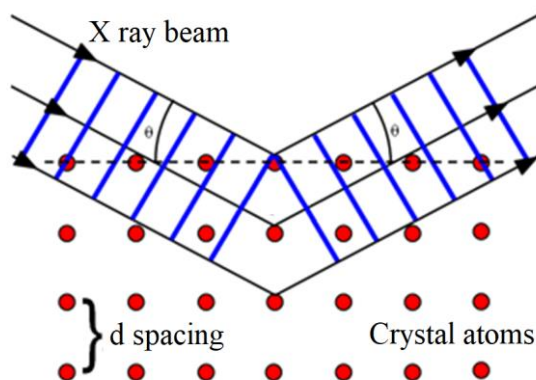
Figure 3.1. Schematic representation of working principle of XRD

According to Bragg's law, "2dsinθ=nλ" and d is specific for every crystal plane; that's why the spectrum can be analyzed deeply for crystal structure analysis. Phase

41

identification of all samples was made by X-ray powder diffraction (XRD) using Rigaku-Ultima IV XRD. The diffraction peaks were scanned between 5-50° with a minimum of 1°/min scan speed. XRD analysis was performed by calculation of integral area of the main 5 peaks of zeolite 4A and zeolite 13X to determine the relative crystallinity of synthesized zeolite samples. The highest value of the compared zeolite was designated as 100%, and the relative crystallinities of the other samples were calculated relative to that sample. The relative crystallinity of zeolite samples was calculated from the obtained diffraction patterns by the equation below.

$$Relative\ Crystallinity\ of\ the\ Sample\ (\%) = \frac{The\ sum\ of\ the\ area\ under\ the\ designated\ peaks\ of\ the\ Sample}{The\ sum\ of\ the\ area\ under\ the\ designated\ peaks\ of\ Reference\ Sample}$$

3.4.2   Scanning Electron Microscopy

Scanning Electron Microscopy is the technique of imaging with the help of electrons with very high magnifications. All the synthesized samples were characterized with FEI Quanta 400F Field Emission Scanning Electron Microscope of Middle East Technical University with attachments of an Energy Dispersive X-Ray Detector (EDX). To avoid the charging problem, all samples were coated with 3 nm Au-Pd before the analysis. SEM was used to generate high magnification images of the surfaces, usually at 20 KeV, while EDX was used to measure the elemental composition of the raw materials and synthesis products.

3.4.3   Thermogravimetric Analysis

The Thermogravimetric Analysis method is used to measure the amount of water adsorbed in the pores of the zeolites synthesized. The static water adsorption amounts were measured as follows: As-synthesized samples were humidified for 24 h in a desiccator with saturated NaCl solution. After 24 h, the weight loss of samples

was measured with a Perkin Elmer Pyris 1 thermogravimetric analysis (TGA) device, and the losses until 200 °C were reported.

3.4.4   X-Ray Fluorescence Spectrometry

The X-Ray Fluorescence spectrometry technique is used to identify the chemical composition of the raw starting materials with semi-quantitative mode. In this technique, the sample of interest is illuminated with a high-energy X-Ray beam, and secondary emission of X-Rays from the sample is measured. These secondary X-Rays are unique to the elements present in the sample and used as a fingerprint. The determination of these unique energy positions identifies the presence of these elements in the sample, while its intensity determines its quantity. Rigaku ZSX Primus II system is used to characterize the raw materials in this study.

3.5   Additional Characterizations

Synthesized zeolites were characterized depending on the applications that they will be used and compared with the commercially available alternatives. These characterizations can be summarized in two main application fields: desiccants and warm mix asphalt. As a desiccant, standard material characterizations were performed, but as a Warm Mix Asphalt (WMA) additive, further characterizations of the zeolite mixed asphalts were performed.

3.5.1   Viscosity Characterizations

The viscosity of the binders in the asphalt was characterized according to ASTM D4402, "Viscosity Determination of Asphalt Binder Using Rotational Viscometer." The procedure of the sample preparation is as follows;

a) Binder is heated to the desired temperature in the oven.
b) 100 gr of binder is filled into a glass beaker.

c) The desired amount of additive is added to the binder.

d) The sample is mixed with the help of a mechanical at a rate of 1000 rpm for 5minutes. Meanwhile, the glass beaker is kept at a constant temperature using a mantle heater, as shown in the figure.

e) 10.5 gr of the sample is filled into the test tube and directly moved to the Brookfield viscometer. For the tests, no.27 spindle is used.

f) The readings are taken as soon as the readings are stabilized.

Figure 3.2. Photographs of the (a) sample preparation setup and (b) Brookfield viscometer.

3.5.2   Compactability Characterizations

Marshall Compactor is used to characterize the warm mix asphalts' compactability. A fine graded mix is selected as the control mixture (HMA) in this study. The mixture gradation consists of 36.2% coarse aggregates, 59.4% fine aggregates, and 4.4% filler. The binder type was determined to be a virgin binder Pen 50-70. The optimum mixing and compaction temperatures for the control mixtures were estimated as 150°C and 140°C, respectively. According to the Marshall mix design procedure, the optimum binder content is determined to be 7.5%.

For all the mixtures, the mixing temperature is kept constant. The compaction temperatures are selected to be 30 and 45 °C lower than the optimum temperature to analyze the compactability.

CHAPTER 4

ZEOLITE SYNTHESIS FROM KAOLIN AS STARTING MATERIAL

Traditionally, zeolite 4A is synthesized by hydrothermal crystallization of a specially prepared solution of silicon, aluminum, and sodium [3,7,79]. In order to meet the requirement of growing demand in zeolites, there is still a continuous search on lowering the production cost by replacing conventional chemicals with cheap raw materials. These cheap raw materials include a variety of clay minerals [20,154], coal ash [12,97], halloysite [155,156], and natural zeolites [85] that will supply the demand of SiO_2 and Al_2O_3 for the synthesis of zeolites in the right proportion.

Among these raw materials, kaolin ($Al_2O_3.2SiO_2.2H_2O$) with $Si/Al = 1$, which is in close agreement with that of zeolite 4A, seems to be the most appropriate source to be used as a starting material for its synthesis [100,106,124,157,158]. The framework structure of kaolin is composed of one layer of alumina octahedron sheet and one layer of silica tetrahedron sheet in a 1:1 ratio. To fully utilize kaolin as a source for zeolite synthesis, the crystalline phase of kaolin must be converted into an amorphous and reactive phase by the metakaolinization process. The metakaolinization involves thermal activation at high temperatures, usually 600-1100°C [115,117]. This step is followed by the hydrothermal synthesis step, which typically involves the hydrothermal reaction of metakaolin with an aqueous alkali medium at proper reaction temperatures.

Kaolin is a well-known source material in various industries such as ceramics [159–161], cosmetics [162–164], and paper production[165,166]. Due to its similar chemical content, kaolin is also a widely used raw material for zeolite synthesis [105]. However, every different source type has unique impurities, i.e., high-impurity type "low-quality kaolin" and low impurity type "high-quality kaolin". All

these impurities in their structure cause different characteristics, and the synthesis parameters should be optimized for each of them. Also, low-quality kaolin has very limited applications in the industry due to the high content of extra impurities, making this material a relatively cheap alternative source for zeolite synthesis. This chapter explains the optimization of zeolite 4A and zeolite 13X synthesis conditions.

4.1   Raw Kaolin Characterization

Raw kaolin obtained from Kaolin Endüstriyel Mineraller San. ve Tic. A.Ş. was treated by suspension process to detect possible non-clay impurities. The sample was well-mixed with 1 lt of water and left in suspension for 8 h. With this process, clay minerals, i.e., kaolin, remained in suspension, and non-clay minerals such as quartz, feldspar, and calcite settled down. This process was repeated many times to remove kaolin from non-clay mineral impurities completely. The initial part obtained from the suspended part of kaolin was characterized by XRD after some pretreatments applied on oriented slides such as air drying, ethylene glycol saturation (PEG Modified), and finally, calcination at 300 and 550°C [167]. The XRD patterns obtained from these oriented slice samples are given in Figure 4.1. Moreover, the non-clay part of the sample was analyzed by XRD to determine types of non-clay impurities in the raw material (B0 extra source), and the results are shown in Figure 4.2.
.
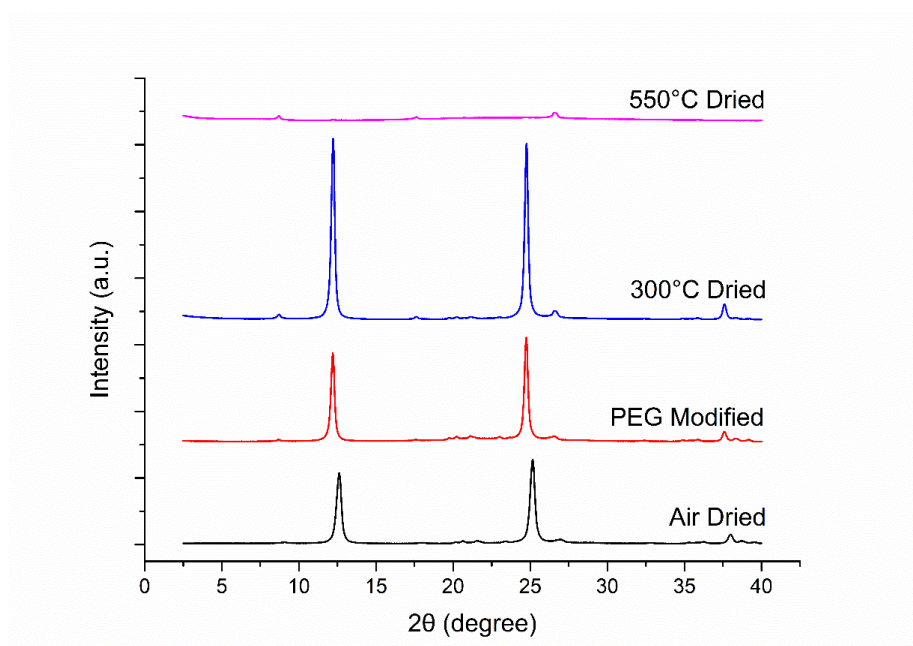
Figure 4.1. XRD patterns of air-dried, EG modified, 300°C and 550°C dried B0 Extra Kaolin source.
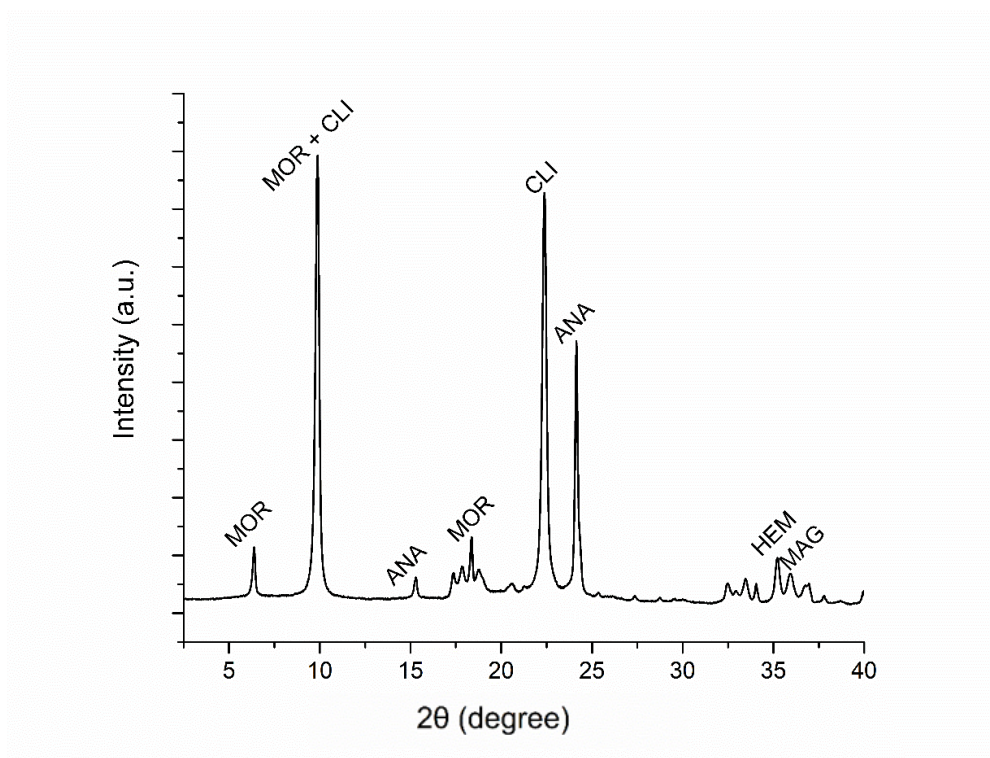
Figure 4.2. XRD pattern of the washed B0 Extra Kaolin source.

49

According to Figure 4.1, only kaolin exists in the B0 Extra source since there is no enhancement in the gallery area upon EG saturation. At the same time, the pattern was kept still after 300°C while the structure was totally destroyed after 550°C calcination [167–169]. Moreover, Figure 4.2 showed that there are minor natural zeolite impurities in the B0 Extra sample, which is around 0.2946 grams in every gram of raw material after washing. These impurities can be identified as mainly mordenite [170,171], clinoptilolite [136,172] and analcime [93,173]. Among these natural zeolites, very loose peaks of hematite and magnetite phases were [174] observed in the spectrum. These impurities in the structure are in agreement with the XRF data given in Table 3.2, which suggests a SiO_2/Al_2O_3 ratio of 2.44. The increase in the SiO_2/Al_2O_3 with respect to the well-known ratio of 2.00 for kaolin can be due to the detected minor impurities with higher SiO_2/Al_2O_3 ratios such as clinoptilolite (SiO_2/Al_2O_3 up to 5) [175] and mordenite (SiO_2/Al_2O_3 up to 25)[176]. Moreover, the presence of iron observed in the XRF spectrum was confirmed by the presence of hematite and magnetite phases in the XRD pattern of the non-clay fraction of washed kaolin B0 Extra sample.

4.2 Optimization of Synthesis Parameters for Zeolite 4A with High-Quality Kaolin

The quality of kaolin to be used as a suitable source depends on the impurity content of that kaolin, such as quartz, mica, feldspar, mullite, etc. High-quality kaolin is defined as a low-impurity, high crystallinity product that consists of almost 100% kaolin. The initial choice of kaolin was "high-quality kaolin" to synthesize zeolite 4A. XRD results obtained from the as-received and calcined kaolin samples are given in Figure 4.3.
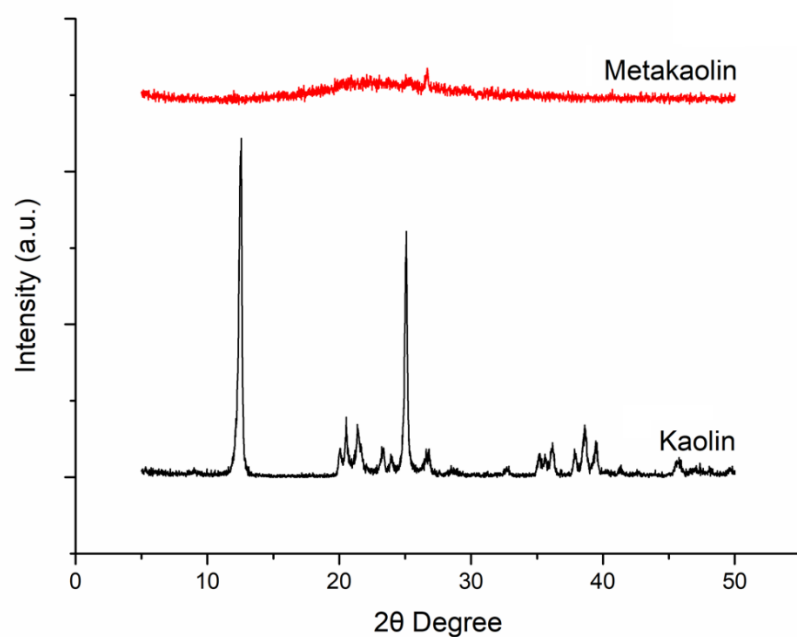
Figure 4.3. XRD patterns of the as-received high-quality kaolin and the calcined
metakaolin.

As seen in Figure 4.3, the crystallinity of the raw material was completely lost after
the calcination was performed at 800°C for 1.5 h. The calcination temperature and
times were picked according to the literature studies reported for the optimum
dehydroxylation of the kaolin structure that is suitable to form an amorphous active
material [21,105,114,122]. Further optimization studies were performed along with
these outputs, and synthesis products out of these kaolin samples were examined.
Synthesis routes and optimized parameters are given in Figure 4.4.
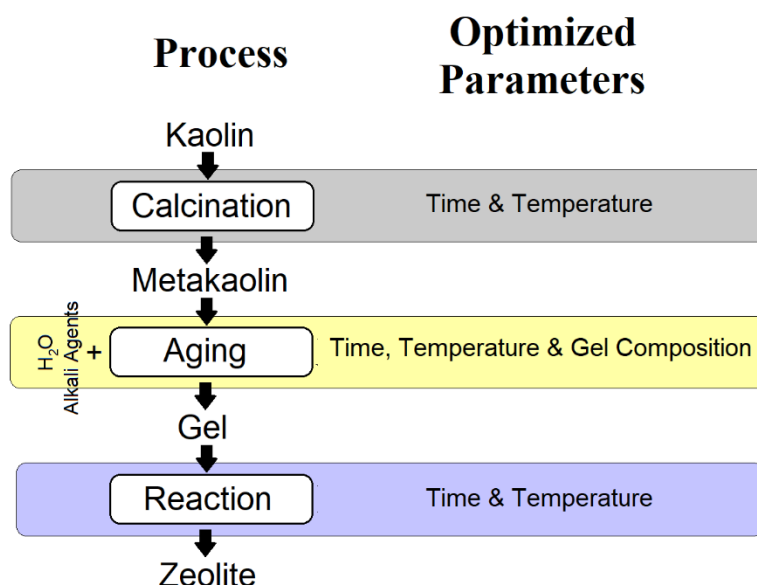
Figure 4.4. Schematic representation of the process flow and the optimized parameters for zeolite 4A synthesis from kaolin.

As shown in Figure 4.4, the time and temperature of each process were aimed to be optimized for each step of the process in addition to the gel composition.

4.2.1   Calcination Conditions

Calcination is a vital activation step of the zeolite synthesis from kaolin since it is the first treatment of the raw material. Calcination is the dehydroxylation of kaolin and generating reactive and X-ray amorphous metakaolin [105,115]. Calcination temperature and calcination time were studied to optimize the calcination conditions.

4.2.1.1   Calcination Temperature

Kaolin samples were placed in a crucible and calcined at three different temperatures for 1.5 h. The calcination temperatures were selected as 800, 850, and 900°C. Synthesis with these calcined kaolins was performed to reach the molar composition

of 2.44 SiO_2: 1 Al_2O_3: 3.14 Na_2O: 110 H_2O [177]. Prepared gels were aged in a 60°C water bath for 4 h, and reactions were performed at 100°C for 4 h, statically. The SEM images of final products and their XRD patterns are shown in Figure 4.5 and Figure 4.6, respectively. The relative crystallinities of all products in comparison with each other are summarized in Table 4.1.
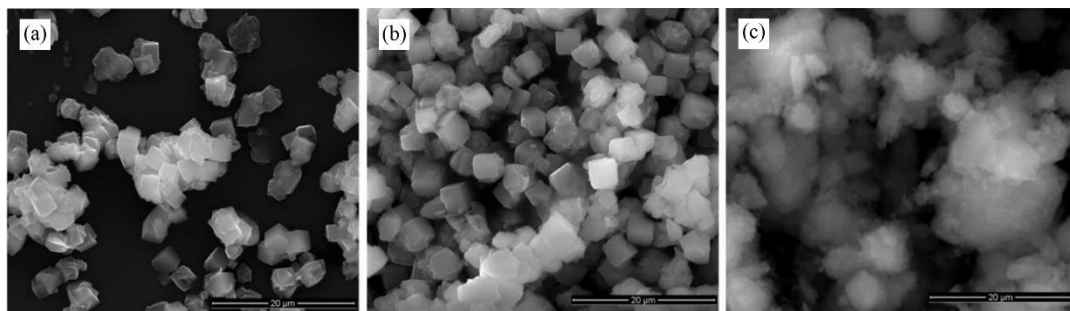
Figure 4.5. SEM images of the zeolite 4A synthesis products from kaolin, calcined at 800°C (a), 850°C (b), and 900°C (c).
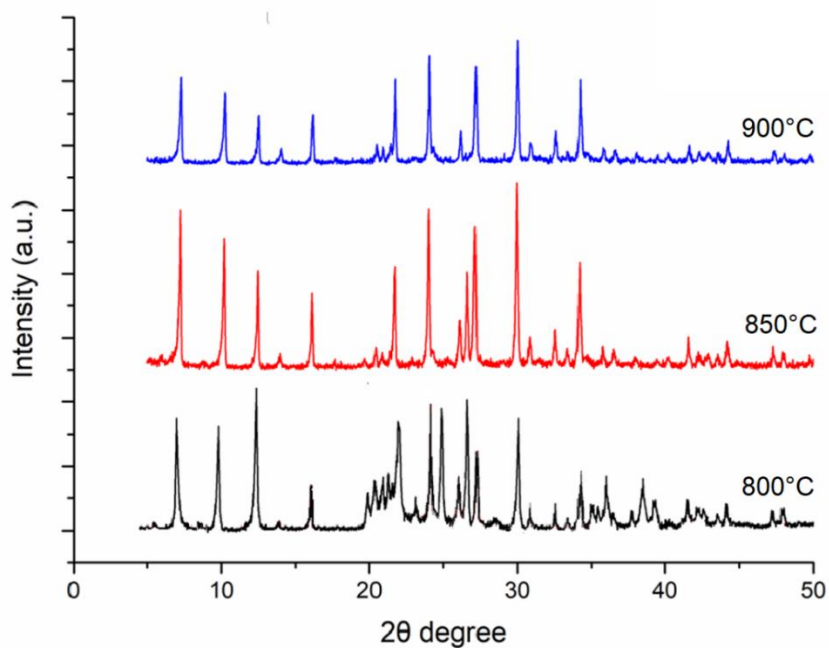
Figure 4.6. XRD patterns of the zeolite 4A synthesis products from kaolin, calcined at 800°C, 850°C, and 900°C.

Table 4.1 Relative crystallinity of zeolite 4A synthesized with different calcination temperatures of kaolin

Calcination Temperature (°C)	800	850	900
Relative Crystallinity, %	82	100	68

According to Figure 4.5, it was observed that the calcination temperature of 850°C resulted in a good quality zeolite 4A product with the highest crystallinity and well-developed cubic morphology. Furthermore, according to Figure 4.6, there is a lack of metakaolinization at a calcination temperature of 800°C, which clearly resulted in less crystalline zeolite 4A product. This situation was improved upon increasing the calcination temperature to 850°C. XRD patterns shown in Figure 4.6 indicate lower crystalline products with respect to those obtained from 850°C calcination. Further increase in calcination temperature to 900°C also resulted in pure zeolite 4A crystals with less crystallinity with respect to 850°C. Accordingly, an optimum calcination temperature of 850°C was chosen for the rest of the experiments.

4.2.1.2   Calcination Time

Calcination time is another critical parameter to dehydroxylate the structure and form metakaolin, the primary starting material for zeolite synthesis. For that purpose, three different durations of 1.5, 3, and 6 h at 850°C were studied. Obtained metakaolins were used as starting materials for hydrothermal synthesis with a molar gel formula of 2.44 SiO_2: 1 Al_2O_3: 3.14 Na_2O: 110 H_2O. Prepared gels were aged in a 60°C water bath for 4 h, and reactions were performed at 100°C for 4 h, statically.

The SEM images of final products and their XRD patterns are given in Figure 4.7 and Figure 4.8, respectively.
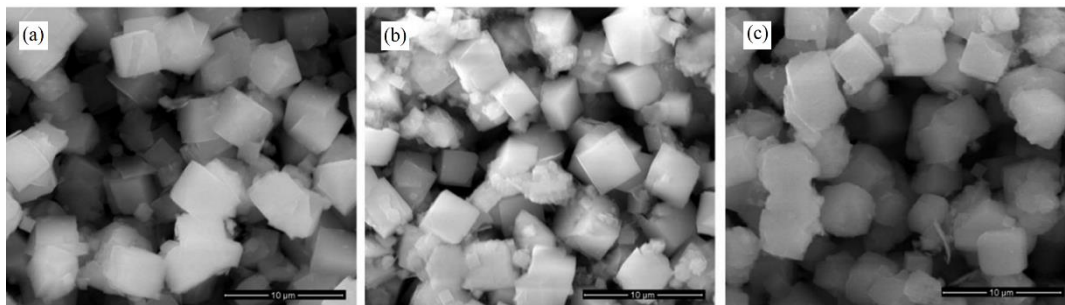
Figure 4.7. SEM images of the zeolite 4A synthesis products from kaolin, calcined at 850°C for 1.5 h (a), 3 h (b), and 6 h (c).
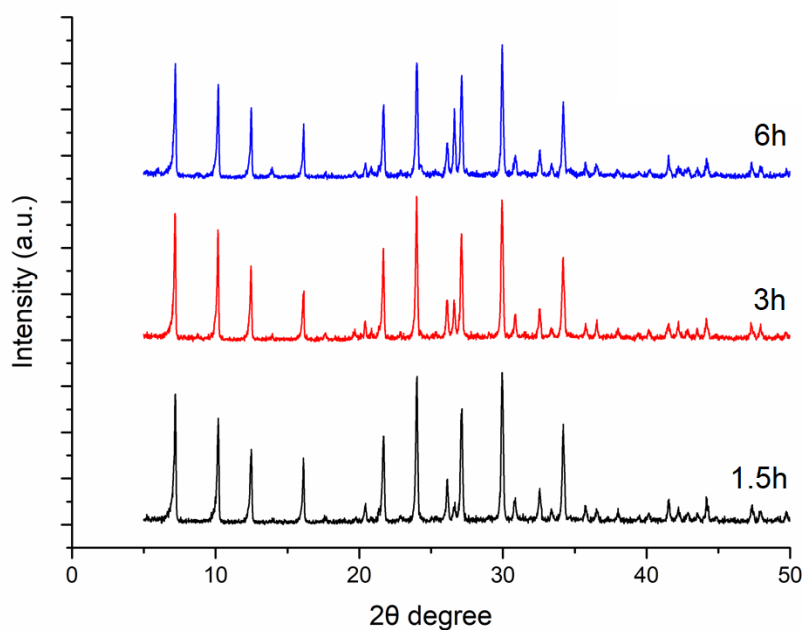
Figure 4.8. XRD patterns of the zeolite 4A synthesis products from kaolin, calcined at 850°C for 1.5 h, 3 h, and 6 h.

Figure 4.7 and Figure 4.8 suggest that no significant change was observed either in the morphology and crystallinity of the zeolite crystals after 1.5 h of calcination.

Also, relative crystallinities were calculated and were found to be around 98% ± 2 for all three samples. It means that the metakaolinization was finalized after 1.5 h of calcination time for this particular kaolin sample. To minimize the production costs, the rest of the experiments were conducted using 1.5 h of calcination time at 850°C.

4.2.2 Aging Conditions

Aging was the second process step of the zeolite synthesis route performed after the metakaolinization step. Metakaolinization was performed at 850°C for 1.5 h. Metakaolin samples were mixed with the pre-calculated amount of sodium hydroxide and sodium aluminate to form a gel with the molar formula of 2.44 SiO_2: 1 Al_2O_3: 3.14 Na_2O: 110 H_2O.

Two different temperatures and three different aging times were performed to investigate the optimum aging conditions.

4.2.2.1 Aging Time

Three different aging times of 2, 4, and 6 h were studied to determine the optimum aging time for zeolite 4A synthesis from kaolin as starting material. Conditions for the metakaolinization step were identical for all synthesis experiments and were performed at 850°C for 1.5 h. Metakaolins were mixed with the calculated amount of sodium hydroxide, sodium aluminate/sodium silicate, and distilled water to form a gel with the molar formula of 2.44 SiO_2: 1 Al_2O_3: 3.14 Na_2O: 110 H_2O. The resulting gels were placed in an HDPE bottle and aged at 60°C water bath with continuous stirring for three durations. Aged gels were placed in a previously heated oven at 100°C for 4 h for the reaction step. The SEM images of final products and their XRD patterns are given in Figure 4.9 and, Figure 4.10, respectively.
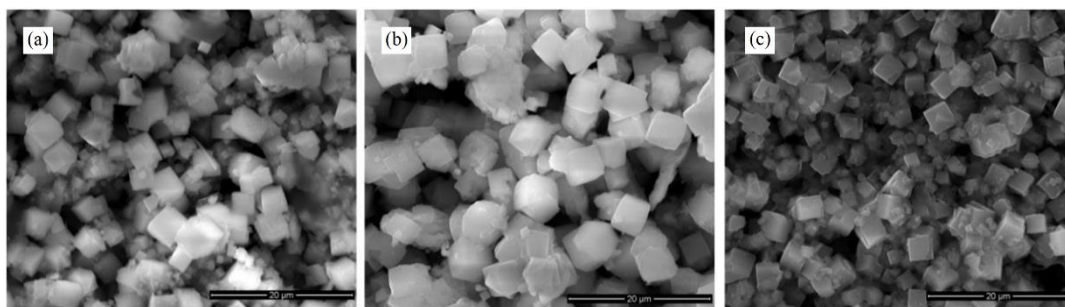
Figure 4.9. SEM images of the zeolite 4A synthesis products from kaolin, aged at 60°C for 2 h (a), 4 h (b), and 6 h (c).
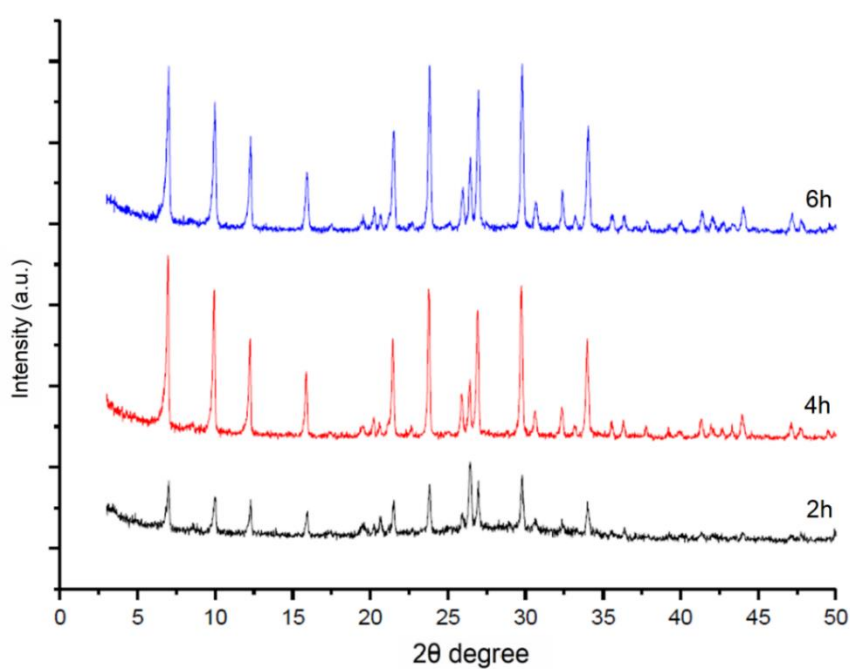
Figure 4.10. XRD patterns of the zeolite 4A synthesis products from kaolin, aged at 60 °C for 2 h, 4 h, and 6 h.

The SEM images suggest no significant difference in the morphologies among the aged samples for 2, 4, and 6 h. According to the XRD patterns, the intensity of the main zeolite 4A peak increased up to 4 h of aging. Relative crystallinities with different aging times were given in Table 4.2.

Table 4.2 Relative crystallinity of zeolite 4A synthesized from kaolin with
different aging times

Aging Time (h)	2	4	6
Relative Crystallinity, %	42	98	100

As reported in the literature, aging has an essential effect on gel chemistry, ultimately affecting nucleation and crystal growth kinetics. It directly affects improved crystallization if the right experimental conditions are assured [77,123]. Caballero et al. reported that no aging resulted in amorphous aluminosilicate gel [90] for zeolite 13X synthesis. Also, it is reported that extended aging times lead to a higher number of nuclei formation, decreasing the final particle size of the zeolites for zeolite Y [178,179]. The parameters for each type of raw material need to be remarkably optimized due to the dissolution limitations [67,177,180,181]. According to the obtained results, further experiments were conducted using 4 h of aging at a 60°C water bath.

4.2.2.2   Aging Temperature

Aging temperature is another critical parameter since it directly affects the nuclei formation, thus zeolite type and particle size. Metakaolinization was performed at 850°C for 1.5 h. Metakaolins were mixed with the calculated amount of sodium hydroxide and sodium aluminate to form a gel with $2.44 SiO_2$: $1 Al_2O_3$: $3.14 Na_2O$: $110 H_2O$ formula. Aging was performed for 4 h at 25°C and 60°C. Aged gels were placed in a previously heated oven at 100°C for 4 h for the reaction step. The resulting solid particles were separated from the mother liqueur and washed by distilled water at least three times by centrifugation at 7500 rpm for 5 minutes and dried in a conventional oven at 70°C overnight. The SEM images of final products and their XRD patterns are given in Figure 4.11 and Figure 4.12, respectively.

58
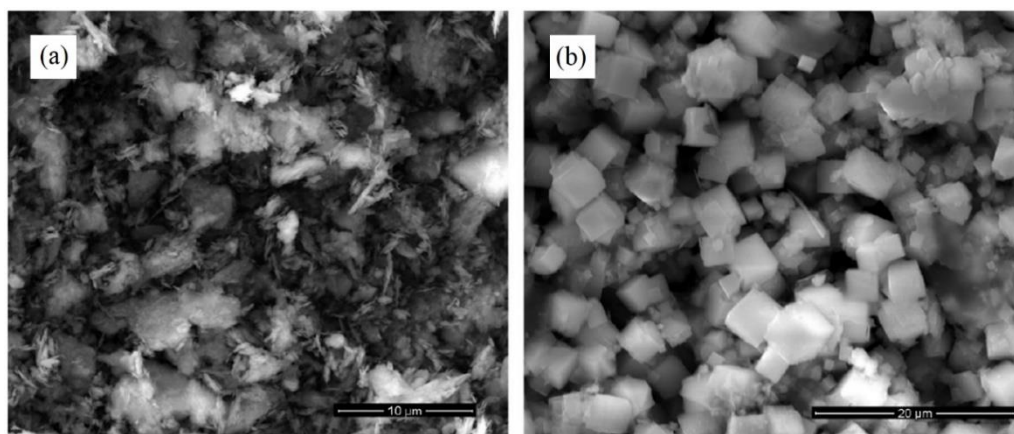
Figure 4.11. SEM images of the zeolite 4A synthesis products from kaolin, aged at 25°C (a) and 60°C (b) for 4 h.
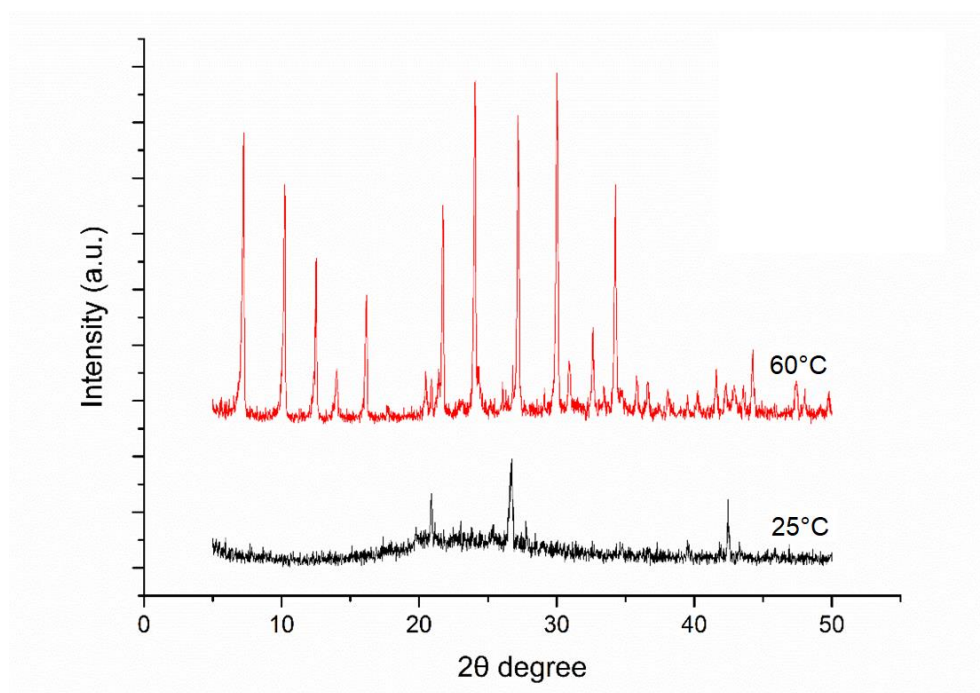
Figure 4.12. XRD patterns of the zeolite 4A synthesis products from kaolin, aged at 25°C and 60°C for 4 h.

It is known that the heat input to the reaction system during the aging step increases the dissolution of Si and Al species in the gel [182]. On the other hand, it is reported that aging temperatures above 70°C do not give any crystalline product for the synthesis of zeolite 13X [90]. Furthermore, it was reported that increasing aging

temperature resulted in losing control over the synthesized product, such as the formation of the uncontrolled formation of zeolite P along with the desired zeolite types [77,154].

Overall, these results confirmed that aging at 25°C resulted in almost no crystalline zeolite product, while 60°C aging has the highest crystallinity with the cubic morphology. The observed amorphous product indicated the necessity of initial heat input applied during the aging step. Another solution was shown to increase aging time for zeolite production out of the kaolin, which correlates with the literature studies [77].

4.2.3   Aging Temperature

Tailoring reaction conditions can be proposed to be the final step for controlling the process of zeolite synthesis, as shown in Figure 4.4. For that particular study, metakaolinization was performed at 850°C for 1.5 h. Metakaolins were mixed with the calculated amount of sodium hydroxide and sodium aluminate to form a gel with 2.44 SiO_2: 1 Al_2O_3: 3.14 Na_2O: 110 H_2O formula. The resulting gels were placed in an HDPE bottle and aged at 60°C with continuous stirring for 4 h. Three different reaction temperatures and three different reaction times were investigated for this particular study.

4.2.3.1   Reaction Temperature

Aged gels were placed in previously heated ovens at 80 and 100°C for 4 h to optimize the reaction condition. The SEM images of final products and their XRD patterns are given in Figure 4.13 and Figure 4.14, respectively.
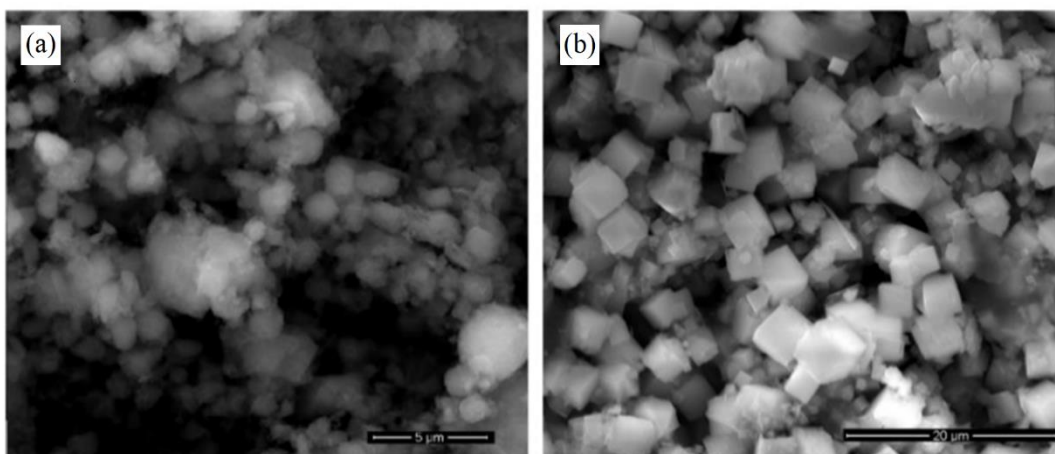
Figure 4.13. SEM images of the zeolite 4A synthesis products from kaolin, with reaction temperatures of 80°C (a) and 100°C (b).
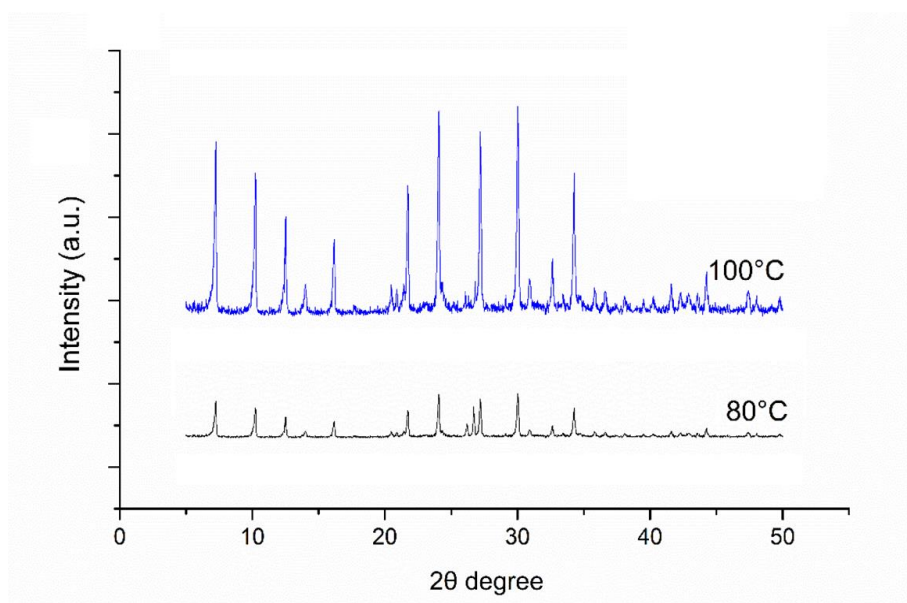
Figure 4.14. XRD patterns of the zeolite 4A synthesis products from kaolin, with reaction temperatures of 80°C and 100°C

Table 4.3 Relative crystallinity of zeolite 4A synthesized from kaolin with different reaction temperatures

Reaction Temperature (°C)	80	100
Relative Crystallinity, %	23	100

According to the SEM images shown in Figure 4.13, the zeolite obtained after 80°C was poor quality. This has been a well-studied topic in the literature alongside various studies reported focused on reaction time and temperatures, such as 6.1 h at 78°C [183], 4 h at 95°C [184], and 24 h at 125°C [47]. It is challenging to find a single solution for all of these studies since each parameter should be optimized for every zeolite source and gel molar formula independently [47,81]. Accordingly, reaction conditions had to be optimized for that particular local source to obtain zeolite 4A successfully. The results obtained from the current study suggested that the highest crystallinity could be obtained at a reaction temperature of 100°C (Figure 4.14, Table 4.3).

4.2.3.2   Reaction Time

Reaction time is one of the most crucial parameters for the zeolite synthesis to form desired particle-sized zeolites with optimum yield avoiding secondary phases as impurities. In the literature, there are various reports with different reaction times from 70°C to 130°C [19,77]. For the current study, metakaolinization was performed at 850°C for 1.5 h. Metakaolins were mixed with the calculated amount of sodium hydroxide and sodium aluminate to form a gel with the molar formula of 2.44 SiO_2: 1 Al_2O_3: 3.14 Na_2O: 110 H_2O. The resulting gels were placed in an HDPE bottle and aged at 60°C with continuous stirring for 4 h. Aged gels were placed in a previously heated oven at 100°C for 2, 4, and 6 h to optimize the reaction time. The SEM images of final products and their XRD patterns are given in Figure 4.15 and Figure 4.16, respectively.

Figure 4.15. SEM images of the zeolite 4A synthesis products from kaolin, at reaction times of 2 h (a), 4 h (b), and 6 h (c).

Figure 4.16. XRD patterns of the zeolite 4A synthesis products from kaolin, with reaction durations of 2 h, 4 h, and 6 h.

Table 4.4 Relative crystallinity of zeolite 4A synthesized from kaolin at different reaction times

Reaction Time (h)	2	4	6
Relative Crystallinity, %	57	99	100

In summary, all obtained results suggested no significant increase in crystallinity after 4 h of reaction time at 100°C. Thus, a reaction time of 4 h and a reaction temperature of 100°C was set for the rest of the experiments.

4.2.4 Gel Formulation

The gel formula is known to be the determining step for the final purity of the product, its crystallinity, and even the type of zeolite crystal obtained at the end of the process. For this purpose, four different gel formulations were prepared using metakaolin calcined at 850°C for 1.5 h, adding an appropriate amount of sodium hydroxide, sodium aluminate, and distilled water. The list of all gel formulas is given in Table 4.5. Afterward, the resulting gels were also placed in an HDPE bottle and aged at 60°C with continuous stirring for 4 h. Aged gels were placed in a previously heated oven at 100°C for 4 h of reaction time. The SEM images of final products and their XRD patterns are given in Figure 4.17 and Figure 4.18, respectively.

Table 4.5 Different molar gel formulas prepared for zeolite 4A synthesis from kaolin

Formula Code	SiO_2 (moles)	Al_2O_3 (moles)	Na_2O (moles)	H_2O (moles)
Gel 1	2.44	1	3.14	110
Gel 2	2.10	1	3.14	110
Gel 3	2.44	1	2.00	70
Gel 4	2.00	1	2.00	70
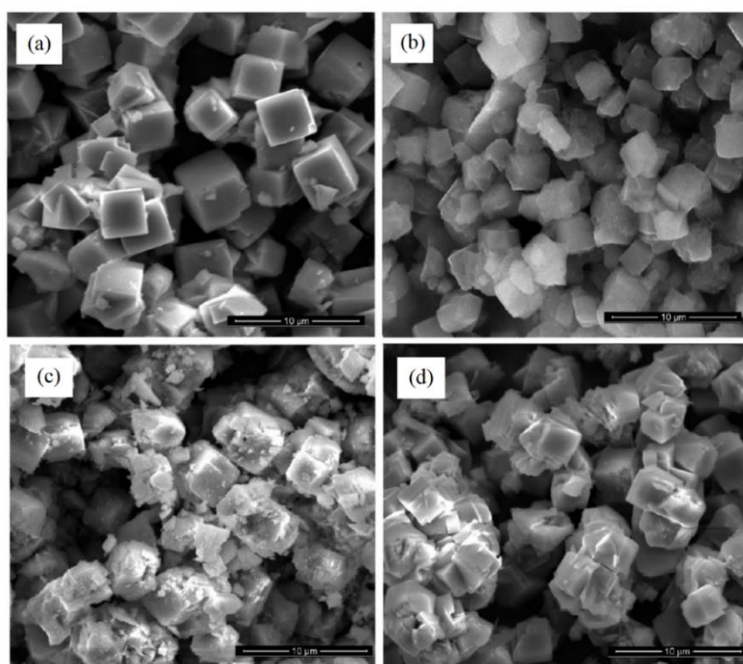
Figure 4.17. SEM images of the synthesis products from kaolin which were produced from 4 different gel formulas; Gel 1 (a), Gel 2 (b), Gel 3 (c), and Gel 4 (d).
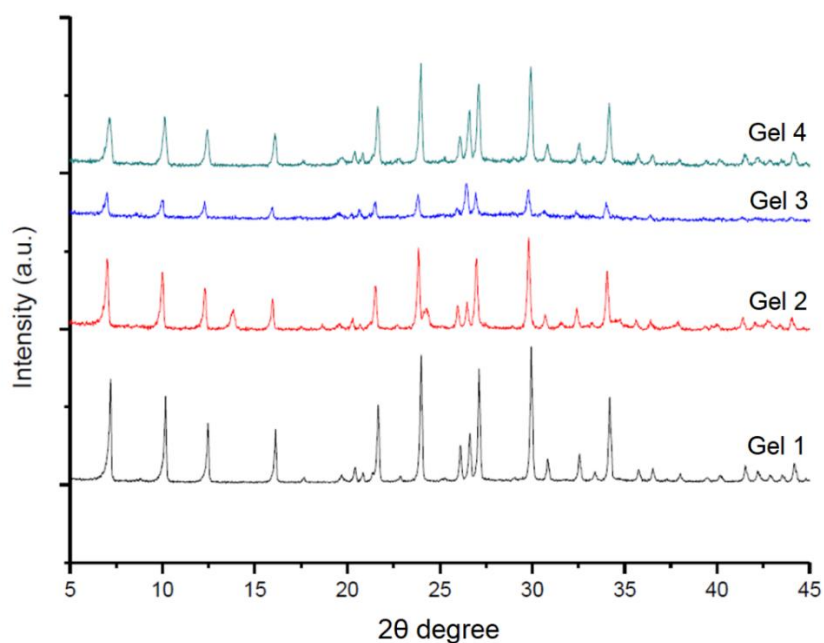
Figure 4.18. XRD patterns of the zeolite 4A synthesis products from kaolin with different gel formulas.

Table 4.6 Relative crystallinity of zeolite 4A synthesized from kaolin with different gel formulations

Gel Formulations	Gel 1	Gel 2	Gel 3	Gel 4
Relative Crystallinity (%)	100	84	38	69

The effect of changing the molar gel formula on the zeolite morphology is shown in Figure 4.17. Accordingly, similar morphologies were observed for all zeolite samples as standard cubic particles of zeolite 4A except for gel 3, which showed a more significant amorphous material formation accompanied by cubic zeolite 4A crystals. Furthermore, the results that are shown in Figure 4.17 and Table 4.6 confirm that gel 3 has the lowest crystallinity among all. Additionally, the crystallinity of the products (Table 4.6) decreased at lower alkalinity, as observed from the results obtained using gels 3 and 4. These results correlate with the reported data suggesting the competing phases between sodalite and zeolite 4A. Alkalinity also directly affects the crystallinity of the final product [101,185]. Gel 1 resulted in the highest crystallinity among all products with a relatively lower yield (89.2 wt.%). In comparison, gel 2 resulted in a higher yield (92.1 wt.%) with lower crystallinity with respect to the zeolite synthesized using gel 1. It can be hypothesized that the lower yield was caused by the excess amount of silica source in the starting gel. Simultaneously, it could increase the crystallinity of the final product, which is one of the most critical parameters considered in industrial zeolite production [177].

4.3 Comparison of Synthesized Zeolite 4A with Commercial Zeolite 4A

The zeolite 4A obtained using locally available high-quality kaolin was named Zeolite 4A HQK (High-Quality Kaolin). The summary of optimized synthesis parameters obtained from the initial part of this thesis study is as follows:

Calcination parameters: 850°C, 1.5 h

Gel Formula: 2.44 SiO_2: 1 Al_2O_3: 3.14 Na_2O: 110 H_2O

Aging Conditions: 60°C water bath for 4 h, continuous agitation

Reaction Conditions: 100°C for 4 h, static

The SEM images and XRD patterns of the commercially available zeolite 4A and the synthesized Zeolite 4A HQK are shown in Figure 4.19 and Figure 4.20, respectively.
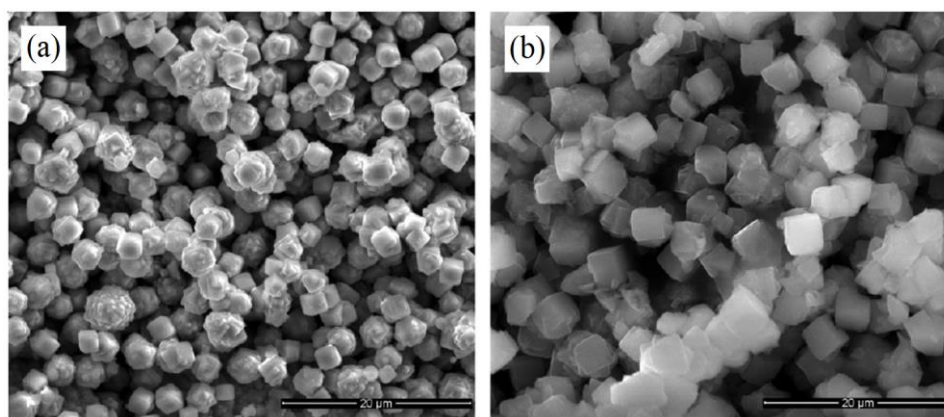
Figure 4.19. SEM images of the commercial zeolite 4A (a) and Zeolite 4A HQK (b).
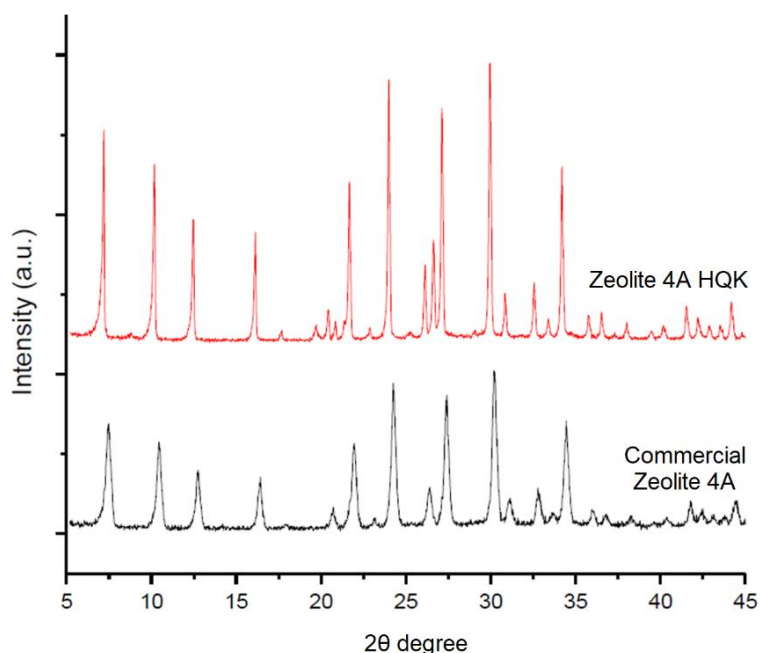
Figure 4.20. XRD patterns of the commercial zeolite 4A and Zeolite 4A HQK.

It was observed that the shapes of the synthesized zeolites have the standard cubic structure of the LTA family while commercial zeolites have rounded corners which is a requirement for detergent grade zeolite. Particle size distribution analysis also confirmed that the average particle size of commercial zeolite was 3.4 μm, while synthesized zeolites have an average particle size of 5.6 μm. According to the XRD patterns of both zeolites, synthesized zeolites showed higher crystallinity, which may be due to larger particle-sized crystals. Water sorption analysis confirmed that synthesized zeolite has 21.1 wt. % in its pores, commercial zeolite has 22.1 wt.%; this might affect the bigger particle-sized zeolites, which decrease the adsorption and desorption characteristics [186,187]. The synthesized zeolites from high-quality kaolin were very promising alternatives compared to the commercially available ones due to their low raw material cost. The particle size and truncated/sharp-cornered geometry of the synthesized zeolite 4A can be altered with further modifications depending on their final use of application.

4.4 Optimization of Synthesis Parameters for Zeolite 13X with High-Quality Kaolin

Synthesis parameters were also optimized in order to obtain Zeolite 13X, which finds use in different industrial applications. Gel formulations, aging, and reaction conditions were optimized by changing one parameter at a time. Synthesis routes and optimized parameters are given in Figure 4.19.
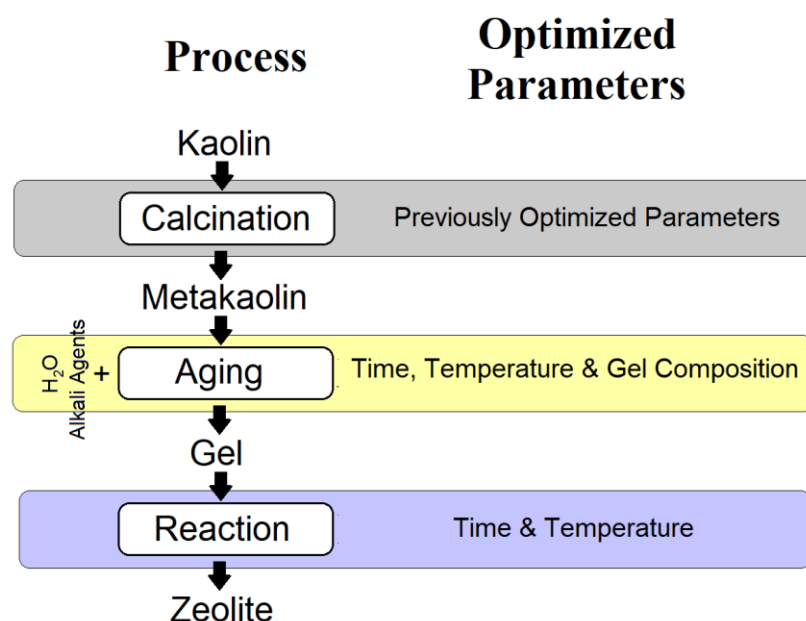
Figure 4.21. Schematic representation of the process flow and the optimized parameters for zeolite 13X synthesis from kaolin

Calcination parameters were previously optimized in Section 4.1. For the controlled experimental setup design, each parameter was controllably changed one at a time while keeping the others identical. The first four parameters were optimized for single gel formula, which is 5 SiO_2: 1 Al_2O_3: 7.5 Na_2O: 337.5 H_2O and these parameters were used to optimize the gel formula of the starting mixture [5].

4.4.1 Aging Conditions

The aging step was the second controlled parameter during the process, carried out after the metakaolinization. It was reported that the aging conditions could define the selection between two competing phases, such as LTA and FAU [102]. The metakaolinization step was performed using the previously optimized parameters of 850°C for 1.5 h. Obtained metakaolins were mixed with the calculated amount of sodium hydroxide, sodium silicate, and distilled water to form a gel with the formula of 5 SiO_2: 1 Al_2O_3: 7.5 Na_2O: 337.5 H_2O. Two different temperatures and three different durations were examined to obtain the optimum aging conditions.

4.4.1.1 Aging Temperature

Aging procedures were investigated using 18 h of duration at 25°C and 60°C. Aged gels were placed afterward in a previously heated oven at 100°C for 18 h for the reaction step. The final products' SEM images and XRD patterns are shown in Figure 4.22 and Figure 4.23, respectively.
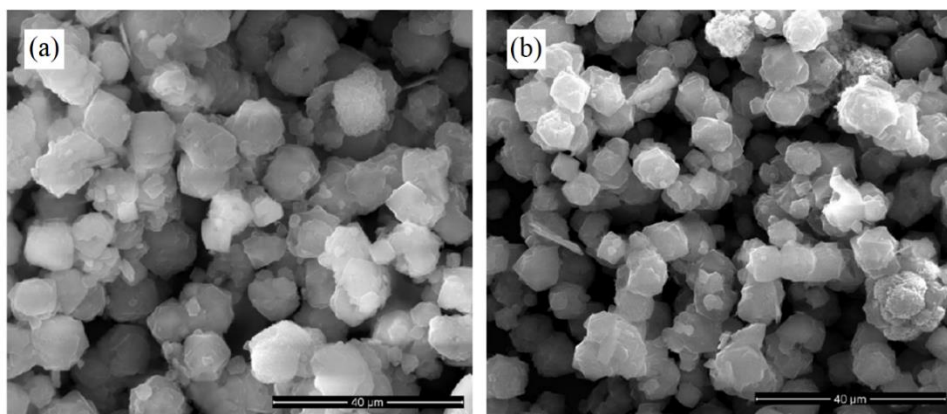
Figure 4.22. SEM images of the zeolite 13X synthesis products from kaolin, aged at 25°C (a) and 60°C (b) for 18 h.
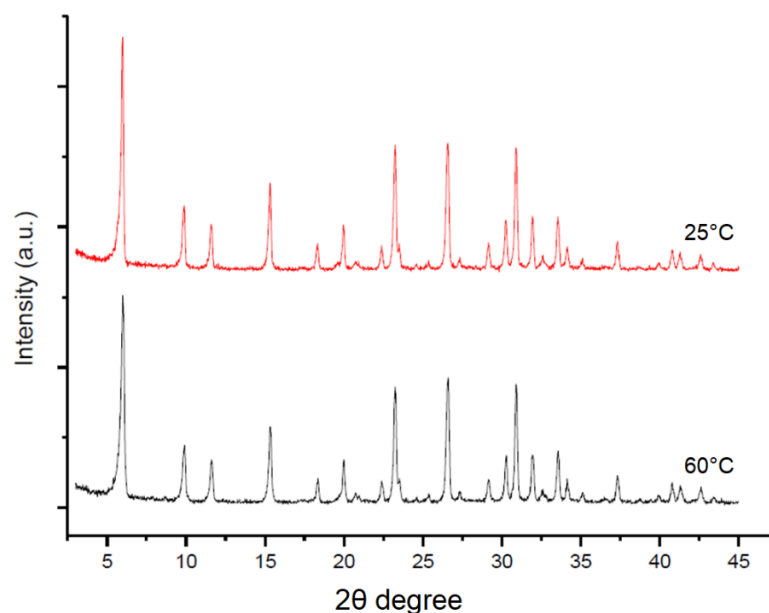
Figure 4.23. XRD patterns of the zeolite 13X synthesis products from kaolin, aged at 25°C and 60°C for 18 h.

Caballero et al. [90] reported that aging temperatures between 25°C and 60°C resulted in zeolite 13X formation, with the highest crystallinity attainable at lower aging temperatures. Various studies suggest different aging temperatures in the range of 20 - 40°C [154] and room temperature [188].

Table 4.7 Relative crystallinity of zeolite 13X synthesis products from kaolin with different aging temperatures

Aging Temperature (°C)	Relative Crystallinity (%)
25	100
60	94

In the current study, more agglomeration was observed among zeolites synthesized using gels aged at 60°C with more significant unreacted chemicals on top of the zeolite crystals (Figure 4.22). These smaller and newly formed crystal formations might be due to the higher number of nuclei growth at an elevated aging temperature

[189,190]. Also, XRD patterns showed that while both products were pure zeolite 13X, the product obtained using the gel aged at 25°C had higher crystallinity (Table 4.7). Smaller zeolite dimensions lead to a drop in the intensity of the diffraction lines because of the presence of a smaller number of network planes [191] and lower unreacted chemicals observed in the final product.

4.4.1.2   Aging Time

For the optimization of aging time, obtained metakaolins were aged at 25°C for different duration of times, which were chosen to be 16 h, 18 h, and 20 h. Metakaolins were mixed with the calculated amount of sodium hydroxide, sodium silicate, and distilled water to form a gel with $5\ SiO_2$: $1\ Al_2O_3$: $7.5\ Na_2O$: $337.5\ H_2O$ formula. The resulting gels were placed in an HDPE bottle and aged at 25°C with continuous stirring for the times stated above. Aged gels were placed in a preheated oven at 100°C for 8 h for the reaction step. The final products' SEM images and XRD patterns are shown in Figure 4.24 and Figure 4.25, respectively.
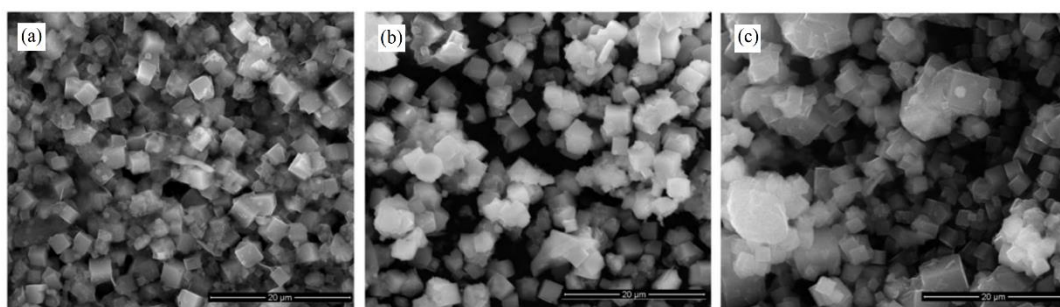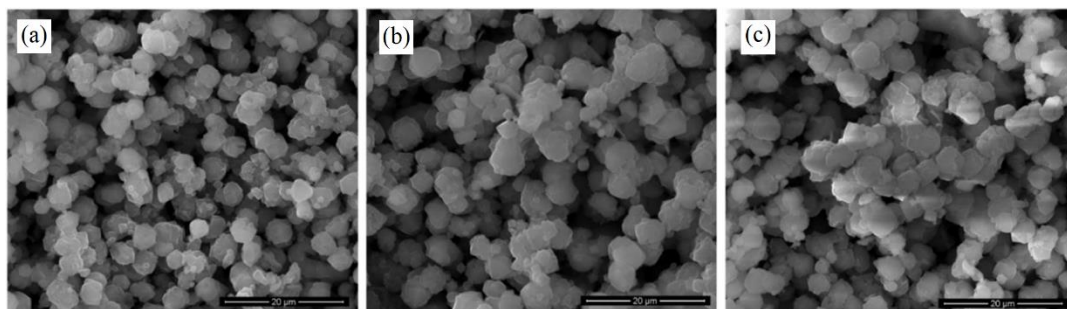

Figure 4.24. SEM images of the zeolite 13X synthesis products from kaolin, aged at 25°C for 16 h (a), 18 h (b), and 20 h (c).
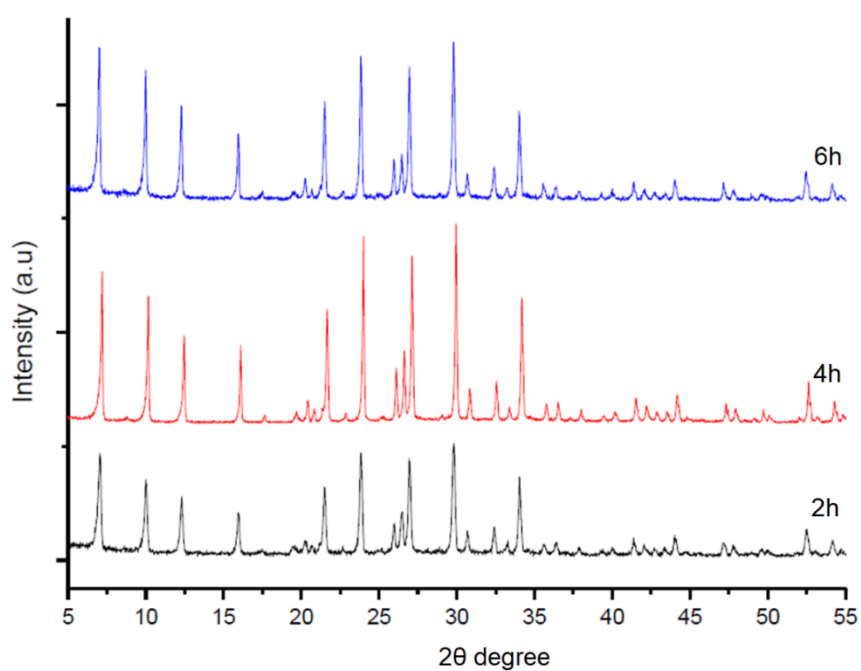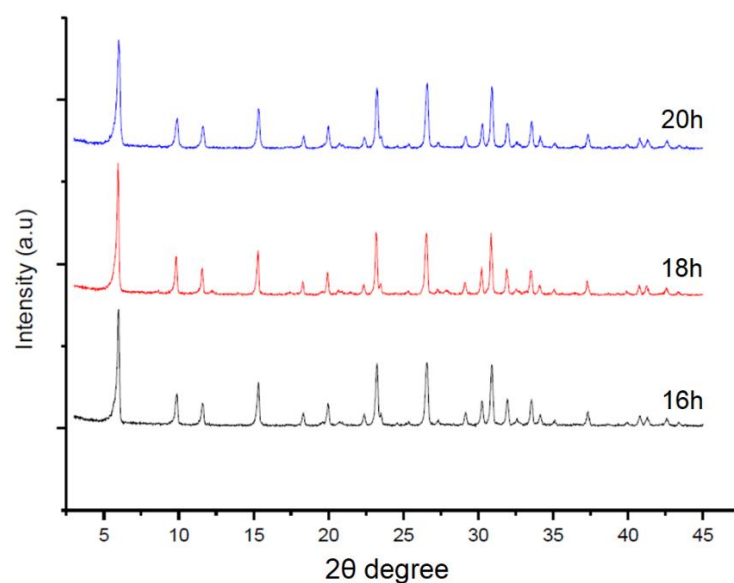
Figure 4.25. XRD patterns of the zeolite 13X synthesis products from kaolin, aged at 25°C for 16 h, 18 h, and 20 h.

Table 4.8 Relative crystallinity of zeolite 13X synthesis products from kaolin with different aging times

Aging Time (h)	16	18	20
Relative Crystallinity (%)	91	100	92

According to the SEM images shown in Figure 4.24, no significant difference was observed in the morphologies among the investigated durations. However, XRD patterns showed that most crystalline products were obtained using an aging time of 18 h (Table 4.8). Accordingly, aging at 25°C for 18 h was selected for conducting the rest of this study. These optimization studies were performed with various raw material types; each source varies to synthesize the same zeolite [90,94,154].

4.4.2   Reaction Conditions

Optimization of reaction conditions was the last step to investigate the zeolite synthesis process of zeolite 13X. For this part of the study, previously optimized meta kaolinization and aging conditions were used for zeolite 13X synthesis. Zeolite synthesis was conducted using two different reaction temperatures and three different duration times of reaction.

4.4.2.1   Reaction Temperature

Previously optimized parameters were used for calcination and aging steps; resulting gels were placed at preheated ovens at 80, and 100°C for 8 h. SEM images and XRD patterns of the final products were given in Figure 4.26 and Figure 4.27, respectively. Also, the relative crystallinity of zeolite 13X was calculated from the XRD patterns and shown in Table 4.9.
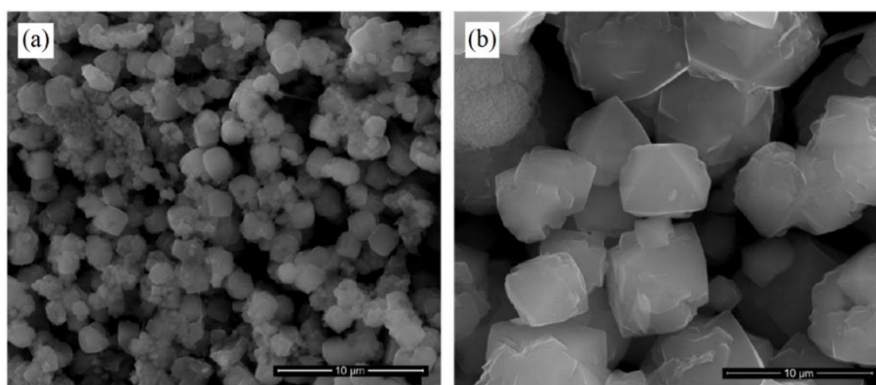
Figure 4.26. SEM images of the zeolite 13X synthesis products from kaolin, with 80°C (a) and 100°C (b) reaction temperatures.
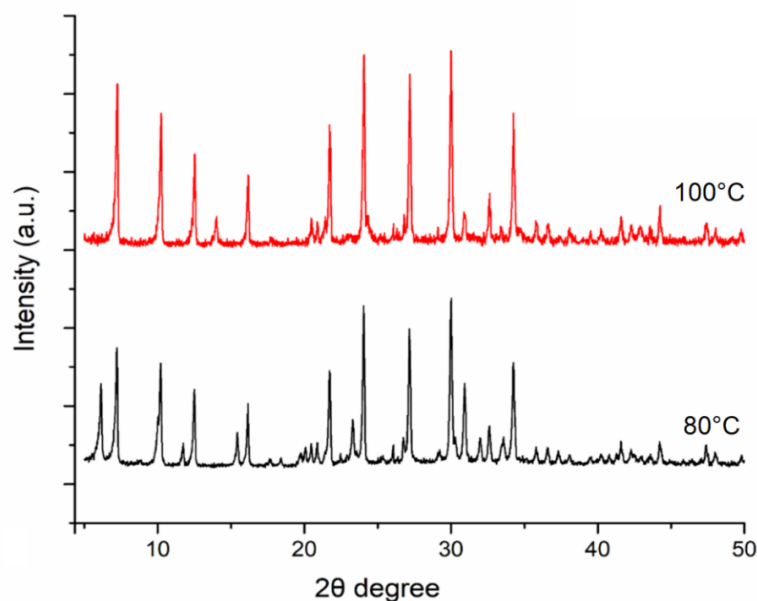
Figure 4.27. XRD patterns of zeolite 13X synthesis products from kaolin, with reaction temperatures of 80°C and 100°C.

Table 4.9 Relative crystallinity of zeolite 13X synthesis products from kaolin with different reaction temperatures

Reaction Temperature (°C)	80	100
Relative Crystallinity (%)	77	100

The SEM images shown in Figure 4.26 suggested the formation of smaller-sized zeolite crystals at 80°C with a more developed zeolite 13X morphology at 100°C. The XRD patterns shown in Figure 4.27, in addition to % crystallinity results summarized in Table 4.10, also suggest a more well-defined crystal formation of zeolite 4A at 100°C. XRD patterns of these products confirmed the formation of zeolite 4A with no other impurities at a reaction temperature of 100°C, while a mixture of zeolite 13X and zeolite 4A was observed at 80°C. Also, the crystallinity of the zeolite 13X phase was relatively lower at 80°C with respect to a reaction temperature of 100°C (Figure 4.27). De Lucas et al. also reported that lower temperatures in various gels resulted in a mixture of zeolite 4A and zeolite 13X

[169]. Similar observations were made in the literature data suggesting higher reaction temperatures result in well-developed zeolite 13X with less secondary phase formation [5,201,204].

4.4.2.2   Reaction Time

In order to optimize reaction time, metakaolinization was performed at 850°C for 1.5 h. The resulting metakaolins were mixed with the calculated amount of sodium hydroxide, sodium silicate, and distilled water to form a gel with the formula of 5 SiO_2: 1 Al_2O_3: 7.5 Na_2O: 337.5 H_2O. The resulting gels were placed in an HDPE bottle and aged at 25°C with continuous stirring for 18 h. Aged gels were placed in a previously heated oven at 100°C for 6 h, 8 h, and 10 h to optimize the reaction time. The final products' SEM images and XRD patterns are shown in Figure 4.28 and Figure 4.29, respectively.
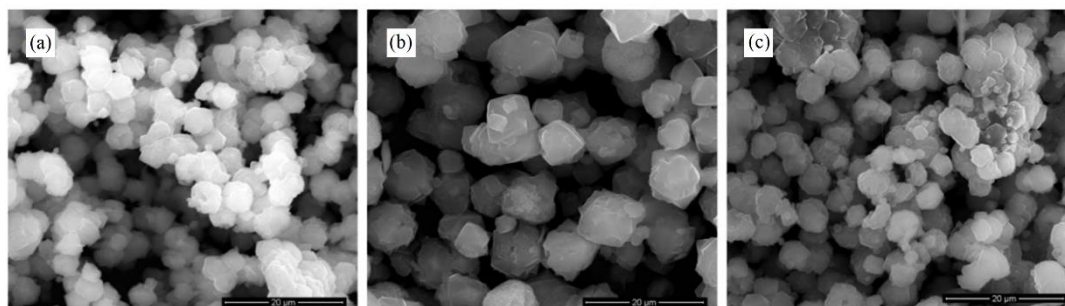
Figure 4.28. SEM images of the zeolite 13X synthesis products from kaolin, with reaction durations of 6 h (a), 8 h (b), and 10 h (c).
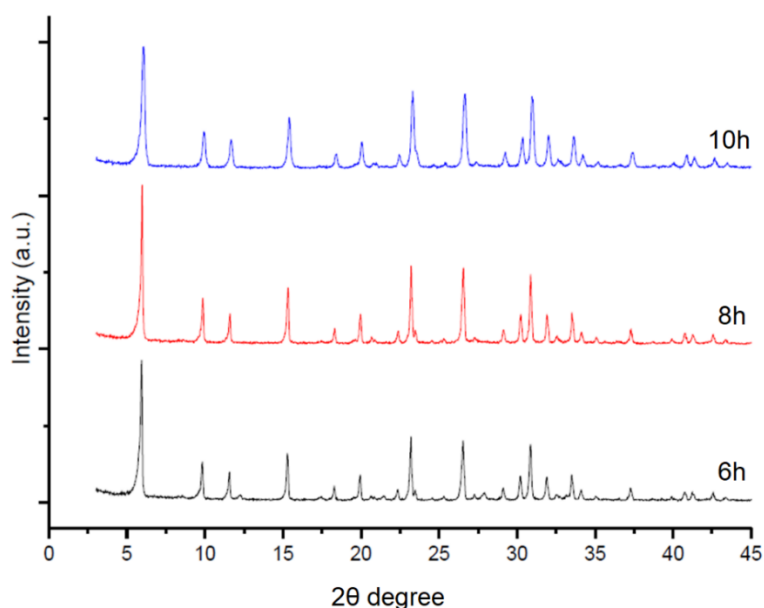
Figure 4.29. XRD patterns of the zeolite 13X synthesis products from kaolin, with reaction durations of 6 h, 8 h, and 10 h.

According to the SEM images shown in Figure 4.28, crystals grew to be larger with an increase in reaction time to 8 h, after which smaller crystals were observed upon a further increase in reaction time. Additionally, the highest % crystallinity was observed at 8 h of reaction time, as also summarized in Table 4.10.

Table 4.10 Relative crystallinity of zeolite 13X synthesis products from kaolin with different reaction times

Reaction Time (h)	6	8	10
Relative Crystallinity (%)	89	100	86

According to these results, 8 h of reaction resulted in well-developed faujasite morphology with the highest crystallinity. Therefore, further studies were conducted using 8 h of reaction time.

4.4.3   Gel Formulation

Four different gel formulations were prepared using readily available metakaolin calcined at 850°C for 1.5 h, sodium hydroxide, sodium silicate, and distilled water to test different gels with the optimized parameters. The molar gel formulations are listed in Table 4.11.

Table 4.11 Gel formulations of the synthesized zeolite 13X from kaolin

Formula Code	SiO_2 (moles)	Al_2O_3 (moles)	Na_2O (moles)	H_2O (moles)
Gel 1	5	1	7.5	337.5
Gel 2	4	1	8.5	325
Gel 3	3	1	7.8	240
Gel 4	2.7	1	7.2	210

The resulting gels were placed in an HDPE bottle and aged at 25°C with continuous stirring for 18 h. Aged gels were placed in a previously heated oven at 100°C for 8 h of the reaction time. The resulting solid particles were separated from the mother liqueur and washed by distilled water at least three times by centrifugation at 7500 rpm for 5 minutes and dried in a conventional oven at 70°C overnight. The final products' SEM images and XRD patterns are shown in Figure 4.30 and Figure 4.31, respectively.
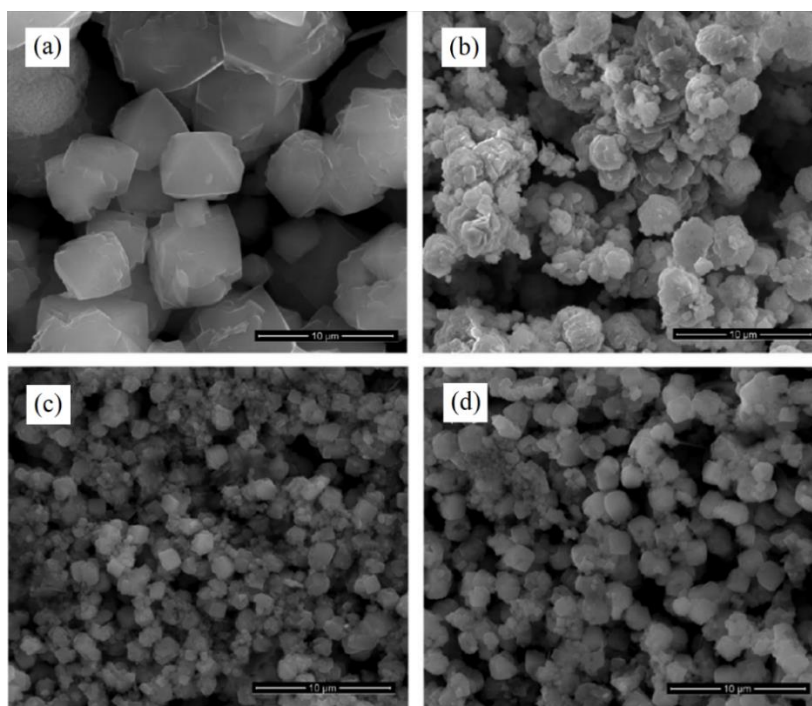
Figure 4.30. SEM images of the zeolite 13X synthesis products from kaolin with 4 different gel formulations; Gel 1 (a), Gel 2 (b), Gel 3 (c), and Gel 4 (d).
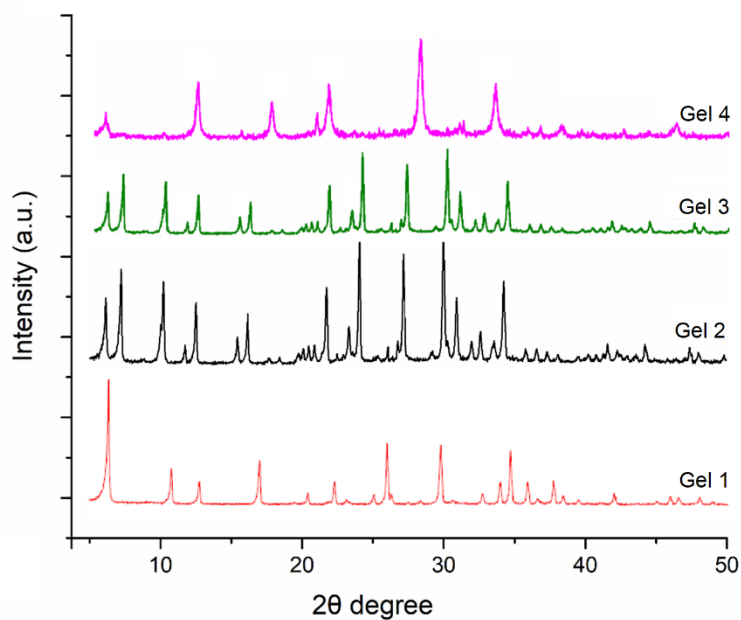
Figure 4.31. XRD patterns of the zeolite 13X synthesis products from kaolin with different gel formulations.

According to the SEM images of the final products, a higher Si/Al ratio in the gel results in larger crystals with lower agglomerations. Also, the shape of each crystal has the well-known structure of the zeolite 13X. XRD analysis confirmed that Gel 1 results in the only pure zeolite 13X form, while a decrease in the Si/Al ratio of the gel results in a mixture of zeolite 4A and zeolite 13X. Gel 4 resulted in the formation of zeolite P, which is the main impurity phase observed during zeolite formation with low silica zeolites, such as zeolite 4A and zeolite 13X. Furthermore, an amorphous gel-like structure was observed in the SEM images of zeolites synthesized from gels 2, 3, and 4. These results agree with the literature data stating that zeolite 13X and zeolite 4A are competing phases in the ternary phase diagram [67,77,188]. Lowering the Si/Al ratio was reported to cause a shift in the region towards the formation of zeolite 4A on the ternary phase diagram. Additionally, Zhou et al. reported that increased alkalinity resulted in zeolite P formation [188].

4.5 Comparison of Synthesized Zeolite 13X with Commercial Zeolite 13X

Synthesis of zeolite 13X, from now on named as Zeolite 13X-HQK (High-Quality Kaolin), was performed with the gel prepared from metakaolins calcined at 850°C for 1.5 h, sodium silicate, and distilled water, with a formula of $5 \, SiO_2: 1 \, Al_2O_3: 7.5 \, Na_2O: 337.5 \, H_2O$. The resulting gels were placed in an HDPE bottle and aged at 25°C with continuous stirring for 18 h. Aged gels were placed in a previously heated oven at 100°C for 8 h of the reaction step. The resulting solid particles were separated from the mother liqueur and washed with distilled water at least three times by centrifugation at 7500 rpm for 5 minutes and dried in a conventional oven at 70°C overnight. SEM images and XRD patterns of the synthesized zeolite 13X and commercial zeolite 13X were given in Figure 4.32 and Figure 4.33.
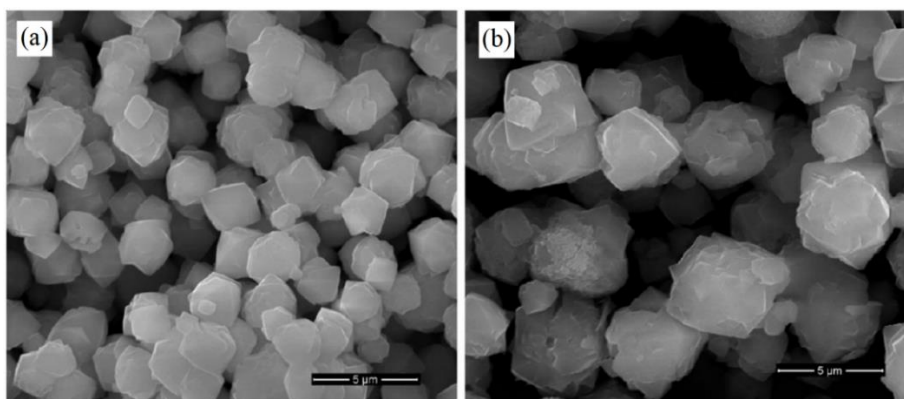
Figure 4.32. SEM images of the commercial zeolite 13X (a) and Zeolite 13X-HQK (b).
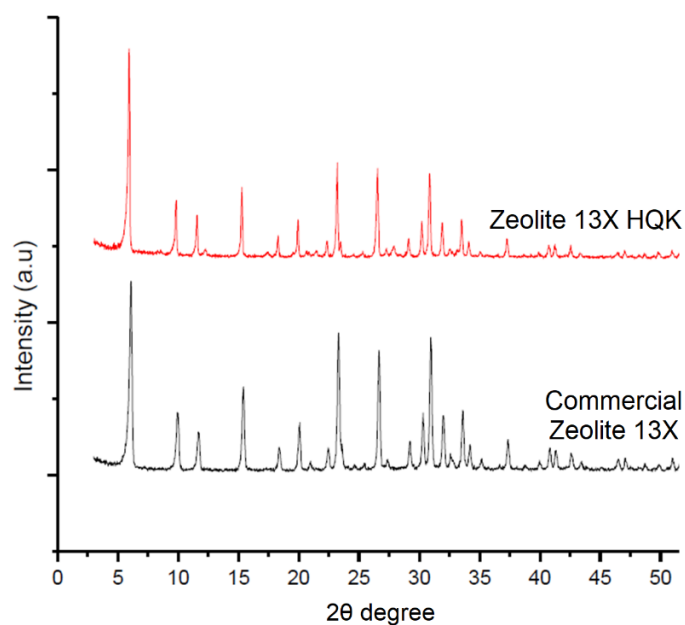
Figure 4.33. XRD patterns of the commercial zeolite 13X and Zeolite 13X-HQK

According to the SEM images of the zeolites, both have the unique structure of zeolite 13X, while commercial zeolite crystals were smaller with respect to the synthesized ones. Also, particle size distribution analysis showed that the average particle size of commercial zeolites was 3.2 µm while synthesized ones were 4.6 µm. XRD patterns showed that both products were pure zeolite 13X with very similar crystallinities.

4.6 Optimization of Activation Parameters for Zeolite 4A with Low-Quality Kaolin

Since kaolin minerals are abundant worldwide, they are highly preferred as low-cost raw materials. However, developed processes using kaolin as source material after thermal activation and synthesis steps are still being investigated due to disagreements on the conditions required to produce metakaolin. Depending on the origin of the raw material, these conflicts can be related to the activation temperature [21,82], impurity and particularly iron content [86,192], Si/Al ratio [19,89,193], quartz content [114,117], and initial crystallinity of raw material [19,194]. In order to resolve these concerns and reduce the cost of the synthesis, the alkali fusion route was developed [82,100]. The chemical content of the starting kaolin samples used in this study is shown in Table 4.12.

Table 4.12 Chemical composition and quartz content (wt%) of raw kaolin samples.

Kaolin Code	Content (wt.%)					
	SiO_2	Al_2O_3	TiO_2	Fe_2O_3	Quartz[α]	Si/Al
K1	51.80	46.20	0.70	0.33	2.1	0.95
K2	52.40	44.90	0.81	0.34	2.4	0.99
K3	52.20	44.10	1.10	0.29	4.6	1.05
K4	62.80	33.50	0.56	1.32	15.3	1.59
K5	61.20	35.90	0.51	0.48	26.2	1.44
K6	61.00	36.40	0,.9	0.30	33.6	1.42

α: Calculated with XRD RIR method

Alkali fusion involves the formation of a fused product by the thermal activation of dry-mixed raw kaolin and sodium hydroxide pellets at temperatures 600°C or above. This method enhances the dissolution of silica and alumina layers more effectively, leading to the dissolution of other mineral phases, such as quartz. Also, this method offers a solution to the need for the purification of kaolin with a cost-effective approach in terms of time and energy [20]. However, the type of zeolite produced at the end of fusion followed by hydrothermal synthesis varies in a wide range,

resulting in different products with differing qualities. This variety of products depends on the origin of the raw material. The initial Si/Al ratio and quartz content as an impurity are still of significant importance. The same kaolin source pre-treated using two different routes of metakaolinization or alkali fusion and then subjected to identical synthesis conditions result in different products. It was shown that the metakaolinization resulted in a mixture of Na-X and Na-P, while alkali fusion resulted in Na-Y after being subjected to hydrothermal synthesis [114]. This is mainly caused by increased alkali conditions during the fusion step, resulting in the dissolution of silica ions from impurities like quartz and leading to a higher Si/Al ratio of the synthesis gel. Thus, the alkali fusion route eliminates the drawback of impurities like quartz [20].

Despite the advantages of using kaolin as raw material and discovering new routes for the metakaolinization step, there are still significant variances in the obtained product type and quality [20,114]. This work aims to eliminate the variances based on the origin of raw kaolin, generating an alternative route for the initial thermal activation step by adding alumina source into the raw materials that will be subjected to activation besides kaolin and the alkali source. Therefore, an alternative methodology was developed during the thermal activation of raw kaolin in addition to the well-known metakaolinization and alkali fusion steps. The new process involves fusing kaolin sources with the proper amount of aluminum hydroxide and sodium hydroxide. This approach not only facilitates the dissolution of insoluble impurities of the initial raw material such as quartz but also makes it possible to arrange the zeolite gel composition. In this work, the one-pot fusion approach was developed to obtain zeolite 4A of good crystallinity from low-quality kaolin using six different kaolin sources with varying characteristics. The one-pot fusion results were compared with those obtained from metakaolinization and alkali fusion approaches, as shown in Figure 4.34. The proposed one-pot activation is a faster, easier, and cheaper process, which eliminates the inconsistent product types of zeolite 4A due to varying kaolin grades.
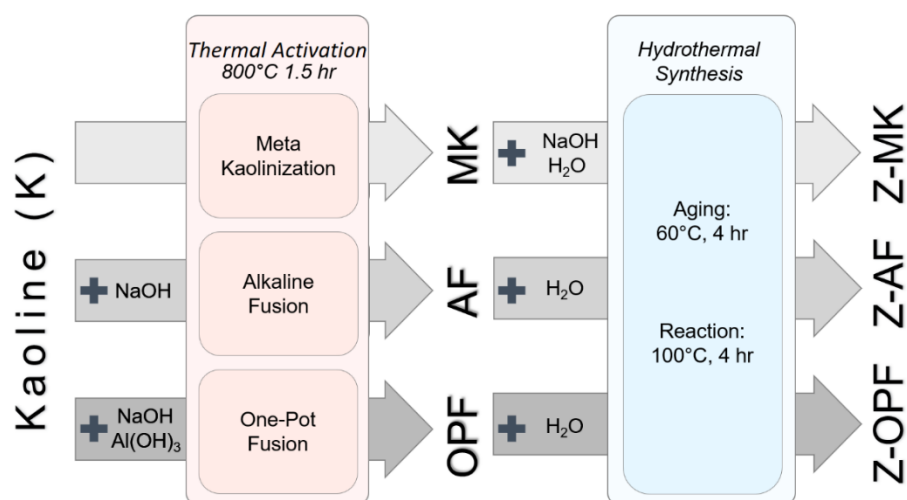
Figure 4.34. Schematic representation of zeolite synthesis methods from kaolin

Characterization results of the synthesis products are shown in Table 4.13.

Table 4.13 Characterization results of zeolite products.

Zeolite Code	Detected Phases	Quartz $(\%)^{\alpha}$	Relative Crystallinity of zeolite 4A (%)	Water Absorbed (wt. %)
Z-MK1	4A	0.3	100	20.3
Z-MK2	4A	3.0	97.9	19.8
Z-MK3	4A	5.1	88.7	19.3
Z-MK4	P, 13X, Quartz	28.4	-	12.4
Z-AF4	P, 13X	2.4	-	12.8
Z-OPF4	4A	3.2	89.8	19.4
Z-MK5	4A, Quartz	26.6	90.7	17.6
Z-AF5	4A, 13X	1.8	87.1	19.6
Z-OPF5	4A	2.4	92.2	19.5
Z-MK6	4A, Quartz	33.7	76.7	17.5
Z-AF6	4A	2.2	89.4	19.5
Z-OPF6	4A	2.3	97.3	19.7

α: Calculated with XRD RIR method.

4.6.1   Metakaolinization

The six kaolin sources obtained from different geological regions can be categorized as high (K1, K2, K3) and low quality (K4, K5, K6) kaolin materials of different characteristics based on their quartz content as impurity level. The XRD patterns of all raw kaolin samples are shown in Figure 4.35, while calcined kaolins are shown in Figure 4.36.
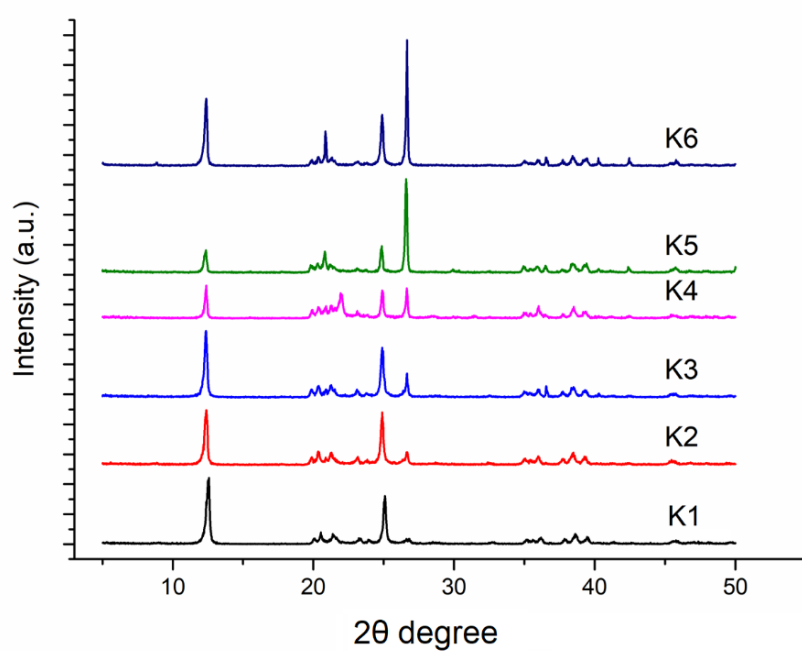
Figure 4.35. XRD patterns of the (K) raw kaolins.
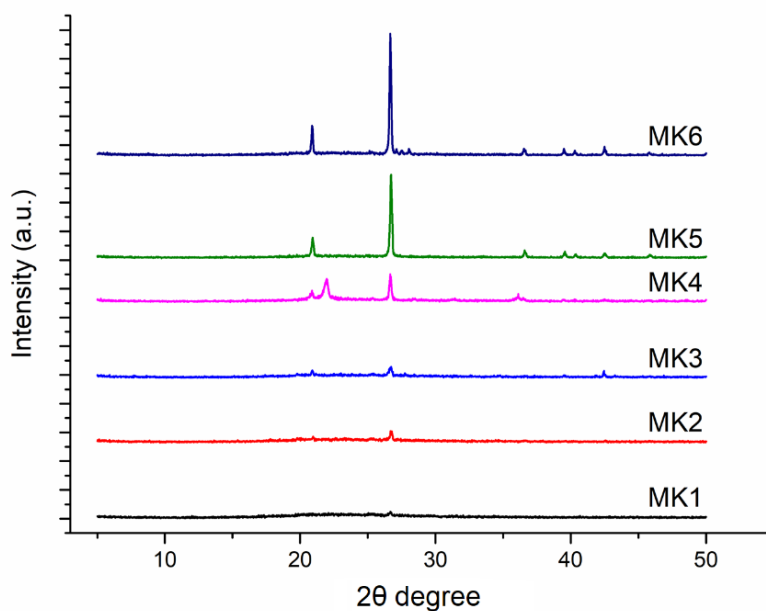
Figure 4.36. XRD patterns of the (MK) metakaolin samples.

The diffraction peaks at 2Θ =12.44, 24.86, and 35-40° indicated the typical characteristic features of kaolin samples. Those at 20.87° and 36.60° correspond to quartz phases. According to Figure 4.35, the raw kaolin samples of K4, K5, and K6 have the highest amount of quartz phase in correlation with the XRF results presented in Table 4.12, which were found to be around 15.3, 26.2, and 33.6, respectively. According to Table 4.12, the raw kaolin sample K4 has the highest SiO_2 and the lowest Al_2O_3 content leading to the highest Si/Al ratio among all other raw kaolin samples. This typically makes K4 unsuitable as a raw kaolin source for zeolite 4A synthesis. After calcination, it can be seen from Figure 4.36 that the structure of kaolin is transformed into amorphous metakaolin, where major kaolin peaks disappeared. It was seen that the samples of MK1, MK2, and MK3 obtained by metakaolinization of high-quality kaolin samples were completely amorphous, which is required for the preparation of zeolite 4A. On the other hand, upon the metakaolinization of low-quality kaolin samples, the quartz peaks observed in the XRD patterns of MK4, MK5, and MK6 samples prolonged to remain, indicating that this phase could not be eliminated. In addition to quartz impurity, the peak at 2Θ equal to 21.12 and 36.48° represent the diffractions of (110) and (111) planes of

α-FeOOH [195,196] in K4 and MK4 samples, which are consistent with the XRF data of the sample K4 showing the highest iron content among all six samples.

The XRD patterns of the products synthesized from kaolin of different sources using the metakaolinization (MK) method (Figure 4.36) are shown in Figure 4.37.
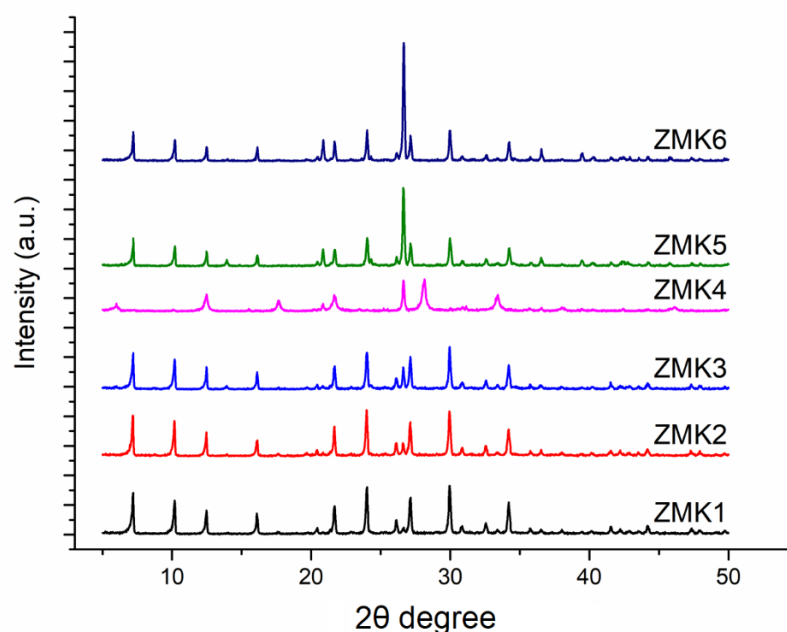
Figure 4.37. XRD patterns of the synthesis products of various kaolin sources activated by the metakaolinization (MK) method.

The products obtained using MK1 and MK2 gave the highest quality zeolite 4A products (Z-MK1 and Z-MK2) with over 95% crystallinity. The product obtained from MK3 resulted in a slightly lower crystallinity of around 89%. It was still possible to observe the quartz peaks of $2\Theta = 26.6°$, which were quantified to be in a range of 3-5% by weight (Table 4.13) in Z-MK2 and Z-MK3. The results obtained upon zeolite 4A products of Z-MK1, Z-MK2, and Z-MK3 suggest that high-quality raw materials with low quartz content resulted in highly crystalline and low impurity products fabricated with the use of the metakaolinization method. Additionally, the results indicated that increasing the amount of quartz from approximately 2.1 to 4.6 in the raw kaolin sample resulted in a decrease in the relative crystallinity of zeolite 4A from 100% for Z-MK1 to ~ 89% for Z-MK3. These results are in good agreement

with the literature suggesting that quartz content can affect the kinetics of zeolite formation [114] and the final crystallinity of the zeolite obtained using the MK method [20,100]. The current study using different high-quality kaolin sources (i.e., K1, K2, and K3) clearly shows that quartz impurity in raw kaolin directly influences the final product crystallinity. The kaolin source with the lowest quartz but the highest iron content (i.e., K1) leads to the best product, which also suggested that iron content did not influence the product significantly. It can be inferred that using high quality raw kaolin with quartz content lower than 5% results in zeolite 4A with acceptable crystallinity requirements for all kaolin sources of K1, K2, and K3 [20,21]. Thus, the application of MK method to high quality kaolin for metakaolinization generating MK1, MK2, and MK3 for hydrothermal synthesis was found to be sufficient to obtain high quality zeolite 4A products.

The hydrothermal synthesis applied using the MK method to low-quality kaolin materials (MK4, MK5, and MK6) showed a variety of products. The XRD profile of zeolite products (Z-MK5 and Z-MK6) obtained using MK5 and MK6 fits well with zeolite 4A, although the peak of quartz was more intense in these samples. The zeolite 4A crystallinities obtained for Z-MK5 and Z-MK6 were around 60%, below the requirements of detergent grade specifications [20,21]. Furthermore, Z-MK5 and Z-MK6 showed poor water sorption properties of around 17.5% due to the impurities in the synthesized products. The sample obtained using MK4 differed from zeolite 4A (i.e., Z-MK4) with the main phase of zeolite P, which is another zeolite type from the Gismondine (GIS) family with varying Si/Al ratios of 1 to 4 [78]. The water sorption properties of Z-MK4 were also very poor in correlation with the observed poor crystallinity of this product. Accordingly, the obtained results suggest that MK methodology was insufficient to obtain high-quality zeolite 4A products using low-quality kaolin samples with high quartz content. The results obtained from metakaolinization studies using different sources of kaolin are in good agreement with the studies, stating the origin of raw material and mineralogical composition as one of the critical factors determining the final product quality [21,78,197].

4.6.2 Alkali Fusion

Another approach was adopted by Ayele et al., who applied a purification method to the raw kaolin with the purpose of attaining a reduction in quartz content [20]. As an alternative to purification, the alkali fusion method was applied on raw kaolin samples resulting in better crystallinity of zeolites synthesized using alkali fused kaolin samples [20]. However, the alkali fusion methodology was shown to provide the direct synthesis of zeolite 13X in another study without any extra Si source addition or dealumination [107]. In our study, the alkali fusion (AF) was investigated using low-quality kaolin (K4, K5, and K6). Our aim was their further utilization in the hydrothermal synthesis of zeolite 4A to decrease quartz impurity level and increase the quality of the final product with respect to the MK method. The XRD patterns of alkali fused kaolin sources (AF4, AF5, and AF6) and the products obtained using them (Z-AF4, Z-AF5, and Z-AF6) are shown in Figure 4.38.
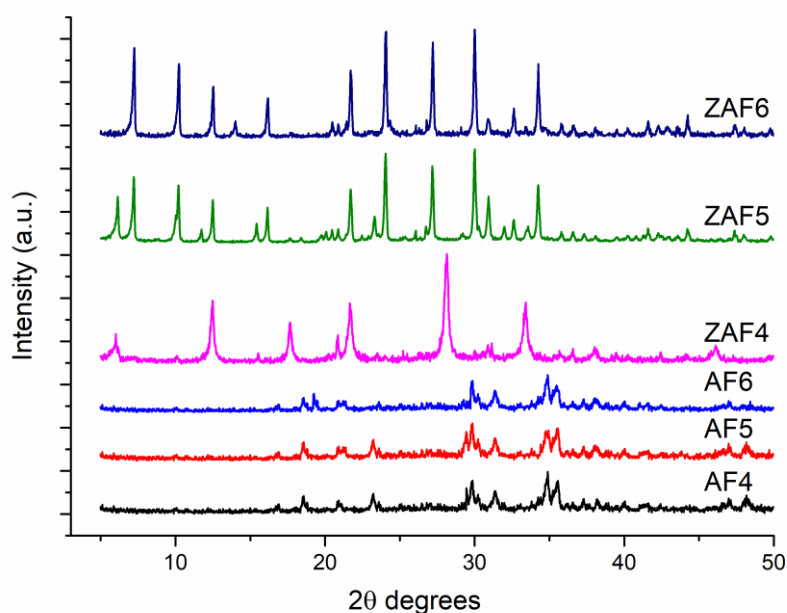
Figure 4.38. XRD patterns of alkali fused kaolin (AF) and zeolites synthesized from the alkali fusion method (Z-AF).

Accordingly, the alkali fusion (AF) process clearly resulted in the disappearance of all quartz peaks in samples AF4, AF5, and AF6 that were observed upon metakaolinization (samples MK4, MK5, and MK6 in Figure 4.36).

According to Figure 4.34, the hydrothermal synthesis products upon using AF4, AF5, and AF6 as raw materials lead to zeolite 4A as the main phase of Z-AF5 and Z-AF6 with the exception of Z-AF4. In the XRD patterns of the synthesized products obtained after the AF method, mainly zeolite P formation with minor zeolite 13X peaks was observed in Z-AF4. On the other hand, Z-AF5 product was mainly composed of zeolite 4A with a secondary phase of zeolite 13X, while Z-AF6 was a single-phase zeolite 4A. These results indicate the conversion of quartz into soluble sodium silicates in alkali fusion [100,115].

It seems to be peculiar that only AF4 resulted in an almost totally different zeolite phase with a 15% quartz content of K4. On the other hand, the products of AF5 and AF6 turned out to be mostly zeolite 4A, while K5 and K6 exhibit a higher amount of quartz with respect to K4. The zeolite P formation was explained on the basis of higher silica content in the gel with respect to the amount necessary to obtain zeolite 4A [113,115]. This result suggests that not only quartz but also the initial Si/Al ratio of kaolin affected the type of zeolite formed in the present work. It seems that the alkali fusion process was not successful in converting low-quality kaolin with the highest Si/Al ratio to zeolite 4A (i.e., Z-AF4). It is known from the literature that, to synthesize high silica zeolites from kaolin, there is the need for an additional source of silica during the hydrothermal step, which can also be used to vary the Si/Al ratio of the reaction mixture [113,114]. Thus, the correct manipulation of the Si/Al ratio of the mixture used for hydrothermal synthesis can also be significant in determining the precise zeolite phase to be obtained as the final product. This manipulation can be of particular interest if the resource belongs to low-quality kaolin characteristics with a higher Si/Al ratio and quartz crystallinity of more than 15%. The Si/Al ratio variation in raw kaolin is reported to be the reason for forming more siliceous

zeolites of different types depending on the heat treatment methodology (i.e., metakaolinization or alkali fusion) [20,82].

4.6.3   One-Pot Fusion

An alternative approach to produce low silica zeolites, i.e., zeolite 4A, using low-quality kaolin with no further purification would require an additional source of alumina. This would possibly eliminate the variations in the quality and type of zeolites occurring due to a wide range of changing kaolin characteristics in different geological regions. For that purpose, a new methodology of one-pot fusion (OPF) was developed, where in addition to kaolin and alkali sources, aluminum hydroxide was also added into the thermal activation process. The effect of OPF was systematically studied by subjecting K4, K5, and K6 into this process and comparing the outcome obtained via MK and AF methods with the aim of producing pure zeolite 4A with the crystallinity of at least 90%.

In Figure 4.39, Figure 4.40, and Figure 4.41, the XRD patterns are shown for all zeolite products obtained following metakaolinization (MK), alkali fusion (AF), and one-pot fusion (OPF) approaches applied on raw kaolin samples.
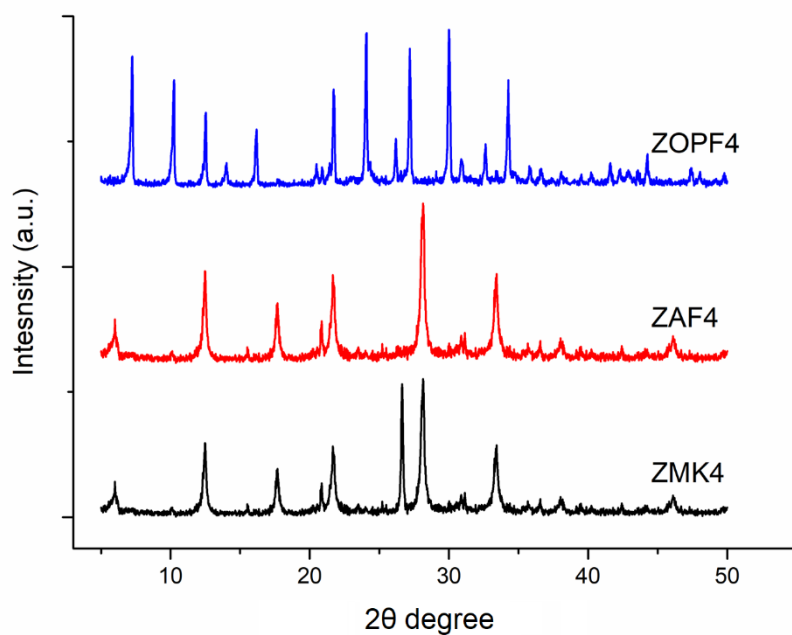
Figure 4.39. XRD patterns of the zeolite products synthesized from K4 using metakaolinization (MK), alkali fusion (AF), and one-pot fusion (OPF) methods.
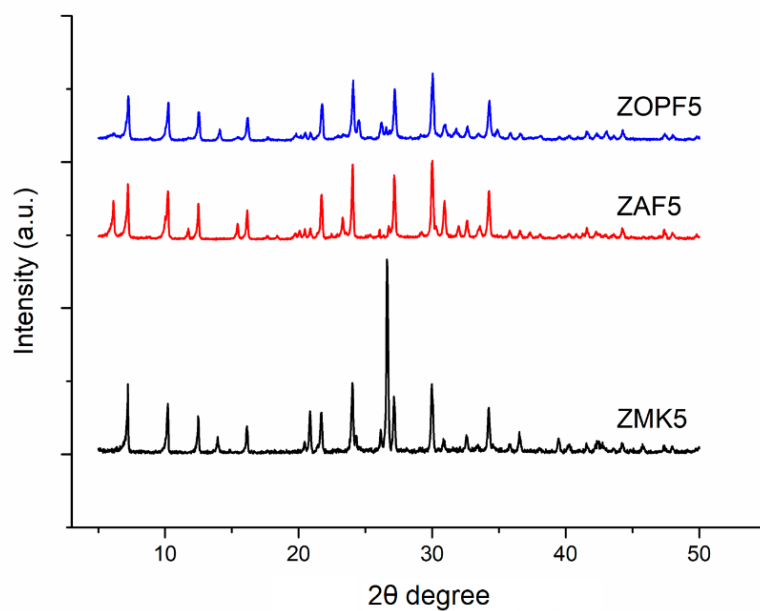
Figure 4.40. XRD patterns of the zeolite products synthesized from K5 using metakaolinization (MK), alkali fusion (AF), and one-pot fusion (OPF) methods.
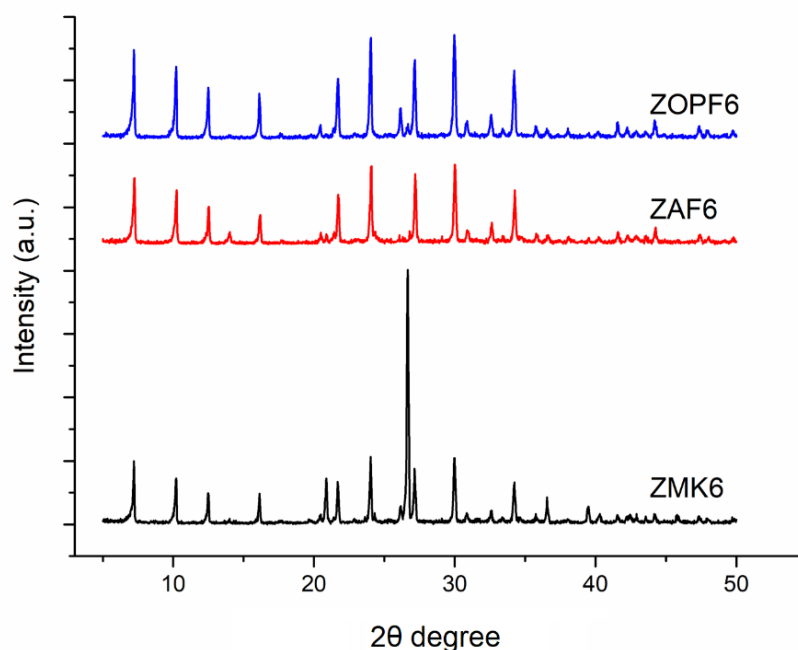
Figure 4.41. XRD patterns of the zeolite products synthesized from K6 using metakaolinization (MK), alkali fusion (AF), and one-pot fusion (OPF) methods.

As shown in Figure 4.39, Figure 4.40, and Figure 4.41, the OPF approach resulted in at least 90% crystallinity of zeolite 4A with respect to MK and AF methods in all low-quality kaolin samples. The zeolite products of P and 13X formed upon MK and AF methods using K4 turned out to be zeolite 4A of ~90% crystallinity upon the OPF method. It seems that eliminating quartz content by the AF method in order to produce zeolite 4A was not sufficient for this particular type of raw kaolin sample K4. However, the OPF approach resulted in the complete conversion of K4 to zeolite 4A (Z-OPF4), and it suggests that the Si/Al ratio of the initially heat-treated material is of significant importance. For the other low-quality kaolin sources of K5 and K6, the OPF methodology resulted in an increase of zeolite 4A crystallinity to higher than 90% (Figure 4.40 and Figure 4.41). According to the results shown in Figure 4.40, the extra zeolite 13X phase obtained using K5 after alkali fusion (Z-AF5) diminished, and the whole material was converted to pure zeolite 4A using the OPF method. Furthermore, Z-OPF6 was found to exhibit the highest crystallinity of 97% among all of the zeolites obtained using low-quality kaolin (Figure 4.41).

93

It is known that properties, like water sorption capacity and cation exchange capacity, are directly related to the crystallinity of zeolite 4A [82]. The synthetic products obtained upon the OPF method exhibited the highest amount of adsorbed water, especially for the sample Z-OPF4 (Table 4.13). In general, the highest values were obtained for Z-MK1 and Z-OPF6, which are the products of high and low-quality kaolin samples, respectively. Thus, the results indicated that higher crystallinity corresponds to higher water adsorption, which agrees with the literature.

The morphologies of all zeolites obtained using low-quality kaolin by MK, AF, and OPF methods are compared in Figure 4.42.
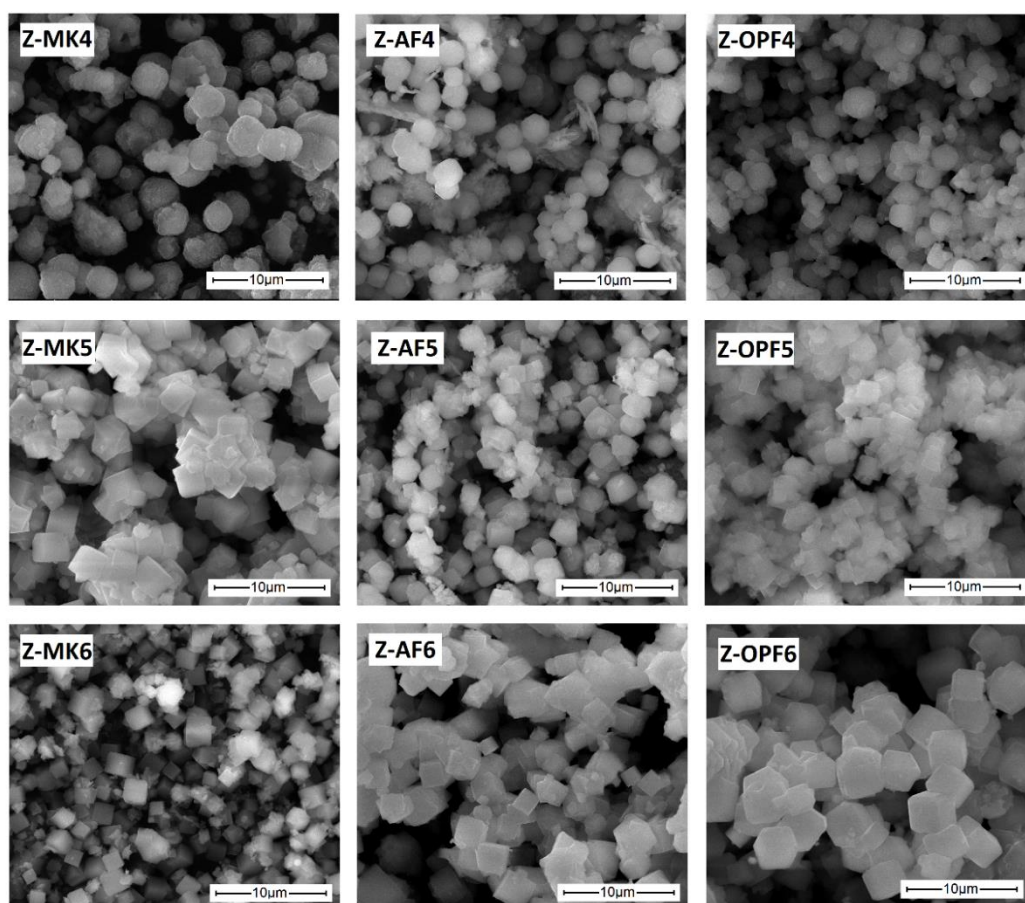
Figure 4.42. SEM images of the zeolite products synthesized from K4, K5, and K6 using metakaolinization (MK), alkali fusion (AF), and one-pot fusion (OPF) methods.

The scanning electron images show that the morphology of MK-4 and AF-4 were predominantly of spherical forms with some indication of unreacted kaolin flakes. The optimum cubic-shaped crystals were formed in the sample Z-OPF4 with rounded edges. The typical cubic morphology of zeolite 4A was more pronounced in the products obtained using K5 and K6. Z-OPF6 exhibited a larger particle size with rounded corners. Commonly, the presence of faceted microcrystals in the powder sample indicated its high crystallinity. This relation was earlier observed for different oxide crystals from different chemical classes when the crystallization time was long enough [198–200]. Respectively, it could be emphasized that this general trend is also observed for the zeolite samples shown in Figure 4.42. In general, the zeolite crystals tend to appear in agglomerates. These results are in agreement with the literature, which attributed these agglomerates to different stages of zeolite formation with respect to the well-known synthetic route [115]. The observed differences in particle size can be due to the differences in the dissolution rate of separate components, resulting in a deviation in the number of nuclei formed during aging [107,113].

4.7   Conclusion

In the first two sections of this study, zeolite 4A and zeolite 13X were successfully synthesized from one high-quality kaolin source with metakaolinization followed by hydrothermal reaction. All metakaolinization, aging, and reaction conditions, and gel formulations were optimized to achieve the most crystalline and impurity-free final product. On the other hand, the metakaolinization method is not the most reliable activation method if there are impurities such as quartz, mullite, etc.[100] which means kaolin is a low-quality one. In that case, the kaolin source should be purified with acid washings [120,201], magnetic separations [202,203], etc., which are undesired due to the increase in the product's final cost. To be able to generate highly pure zeolites out of these low-quality kaolins, Ayele et al. proposed alkali fusion to generate water-soluble silicates from quartz impurity [100].

In the last part of the study, a new methodology of one-pot fusion (OPF) was developed by adding the alumina source in addition to kaolin and alkali sources into the initial thermal activation process of kaolin to be able to generate desired gel in the activation step of the raw material. The effect of OPF proved itself to be useful for obtaining low Si/Al ratio zeolites, i.e., zeolite 4A with at least 90% crystallinity from low-quality kaolin sources containing high quartz and silica content. The zeolite products of P and 13X formed upon metakaolinization (MK) and alkali fusion (AF) methods resulted in zeolite 4A of ~90% crystallinity upon the newly developed OPF method. Eliminating quartz content by the AF method resulted in synthetic zeolite 13X and zeolite P. On the other hand, the OPF approach resulted in the complete conversion of that particular type of low-quality kaolin (K4) to zeolite 4A (Z-OPF4). These results suggest that the OPF method is an innovative way of activating kaolin, which overcomes two significant problems; (i) the quartz content of the raw material (ii) the variations in the Si/Al ratio of the raw kaolin leading to different types of synthetic zeolites.

The second problem was mainly solved by arranging the gel formula using an additional aluminum source, eliminating the need for costly and time-consuming purification of kaolin. Furthermore, the OPF approach resulted in increased crystallinity of zeolite 4A obtained using other low-quality kaolin sources. In summary, it was shown that Zeolite 4A could be synthesized properly through the OPF method from almost any type of kaolin source, getting rid of the precautions necessary to be taken while using low-quality kaolin sources with higher quartz content or Si/Al ratio.

CHAPTER 5

ZEOLITE SYNTHESIS FROM SODIUM FELDSPAR AS STARTING MATERIAL

For decades, lowering the cost of raw material and production for zeolite has been of interest [7]. The primary motivation of these cost-effectiveness studies was to use natural raw materials with similar chemical content with desired zeolites. These raw materials are usually kaolin, halloysite, diatomite, or similar aluminosilicates, which can be easily dehydroxilized, and an amorphous form can be obtained. Even though some of the natural raw materials, such as feldspars, have similar chemical content as zeolites, these materials require high-temperature treatments to break down the structure. During this process, secondary crystallization could occur during the cooling down procedure. The Alkali fusion route was proposed to generate desired aluminosilicates out of these materials [100,150]. Above the melting point of the alkali source, these materials diffuse into the primary raw material and result in the generation of soluble sodium silicates and sodium aluminates. These soluble aluminosilicates can be easily transformed into zeolites with the standard hydrothermal method. This thesis chapter is about optimizing alkali fusion and synthesis conditions for zeolite 4A and zeolite 13X.

5.1   Optimization of Zeolite 4A Synthesis Parameters with Sodium Feldspar and Sodium Hydroxide

Zeolite synthesis from kaolin is a well-known procedure, while sodium feldspar utilization as silica, alumina, and partially sodium source for zeolite synthesis has not been deeply investigated yet. The studies focused on the extraction of silica and alumina out of feldspar [147] or using potassium feldspar for zeolite synthesis [88,204]. In the light of these studies, a procedure was achieved and listed as;

1) Alkali fusion of sodium feldspar with NaOH

2) Sodium hydroxide and sodium aluminate solution preparation in distilled water.

3) Addition of fusion products into an alkali solution.

4) Aging the mixture with continuous agitation in a water bath at the desired temperature and duration.

5) Reaction step of the gel in an oven at the desired temperature and duration.

6) Separation of solid particles from alkali medium with centrifugation, washing with distilled water three times, and drying in an oven.

Several key synthesis parameters were optimized while performing the synthesis procedure in accordance with the earlier stated reaction conditions. Optimized parameters such as aging temperature, reaction temperature, and gel formula in Chapter 4 were used in this part of the study. In this regard, durations were optimized for this particular new source of sodium feldspar since dissolution and nuclei formation rates may vary with a change in the raw material. Parameters studied particularly for this section are given in Figure 5.1.
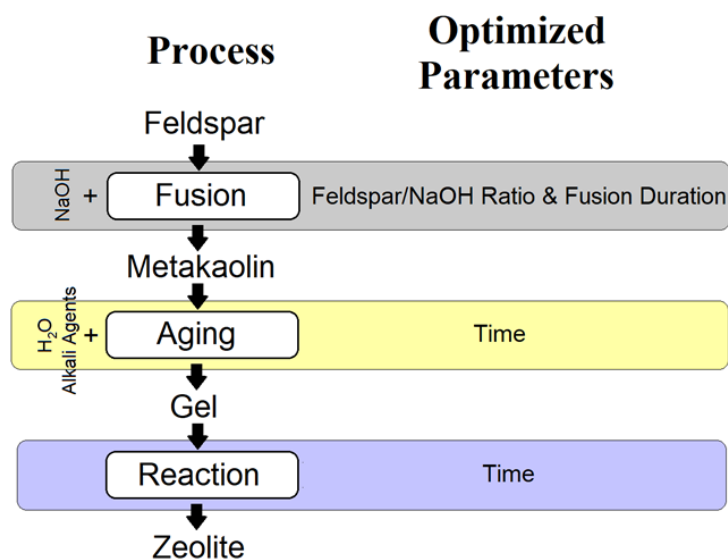
Figure 5.1. Schematic representation of the process flow and the optimized parameters for zeolite 4A synthesis from sodium feldspar

For a controlled experimental setup design, one parameter at a time was changed, keeping the rest identical. Gel formula of 2.44 SiO_2: 1 Al_2O_3: 3.14 Na_2O: 110 H_2O was used in this study, which was pre-selected as summarized in Chapter 4.

5.1.1   Fusion Alkalinity Adjustments

Unlike kaolin activation (metakaolinization), there was an additional parameter of optimizations, which was the alkali source used during fusion in the activation method. The optimization of the ratio of sodium feldspar to NaOH is critical to achieving the desired level of fusion without any unfused silica and alumina source remaining in the fusion product. Accordingly, four different sodium feldspar/NaOH ratios (wt./wt.), 1/1, 1/1.5, 1/2/, and 1/3, were examined. Fusion mixtures were placed in a crucible and fused at 850°C for 1.5 h. The calculated amount of sodium aluminate was mixed with distilled water and fused product to generate the gel of 2.44 SiO_2: 1 Al_2O_3: x Na_2O: 110 H_2O, for which "x" varies with the ratio of the fusion mixture (sodium feldspar/NaOH). The resulting gels were aged at 60°C water bath for 4 h, and aged gels were placed in a previously heated oven at 100°C for 4 h

for the reaction step. The SEM images and XRD patterns of final products are shown in Figure 5.2 and Figure 5.3.
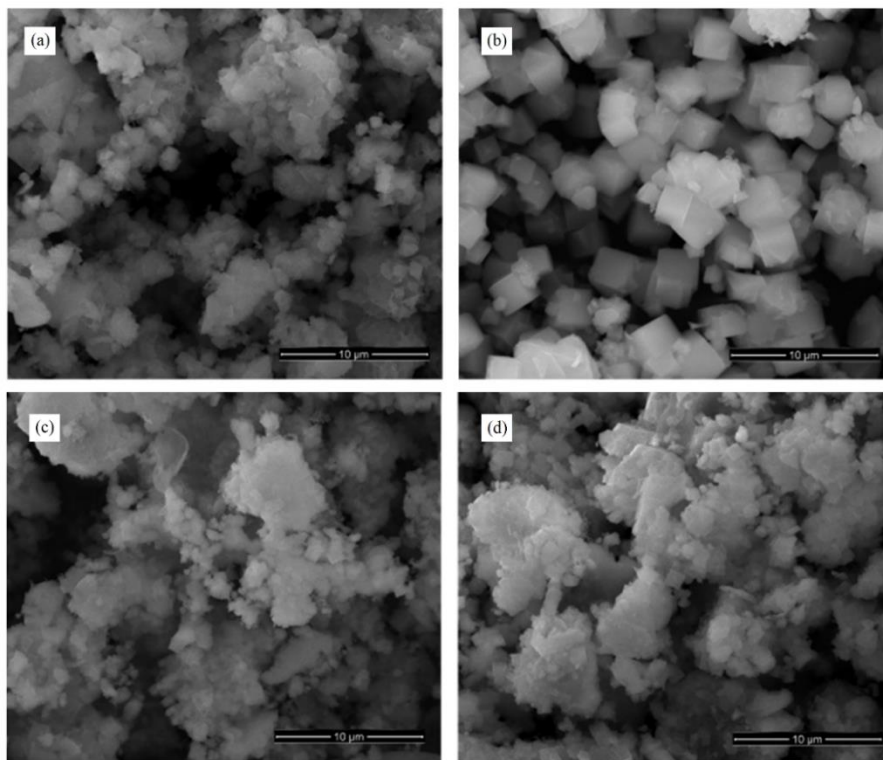
Figure 5.2. SEM images of zeolite 4A synthesis products with ratios of 1/1 (a), 1/1.5 (b), 1/2 (c), and 1/3 (d) by weight of sodium feldspar/ NaOH.

From Figure 5.2, it was observed that the typical cubic morphology of zeolite 4A was achieved with a sodium feldspar/NaOH ratio of 1/1.5. Also, XRD patterns confirmed that the highest crystalline products were obtained from the same product, while secondary phases such as zeolite P and zeolite 13X were observed in the other products. This may be due to the lack of proper fusion due to the less or excess NaOH used in the fusion step. The rest of the experiments were conducted with the sodium feldspar/NaOH ratio of 1/1.5.
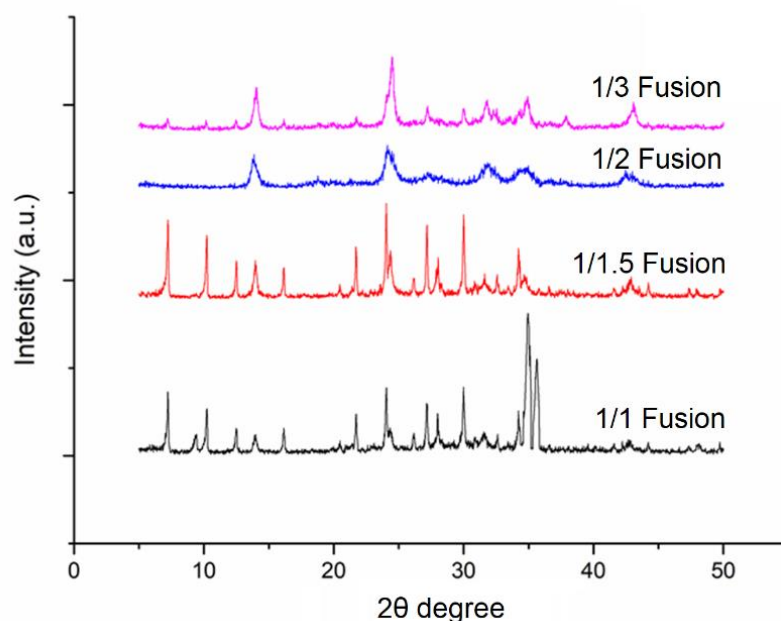
Figure 5.3. XRD Patterns of zeolite 4A synthesis products with ratios of 1/1, 1/1.5, 1/2, and 1/3 by weight of sodium feldspar/NaOH

5.1.2   Alkali Fusion Time

Alkali fusion is a crucial part of this process since sodium feldspars can not be converted into amorphous phases with relatively mild conditions such as kaolin at 600-1000°C [105,113,157]. Due to this phenomenon, alkali sources with lower melting points are introduced, such as sodium hydroxide. This low melting point alkali material melts at elevated temperatures and reacts with the solid phase to form soluble silicates and aluminates. Most of the crystalline phases could be converted into soluble phases and transformed into zeolite crystals by alkali fusion. To be able to generate desired soluble phases, enough time should be given for a proper and complete conversion. Three different durations were performed, which are 1.5 h, 3 h, and 6 h.

The calculated amount of sodium aluminate was mixed with distilled water and subjected to fusion to generate the 2.44 SiO_2: 1 Al_2O_3: 3.14 Na_2O: 110 H_2O gel. The

resulting gels were aged at 60°C water bath for 4 h, and aged gels were placed in a previously heated oven statically at 100°C for 4 h for the reaction step. The SEM images and XRD patterns of final products are shown in Figure 5.4 and Figure 5.5.
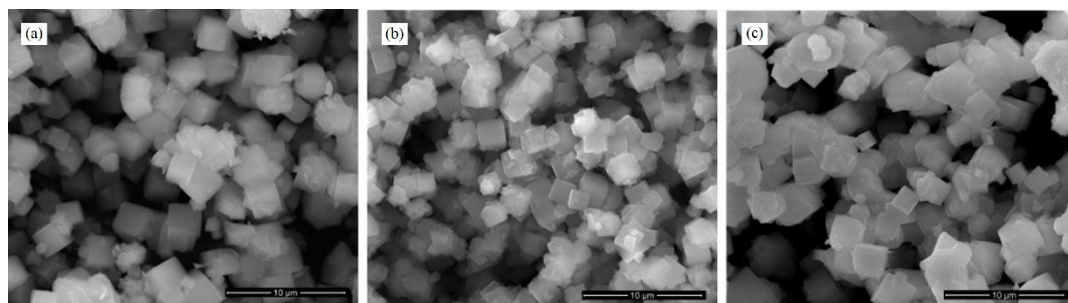
Figure 5.4. SEM images of zeolite 4A synthesis products from sodium feldspar with 1.5 h, 3 h, and 6 h of fusion times.
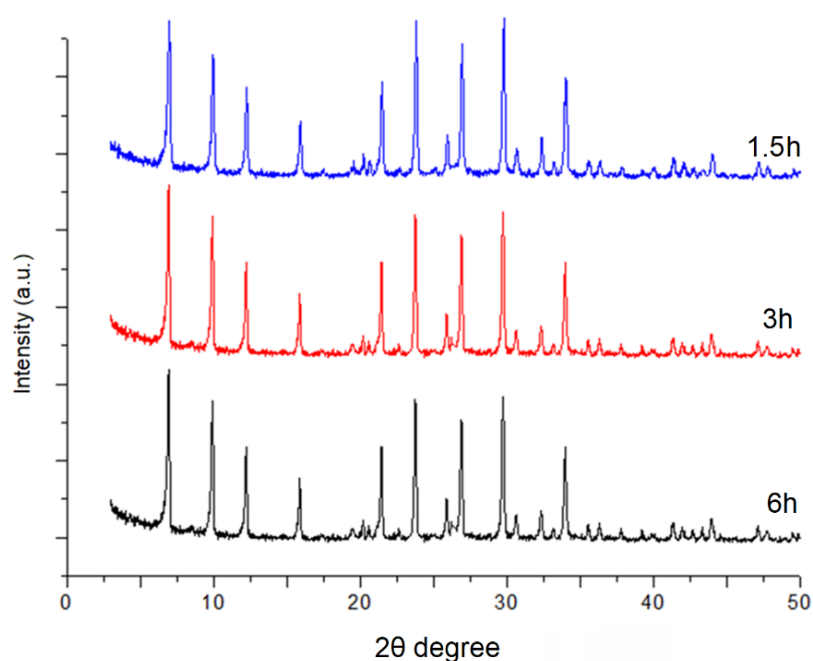
Figure 5.5. XRD patterns of zeolite 4A synthesis products ffrom sodium feldspar with 1.5 h, 3 h, and 6 h of fusion times.

It was observed from both SEM images and XRD patterns that fusion duration was not significantly affected on the final product quality. The relative crystallinity of

the final products was calculated as 98, 100, and 99 with increasing durations of fusion. The lowest duration, which is 1.5 h, was chosen for the rest of the study.

5.1.3   Aging Time

Aging conditions were optimized with the previously optimized gel formula, which is 2.44 SiO_2: 1 Al_2O_3: 3.14 Na_2O: 110 H_2O. To achieve this gel formula, the calculated amount of Sodium feldspar: NaOH (1.5:1 wt.) was fused at 850°C for 1.5 h. After the fusion process, solid particles were mixed in calculated amounts of sodium aluminate and DI water. Three different aging durations were performed for this particular study, which are 2 h, 4 h, and 6 h at 60°C with continuous agitation with 400 rpm. The resulting gels were subjected to reactions that were performed statically at 100°C preheated oven for 4 h. The resulting solid particles suspended in alkali solution were centrifuged and washed with distilled water four times before overnight drying at 80°C in a conventional oven. SEM images and XRD patterns of the final products were given in Figure 5.6 and Figure 5.7, respectively.
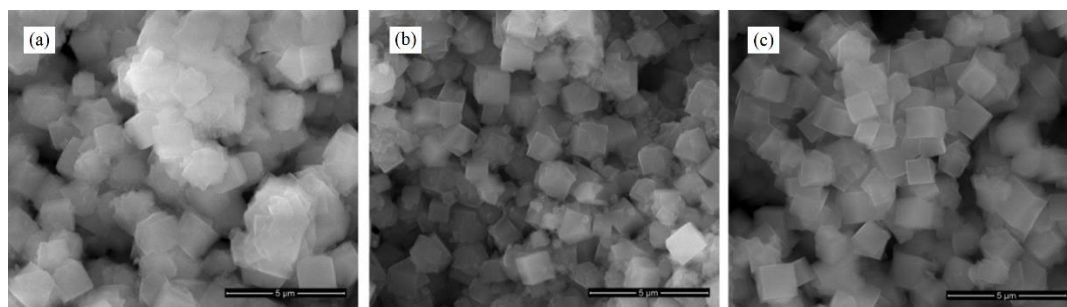
Figure 5.6. SEM images of the zeolite 4A synthesis products from sodium feldspar with 2 h aging (a), 4 h aging (b), and 6 h aging (c).
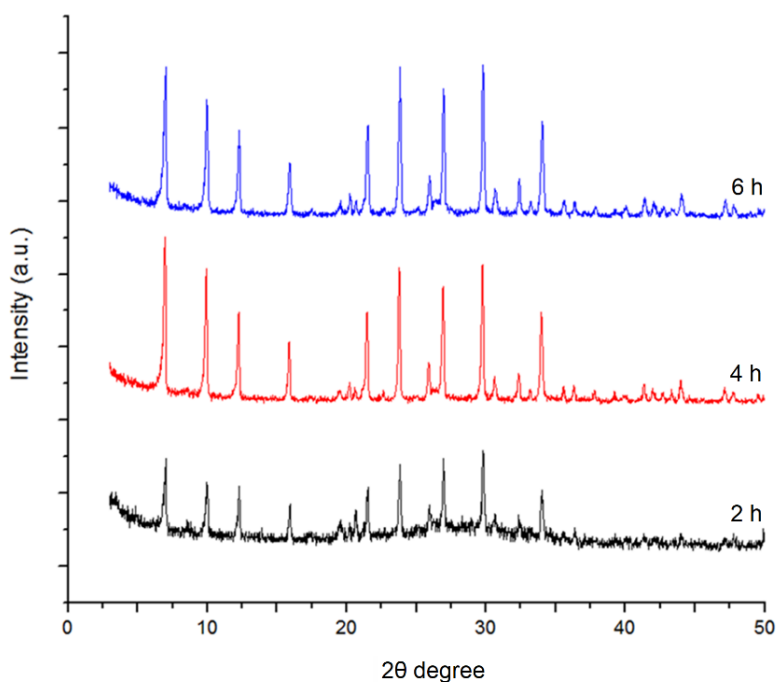
Figure 5.7. XRD patterns of the zeolite 4A synthesis products from sodium feldspar with different aging times.

Table 5.1 Relative crystallinity of zeolite 4A synthesis products from sodium feldspar with different aging times

Aging Time (h)	2	4	6
Relative Crystallinity (%)	52	100	97

Although there was no significant difference observed in the SEM images, XRD patterns shown in Figure 5.7 showed that the crystallinity of the products with 2 h aging is low, with no significant change between 4 to 6 h (Table 5.1). In accordance with the relative crystallinity results and SEM images, 4 h of aging was chosen for further studies.

5.1.4   Reaction Time

In this study, zeolite 4A crystals were synthesized with three different reaction times, which are 2 h, 4 h, and 6 h, while the rest of the parameters were kept identical. Sodium feldspar: NaOH (1.5:1 wt.) was calcined at 850°C for 1.5 h, and the gel formula was adjusted with sodium aluminate and DI water to be 2.44 SiO_2: 1 Al_2O_3: 3.14 Na_2O: 110 H_2O. Aging took place at 60°C for 4 h. Aged gels were placed in a 100°C oven for 2, 4, and 6 h. The final products' SEM images and XRD patterns were given in Figure 5.8 and Figure 5.9, respectively.
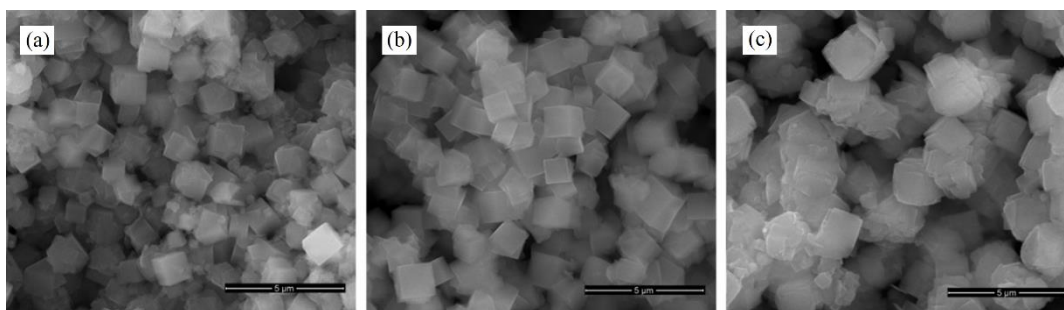
Figure 5.8. SEM images of the zeolite 4A synthesis products from sodium feldspar with 2 h (a), 4 h (b), and 6 h (c) of reaction.
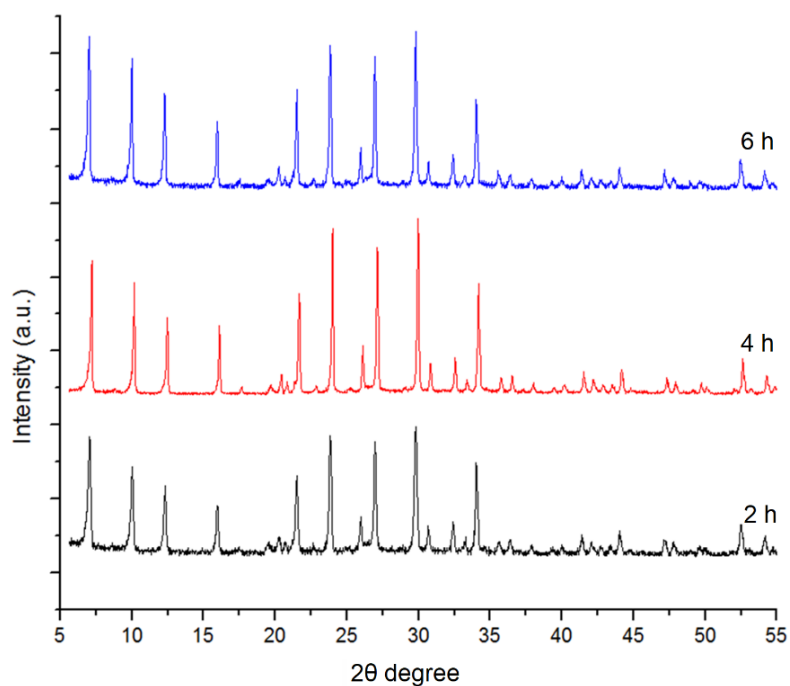
Figure 5.9. XRD patterns of the zeolite 4A synthesis products from sodium feldspar with different reaction times.

Table 5.2 Relative crystallinity of the zeolite 4A synthesis products from sodium feldspar with different reaction times

Reaction Time (h)	2	4	6
Relative Crystallinity (%)	69	96	100

According to the SEM images, all the products showed the standard cubic structure of zeolite 4A. XRD patterns showed that crystallinity increased until 4 h of reaction, and there was no significant increase after that point. For better understanding, relative crystallinities were calculated (Table 5.2), and the most crystalline product was found with 6 h of aging. Since there is a minor difference between 4 and 6 h of aging, and it is beneficial for production to have the same amount of time for aging and reaction, 4 h of reaction will be performed in the further experiments.

5.1.5 Comparison of Synthesized Zeolites with Commercial Zeolites

Synthesis of zeolite 4A was performed with the gel prepared from the fusion products of sodium feldspar and sodium hydroxide with ratios of 1/1.5 (wt./wt.) fused at 850°C for 1.5 h, sodium aluminate, and distilled water, with a formula of 2.44 SiO_2: 1 Al_2O_3: 3.14 Na_2O: 110 H_2O. The resulting gels were placed in an HDPE bottle and aged in a 60 °C with continuous stirring for 4 h. Aged gels were placed in a previously heated oven at 100°C for 4 h of the reaction step. The resulting solid particles separated from the mother liqueur and washed with distilled water at least three times by centrifugation at 7500 rpm for 5 minutes and dried at a conventional oven at 80°C overnight. The resulting zeolites will be named Zeolite 4A-Feldspar-NaOH, and SEM images and XRD patterns of the synthesized zeolite 4A and commercial zeolite 4A are given in Figure 5.10 and Figure 5.11, respectively.
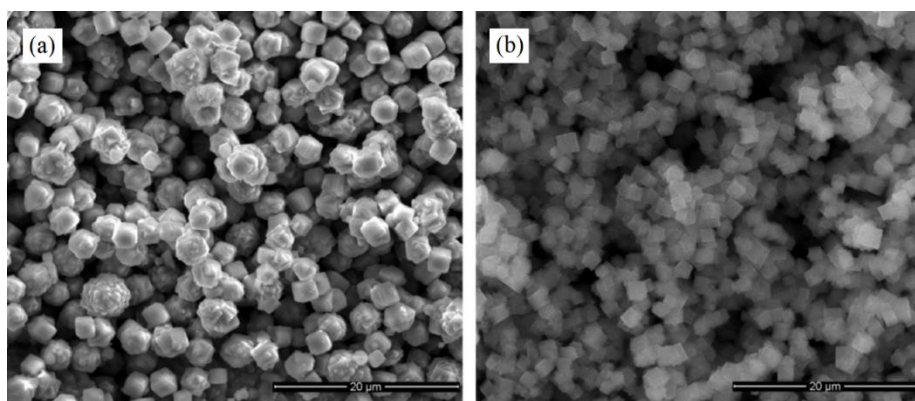
Figure 5.10. SEM images of the commercial zeolite 4A (a) and Zeolite 4A-Feldspar-NaOH (b).
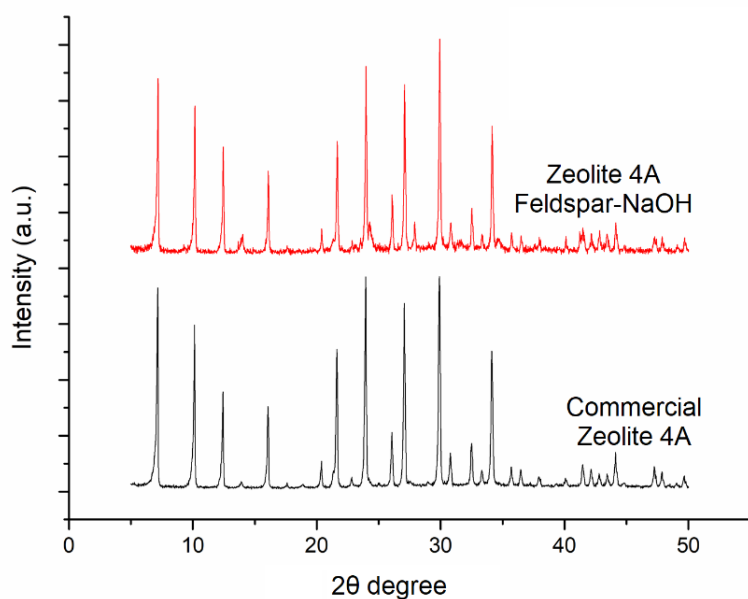
Figure 5.11. XRD patterns of the commercial zeolite 4A and Zeolite 4A-Feldspar-NaOH.

According to the SEM images of the zeolites, both zeolites have the unique structure of zeolite 4A, while Zeolite 4A-Feldspar-NaOH was smaller with respect to commercial zeolites. One significant difference between the morphologies of commercial and synthesized zeolites is the rounder-edged morphology of the commercial zeolites, which makes them more advantageous to be used as an additive in the detergent industry as water softeners. Also, particle size distribution analysis showed that the average particle size of commercial zeolites was 5.8 µm while synthesized ones were 4.2 µm. XRD patterns proved that both products were pure zeolite 4A with no additional impurities.

5.2 Optimization of Zeolite 13X Synthesis Parameters with Sodium Hydroxide

Zeolite 13X synthesis using sodium feldspar as silica, alumina, and partially sodium sources was proposed for the first time since the Si/Al ratio of the source was found to perfectly match for the synthesis of zeolite 13X. An identical activation procedure

of sodium feldspar was used, as explained in the previous section, followed by the hydrothermal synthesis procedures. Basic production steps were given below;

1) Alkali fusion of sodium feldspar with the calculated amount of NaOH
2) Sodium hydroxide and other silicon or aluminum solution preparation in distilled water.
3) Addition of fusion products into an alkali solution.
4) Aging the mixture with continuous agitation in a water bath at the desired temperature and duration.
5) Reaction step of the gel in an oven at the desired temperature and duration.
6) Separation of solid particles from alkali medium with centrifugation, washing with distilled water three times, and drying in an oven.

Several synthesis parameters were optimized while performing the synthesis procedure as mentioned above. In Chapter 4, optimized parameters such as aging temperature, reaction temperature, and gel formula were used in this study. Durations were optimized to achieve a successful synthesis since dissolution and nuclei formation rates may vary with a change in the source used as raw material. Also, the alkali ratio used for preparing the mixture of fusion and duration of fusion were kept constant as 1:1.5 wt./wt. and 1.5 h, respectively. Parameters that were studied particularly for this section are given in Figure 5.12.
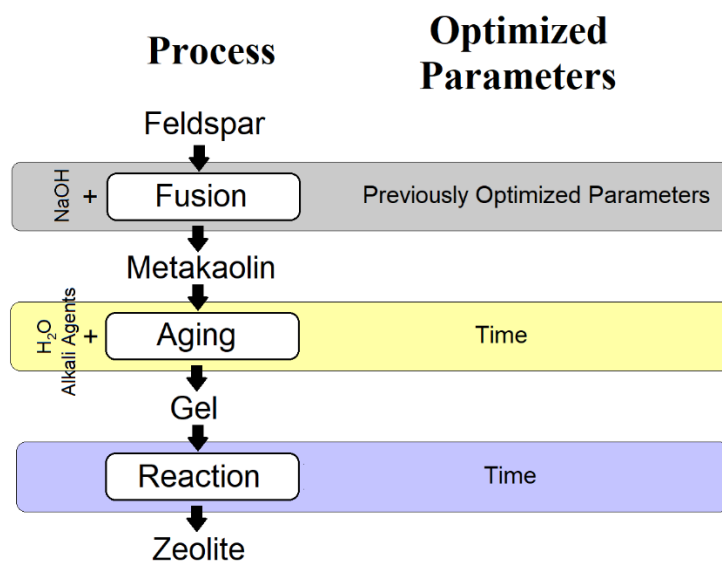
Figure 5.12. Schematic representation of the process flow and the optimized parameters for zeolite 13X synthesis from sodium feldspar

For a controlled experimental setup design, one parameter was changed one step at a time, keeping the others identical. Gel formula of 5 SiO_2: 1 Al_2O_3: 7.5 Na_2O: 337.5 H_2O was used in this study.

5.2.1   Aging Time

Effect of aging time was investigated for the gelation process of 5 SiO_2: 1 Al_2O_3: 7.5 Na_2O: 337.5 H_2O from alkali fusion process of NaOH and sodium feldspar mixture at 850°C for 1.5 h. The obtained product was aged at 25°C for three different durations of aging, which were 16, 20, and 24 h. The resulting gels were placed in previously heated 100°C ovens for 8 h of duration. Then the formed suspension was washed four times with distilled water and dried in an oven at 60°C, overnight. The resulting solid particles were characterized with SEM and XRD, and results were given in Figure 5.13 and Figure 5.14, respectively.
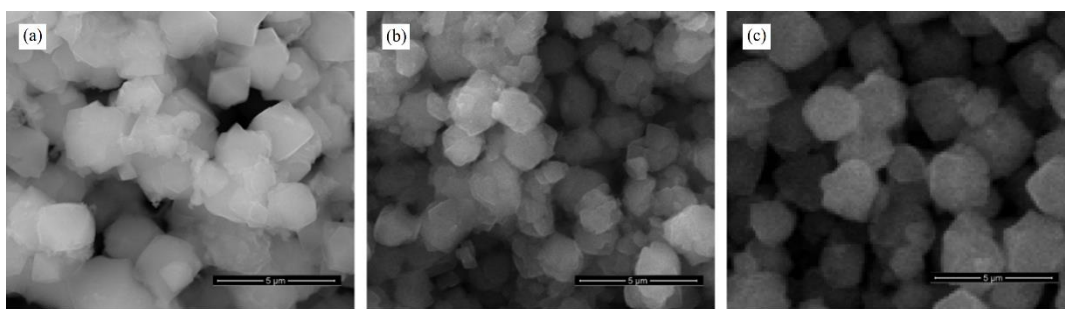
Figure 5.13. SEM images of the zeolite 13X synthesis products from sodium feldspar, obtained with 16 h (a), 20 h (b), and 24 h (c) of aging.
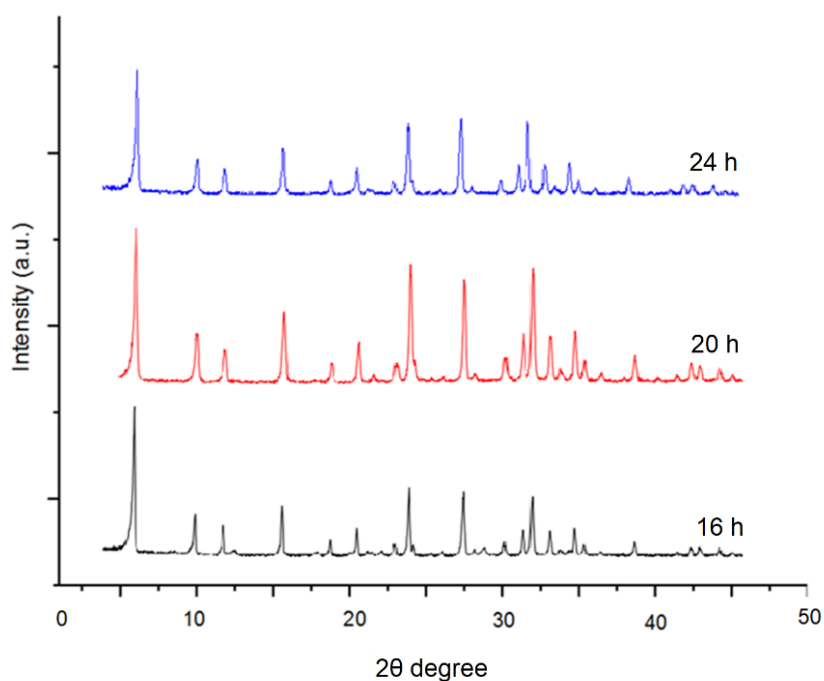
Figure 5.14. XRD patterns of the zeolite 13X synthesis products from sodium feldspar after 16 h, 20 h, and 24 h of aging.

Table 5.3 Relative crystallinity of the zeolite 13X synthesis products from sodium feldspar with different aging times

Aging Time (h)	16	20	24
Relative Crystallinity (%)	92	100	88

According to the SEM images, there was no significant effect of the aging time on the morphology of the final product. However, XRD patterns showed that the intensities of major peaks for zeolite 13X were maximum for 20 h of aging time. In order to enhance % crystallinity of the final product (Table 5.3), 20 h of aging at 25°C was used for the rest of this study.

5.2.2   Reaction Time

The studies conducted on zeolite 13X formation continued with investigating the effect of reaction time on % crystallinity of synthesized products. For this particular case, sodium feldspar sources were subjected to an alkali fusion process with sodium hydroxide using a ratio of 1.5/1 (wt./wt). The resulting fused product was mixed with the proper amount of aluminum hydroxide, sodium hydroxide, and water and aged at 25°C for 20 h with continuous agitation at 400 rpm. Aged samples were placed in a previously heated oven at 100°C for three different durations: 4 h, 6 h, and 8 h. The resulting solid particles were washed with distilled water four times and dried overnight at a 60°C oven. SEM and XRD analysis results are shown in Figure 5.15 and, respectively.
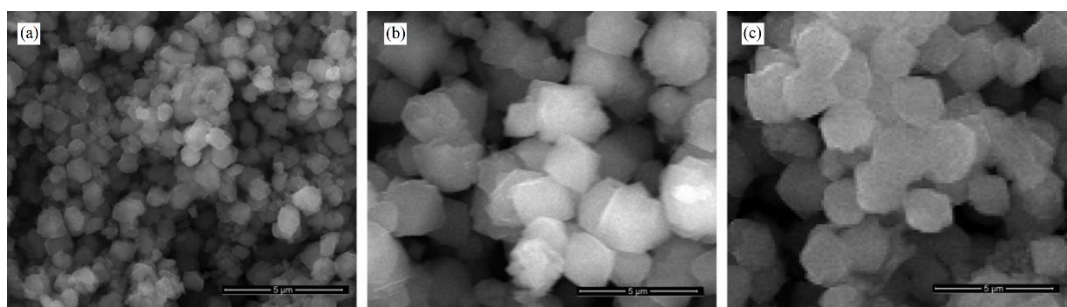
Figure 5.15. SEM images of the zeolite 13X synthesis products from sodium feldspar, using 4 h (a), 6 h (b), and 8 h (c) of reaction.
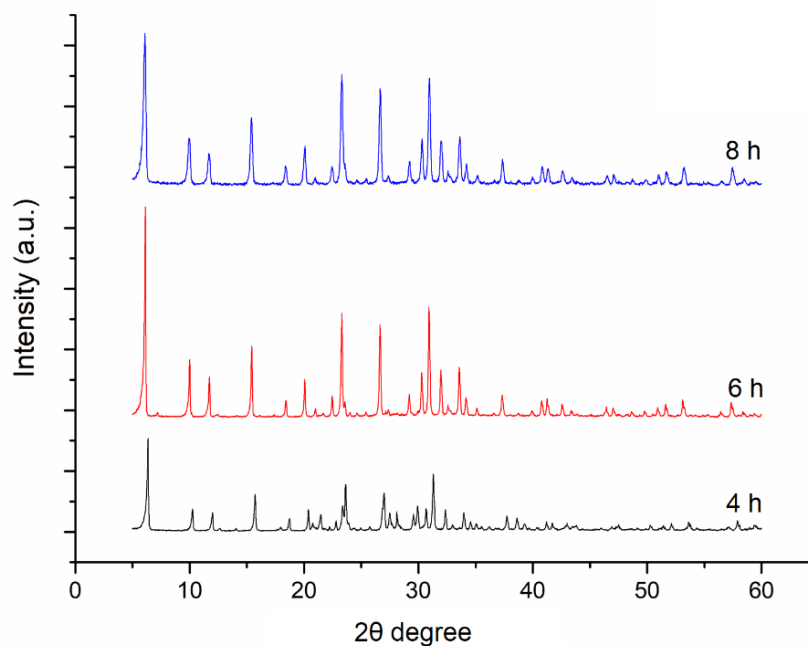
Figure 5.16. XRD patterns of the zeolite 13X synthesis products from sodium feldspar, using 4 h, 6 h, and 8 h of reaction.

According to the SEM images, 4 h of reaction resulted in smaller but agglomerated particles. In comparison, 6 and 8 h showed well-known faujasite zeolite morphology with no significant difference with respect to each other. XRD patterns showed that 6 h of reaction resulted in higher crystallinity with respect to 8 h. Also, relative crystallinities were calculated and shown in Table 5.4. The highest crystallinity was calculated using 6 h of reaction time.

Table 5.4 Relative crystallinity of the zeolite 13X synthesis products from sodium feldspar with different reaction times

Reaction Time (h)	4	6	8
Relative Crystallinity (%)	42	100	88

5.2.3   Comparison of Synthesized Zeolites with Commercial Zeolites

Synthesis of zeolite 13X was performed using the gels prepared from the fusion products of sodium feldspar and sodium hydroxide with ratios of 1/1.5 (wt./wt.) fused at 850°C for 1.5 h, sodium aluminate, and distilled water, with a formula of 5 SiO_2: 1 Al_2O_3: 7.5 Na_2O: 337.5 H_2O. The resulting gels were placed in an HDPE bottle and aged at 25°C with continuous stirring for 20 h. Aged gels were placed in a previously heated oven at 100°C for 6 h of the reaction step. The resulting solid particles were separated from the mother liqueur and washed with distilled water at least three times by centrifugation at 7500 rpm for 5 minutes and dried in a conventional oven at 80°C overnight. SEM images and XRD patterns of the synthesized zeolite 13X, which will be named Zeolite 13X-Feldspar-NaOH from now on, and commercial zeolite 13X were given in Figure 5.17 and Figure 5.18, respectively.
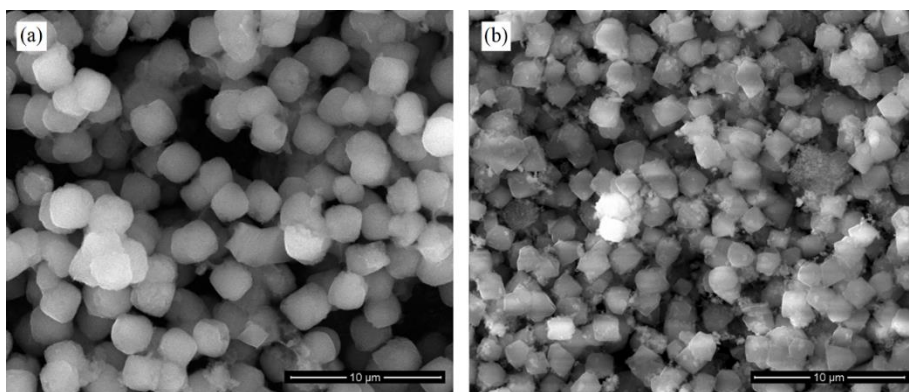
Figure 5.17. SEM images of the commercial zeolite 13X (a) and synthesized Zeolite 13X-Feldspar-NaOH (b).

114
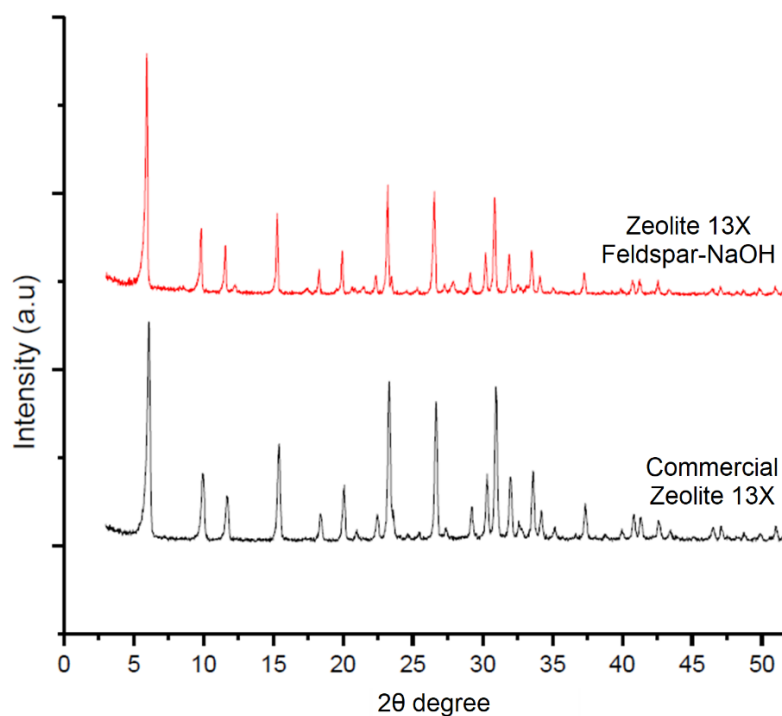
Figure 5.18. XRD patterns of the commercial zeolite 13X and synthesized zeolite 13X with optimized parameters.

According to the SEM images of the zeolites, commercial zeolite 13X had a larger particle size distribution (~5μm) with respect to the synthesized zeolites (~3μm) using sodium feldspar. The size of the zeolite crystals can be manipulated according to the final application area, given that the species formed during alkali fusion can be controllably transformed into the crystal growth phase during the aging step. Figure 5.18 showed that the overall crystallinity of the synthesized zeolite 13X has similar crystallinity with respect to the commercial zeolite13X. In summary, the developed procedure offered a more environmentally friendly and economical approach offering similar morphological and similar crystallinity of zeolite 13X compared to its commercial counterpart.

5.3 Zeolite 4A Synthesis with Sodium Feldspar and Sodium Carbonate

Sodium hydroxide is a well-known and high-demand chemical also known as caustic soda. It has an expensive production method that produces chlorine gas that is very toxic and hard to work safely. Due to the high demand for caustic soda in the industry and its dependency on the chlorine market, it is not the best choice for zeolite production. Sodium carbonate, also known as soda ash, is another candidate as a sodium source, more cost-effective with respect to caustic soda, and safer to work with. Since it will be used as an alkali source, it is crucial to work at higher temperatures than the melting point of sodium carbonate, which is 851°C. In the proposed synthesis route that eliminates sodium hydroxide, all alkalinity was provided from sodium carbonate and aluminum hydroxide during the fusion step to achieve the desired gel formula. Similar to the procedure used in Section 4.3.3, the one-pot fusion approach was applied to all sources used for zeolite synthesis. The resulting fusion product was crushed and mixed with the calculated amount of distilled water. Optimized synthesis procedures were applied to obtain zeolite 4A out of fused sodium feldspar and sodium carbonate mixture. Detailed calculations and experimental procedures were given in Chapter 3. SEM images and XRD patterns of synthesized zeolite 4A samples were given in Figure 5.19 and Figure 5.20, respectively.
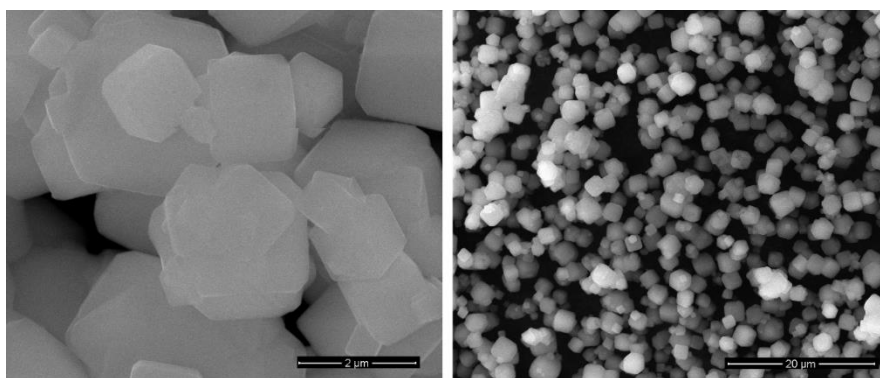
Figure 5.19. SEM images of Zeolite 4A-Feldspar-Na_2CO_3
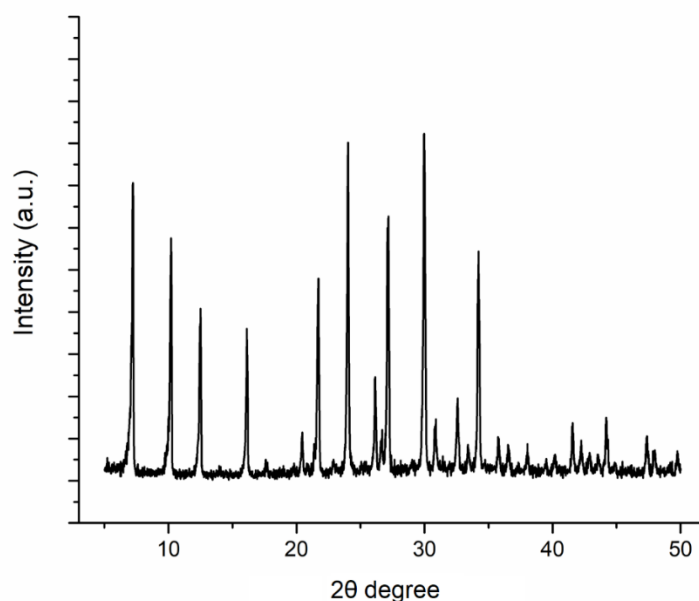
Figure 5.20. XRD pattern of the Zeolite 4A-Feldspar-Na_2CO_3

As observed from the SEM images, the standard cubic structure of zeolite 4A crystals was formed after the synthesis. Furthermore, the XRD patterns confirmed the pure zeolite 4A formation. The particles were non-monodispersed in sizes that were previously observed with one-pot synthesis routes since the dissolution of sodium aluminosilicates and nuclei formation occurs in the same process step of aging.

In this synthesis procedure, the one-pot fusion procedure was used to obtain pure zeolite 4A, and all the reactants except DI water were mixed in the solid phase, and fusion took place to generate "instant soup" like premix. This procedure is a fast, easy, and relatively cheap method to generate desired sodium aluminosilicates from unsoluble phases such as sodium feldspar. This method is also easy to use since the fusion product (semi-product) can be stored, and synthesis can be performed after a while. In that way, this method helps to make the system work in batch formation.

5.4 Zeolite 13X Synthesis with Sodium Feldspar and Sodium Carbonate

As explained in section 5.3, the one-pot fusion method is applicable for synthesizing zeolites out of unsoluble aluminosilicate sources such as sodium feldspars. This production route is applied to synthesize zeolite 13X with the mixture of calculated amounts of sodium feldspar, sodium carbonate, and aluminum hydroxide. The addition of aluminum hydroxide was either eliminated or was very low in comparison with the amount used for zeolite 4A synthesis; since the Si/Al ratio of the sodium feldspar was almost identical to what was needed for zeolite 13X. Thus, there was almost no need to compensate for the difference with an additional alumina source. SEM images and XRD patterns of synthesized zeolite 4A samples are given in Figure 5.21 and Figure 5.22, respectively.
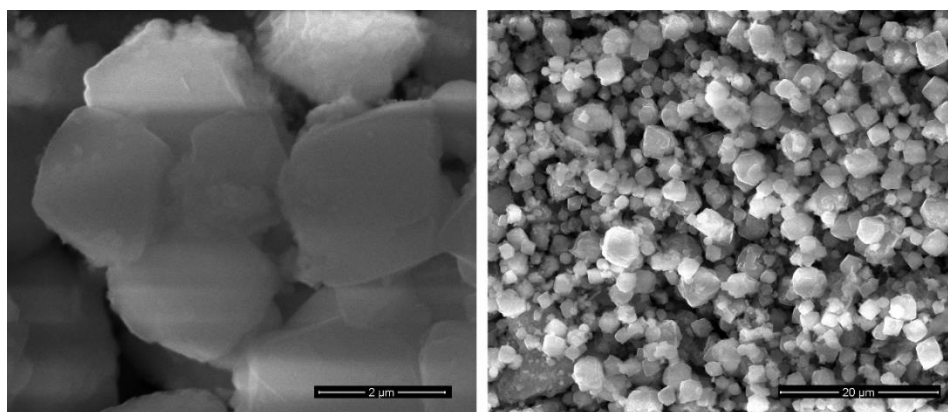
Figure 5.21. SEM images of the Zeolite 13X-Feldspar-Na_2CO_3
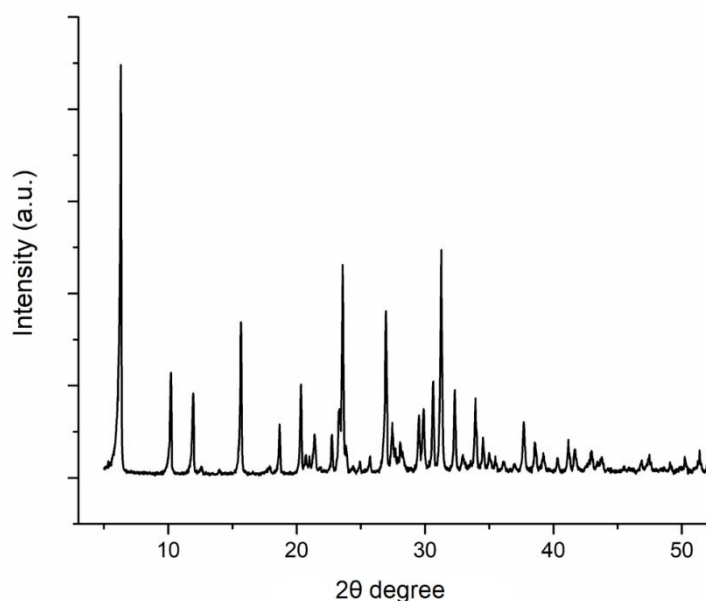
Figure 5.22. XRD pattern of the Zeolite 13X-Feldspar-Na$_2$CO$_3$

SEM images shown in Figure 5.21 confirmed the typical morphology of faujasite type zeolite of truncated bi-pyramids. Moreover, the XRD pattern shown in Figure 5.22 proved no additional secondary phase formation. The same problem with poly-dispersion of particles was observed in this synthesis route due to the one-pot fusion method.

5.5   Conclusions

In this part of the study, zeolite 4A and zeolite 13X were successfully synthesized from sodium feldspar with the alkali fusion method followed by hydrothermal synthesis. Mainly previously optimized parameters were used to synthesize zeolites out of sodium feldspar.

In the first part of the study, alkali fusion was applied with sodium feldspar and sodium hydroxide. Hydrothermal synthesis was applied to the fusion products with additional sodium aluminate and/or sodium aluminate and DI water.

However, in the second part of the study, one-pot synthesis was applied for the activation of sodium feldspar and aluminum hydroxide with the help of sodium carbonate as an alkali agent for the first time. This unique one-pot fusion method helps to generate a semi-product, which can be converted into zeolites at any time with the addition of the calculated amount of distilled water.

Zeolite 4A and zeolite 13X were successfully synthesized with two different fusing agents, and XRD patterns of these zeolites are shown in Figure 5.23 and Figure 5.24.
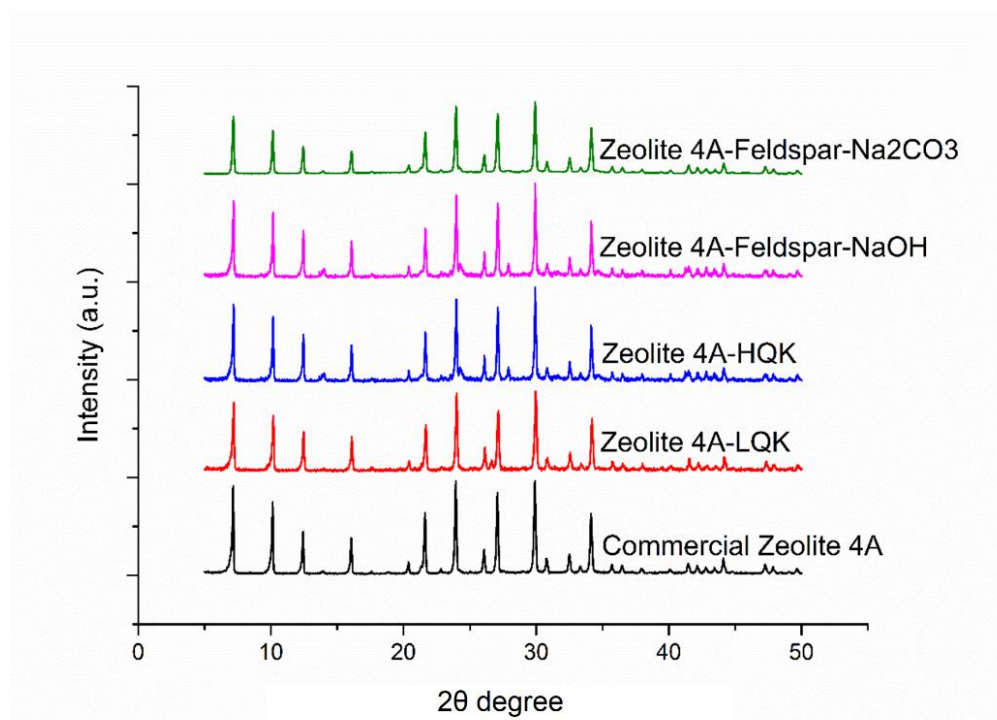
Figure 5.23. XRD patterns of commercial zeolite 4A and synthesized zeolite 4As
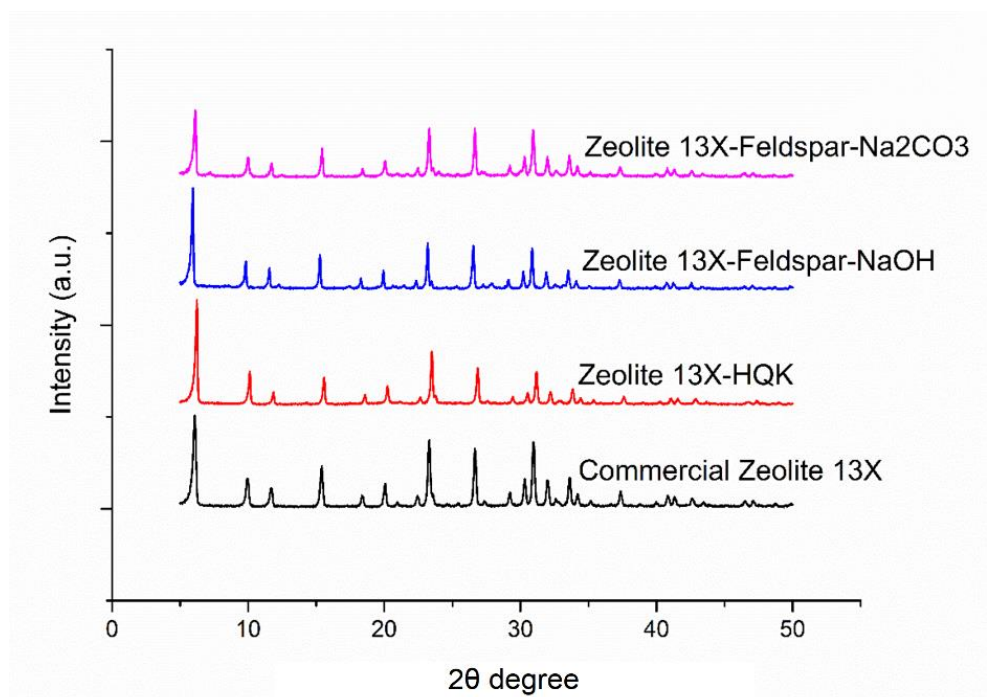
Figure 5.24. XRD patterns of commercial zeolite 4A and synthesized zeolite 13Xs

In conclusion, both alkali agents worked adequately to convert the water-insoluble sodium feldspar raw material into a soluble sodium aluminosilicate source, and proper zeolites were synthesized from the fused materials.

Sodium feldspar is a crucial mine that is highly used in various industries such as ceramics, paper, cosmetics, etc. [160,161,205,206]. Sodium feldspar is a unique material for zeolite synthesis, and it is highly abundant in Turkey. It is reported for the first time that it can be utilized as a zeolite starting material for a cost-effective alternative for standard laboratory-grade chemicals.

CHAPTER 6

DIRECT SYNTHESIS OF ZEOLITE 3A & ZEOLITE 5A

Zeolite 3A is the potassium exchanged form of zeolite 4A, while zeolite 5A is the calcium exchanged form of the same zeolite. In industry, the production of zeolite 3A and 5A is achieved by applying ion-exchange procedures to zeolite 4A. Thus, the success underlying successful zeolite 3A and 5A production is dependent on the synthesis of zeolite 4A through traditional methods. For that purpose, the synthesized zeolite 4A samples need to be ion-exchanged in an aqueous medium with potassium (3A) and calcium (5A) salts. This chapter aims to explain the direct synthesis of zeolite 3A and zeolite 5A with desired K/Na and Ca/Na ratios. The advantages of the proposed direct synthesis method are its ability to lower the number of the process steps and thus decreased energy & time spent to obtain ion-exchanged forms of zeolites. The schematic representation of the production route is shown in Figure 6.1.
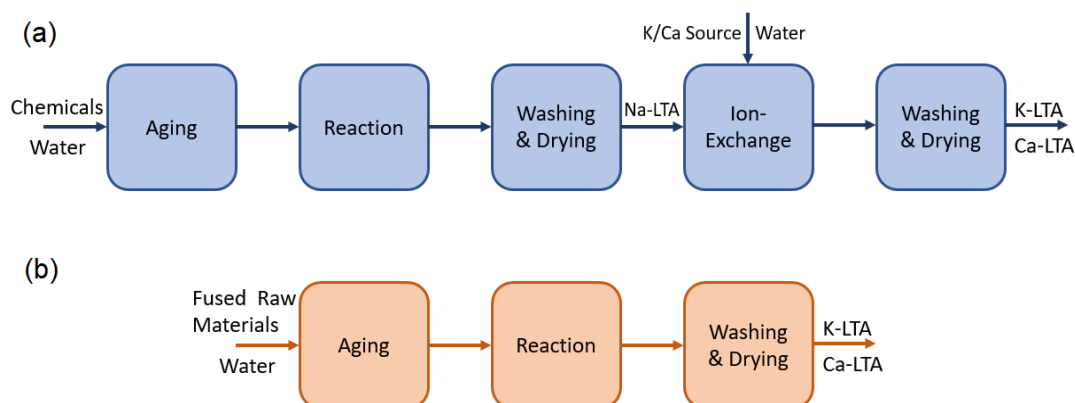
Figure 6.1. Schematic representation of (a) the standard synthesis and ion-exchange procedure and (b) proposed direct zeolite 3A and zeolite 5A synthesis procedure.

6.1　Direct Synthesis of Zeolite 3A

For industrial purposes, the specifications do not require zeolite 3A to be fully ion-exchanged; in fact, it is expected to be partially ion-exchanged with K^+ ions for de-humidifying applications [42]. Accordingly, the existing procedure involves exposing zeolite 4A samples to an ion-exchange procedure with varying K/Na ratios at tailored conditions such as different K^+ concentrations or durations of washing [70,207,208]. The one-pot synthesis route developed in this thesis study was adapted by changing the desired amount of sodium source with potash as an alternative raw material in the current study.

Two different K/Na ratio zeolites at low and high K^+ concentrations were synthesized through the one-pot process by changing the proper amount of sodium carbonate with a fine powder of potash. SEM images of the synthesized zeolites and Energy Dispersive X-Ray (EDX) Spectroscopy results were given in Figure 6.2 and Table 6.1.
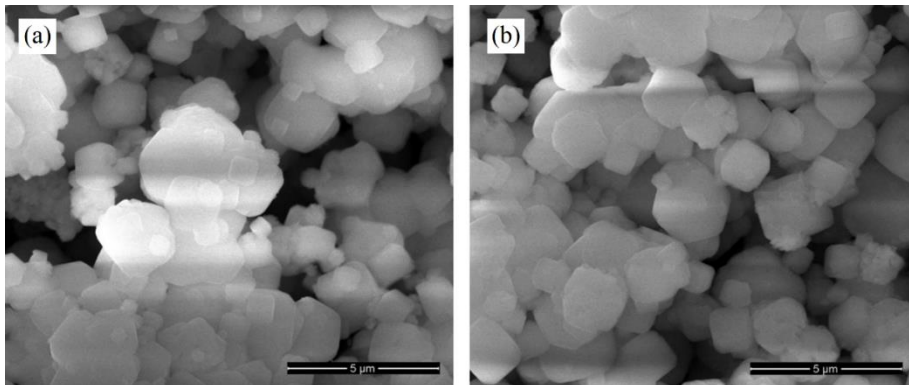
Figure 6.2. SEM images of zeolite 3A synthesized using the one-pot process with low K^+ (a) and high K^+ content (b).

124

Table 6.1 K^+ and Na^+ content of zeolite 3A synthesized through one-pot process and commercial zeolite 3A.

Zeolite	Na (atomic %)	K (atomic %)
Zeolite 3A-Low K	9.74	5.12
Zeolite 3A-High K	6.43	8.36
Commercial Zeolite 3A	8.86	6.15

Synthesized zeolite 3A crystals showed the general morphology of the LTA family with a truncated cubic morphology. Furthermore, XRD patterns of the synthesized zeolite 3A samples are given in Figure 6.3.
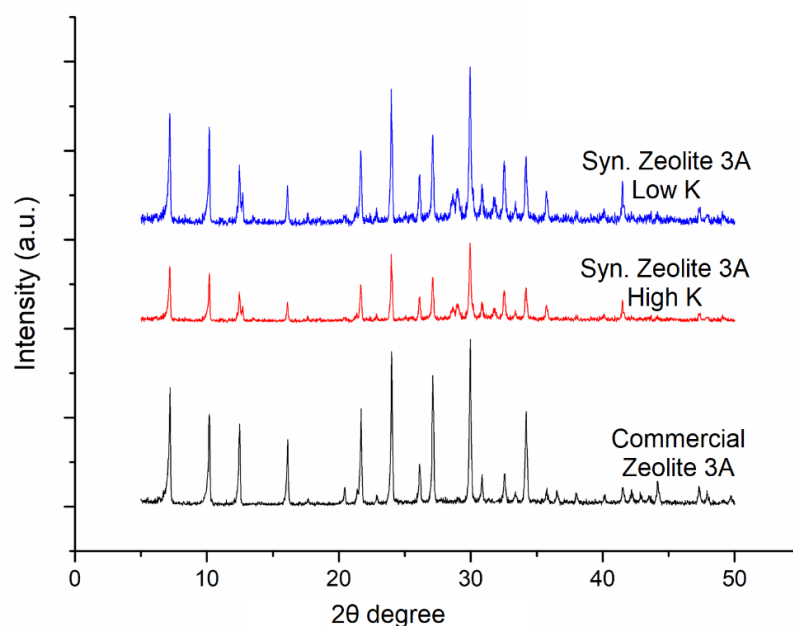
Figure 6.3. XRD patterns of zeolite 3A samples synthesized through the one-pot process and commercial zeolite 3A.

Commercial zeolite 3A was supplied from NEDEX group, which is the company that uses zeolite 3A to build the desiccant beads to be utilized in between insulating windows. Low K^+ content zeolite 3A had higher crystallinity (95.2%) with respect

to the high K^+ content counterpart (52.6%), which might be due to the inhibiting effect of larger ion-sized K^+ in the nucleation and growth rate of the crystals. It was shown in the literature that higher K^+ content resulted in decreased relative crystallinity [209,210]. Seeding was shown to enhance the nucleation and crystal growth rates [7,211], which can be applied in the future to the developed one-pot zeolite 3A synthesis procedure resulting in an increased relative crystallinity of the final products.

6.2   Direct Synthesis of Zeolite 5A

A similar procedure was proposed to directly synthesize zeolite 5A, eliminating the extra ion-exchange step currently used in industrial processes (Figure 6.1). In this proof of concept study, the desired amount of sodium source was changed with calcium carbonate during the one-pot synthesis route developed in this thesis. After calcination, the obtained product was seen to be an agglomerated solidified product, which needed to be crushed with the help of a mortar. The obtained powder was mixed with the desired amount of water for the aging and reaction processes. SEM images of the synthesized products and Energy Dispersive X-ray (EDX) Spectroscopy results were given in Figure 6.4 and Table 6.2.
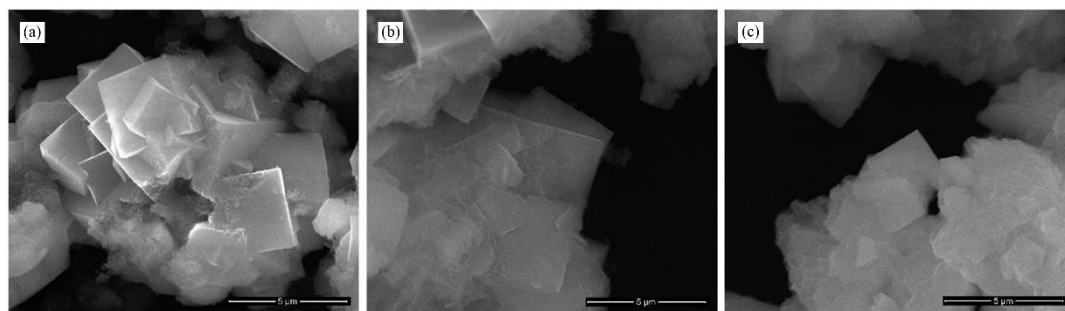
Figure 6.4. SEM images of zeolite 5A synthesized through the one-pot process with low Ca^{2+} (a), medium Ca^{2+} (b), and high Ca^{2+} content (c).

Table 6.2. Ca^{2+} and Na$^+$ content of zeolite 5A synthesized through the one-pot process and commercial zeolite 3A.

Zeolite	Na (atomic %)	Ca (atomic %)
Zeolite 5A-Low Ca	8.74	2.12
Zeolite 5A-Medium Ca	6.91	3.67
Zeolite 5A- High Ca	3.16	6.56
Commercial Zeolite 5A	3.98	6.15

SEM images of the synthesis products showed a significant amount of intergrown particles, creating agglomerations of the crystals. There was a loss in the typical morphology of LTA crystals with increasing Ca^{2+} content. Also, XRD patterns shown in Figure 6.5 displayed a significant loss in % crystallinity with increasing Ca^{2+} content. This may be due to the +2 charge of the calcium atom placed into the pores of the zeolite framework.
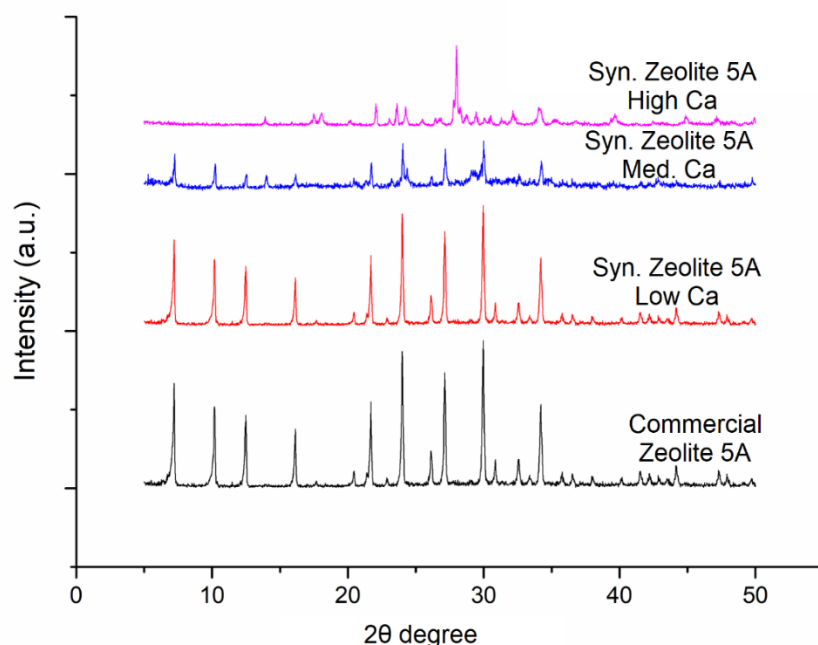
Figure 6.5. XRD patterns of zeolite 5A synthesized through the one-pot process with different Ca^{2+} content and commercial zeolite 5A.

127

Relative crystallinity of the synthesis products was calculated, and high Ca^{2+} content zeolite 5A showed almost no peaks of zeolite 5A. The % crystallinity increased from 35.7% to 89.8% for medium and low Ca^{2+} containing zeolite 5A samples, respectively. These results were in agreement with the SEM images shown in Figure 6.4.

6.3   Application Based Performance of Synthesized Zeolites

Performance-based characterizations were performed on synthesized zeolites such as water sorption capacity, particle size distribution, and color data, which were the most crucial parameters that had to be met for zeolite-based applications[44,104,212]. Color analysis results are summarized in Table 6.3 for all samples prepared in this part of the thesis study.

Table 6.3 Colorimetric analysis of synthesized zeolites and commercial zeolites

Zeolite	a	b	L
Syn. Zeolite 3A-Low K	*-1*	*2*	*73*
Syn. Zeolite 3A- High K	2	6	72
Commercial Zeolite 3A	*1*	*2*	*71*
Syn. Zeolite 5A- High K	-2	*5*	74
Syn. Zeolite 5A- Medium K	-2	*4*	70
Syn. Zeolite 5A- Low K	*-1*	*2*	*71*
Commercial Zeolite 5A	*1*	*2*	72

As shown in Table 6.3, color analysis of the synthesized products showed comparable results with that of the commercial zeolites. The product's color to be used in industry is of significant importance for many applications, and only particular values are accepted before use [44]. Another specification to be met is the particle size distribution, which is user-specific for each separate procedure. Smaller particle-sized samples were desired since increased particle size results in slower

adsorption/desorption behavior [37,213]. Thus, an average particle size of 5µm is commonly desired for desiccant-type zeolites. Particle size analyses of the synthesized zeolites are given in Table 6.4.

Table 6.4 Particle size analysis results of synthesized zeolites and commercial zeolites.

Zeolite	d10	d50	d90
Syn. Zeolite 3A-Low K	1.752	3.166	6.545
Syn. Zeolite 3A- High K	1.984	3.918	7.129
Commercial Zeolite 3A	1.862	3.170	5.170
Syn. Zeolite 5A- High K	*1.198*	*4.140*	*8.198*
Syn. Zeolite 5A- Medium K	*3.118*	*6.148*	*9.954*
Syn. Zeolite 5A- Low K	*3.349*	*8.763*	*13.745*
Commercial Zeolite 5A	*2.187*	*4.492*	*6.587*

Particle size analysis results showed that zeolite 3A could be synthesized within the ranges of the requirements for desiccant-type zeolite production. However, synthesized zeolite 5A samples showed higher d50 values with respect to the commercial zeolite 5A.

One of the most crucial characteristic behavior of the LTA family, besides the high ion exchange capacity, is the water sorption capacity. These analyses were performed with the help of a TGA system, and the results are given in Table 6.5.

Table 6.5 Water sorption results of synthesized zeolites and commercial zeolites

Zeolite	Water Sorption (%)
Syn. Zeolite 3A-Low K	19.3
Syn. Zeolite 3A- High K	17.3
Commercial Zeolite 3A	19.9
Syn. Zeolite 5A- High K	9.9
Syn. Zeolite 5A- Medium K	16.4
Syn. Zeolite 5A- Low K	18.8
Commercial Zeolite 5A	20.2

Water sorption studies indicated that zeolite 3A with low K content showed superior characteristics of the desired product. The zeolite 3A synthesized in the current study was shown to fully meet the industrial requirements expected as desiccants showing comparable water sorption capacity, particle size distribution, and color analysis data with respect to the commercially available one. NEDEX group tested the zeolite samples developed in the current study and concluded that zeolite 3A with low K^+ content was suitable for commercial applications meeting their water retaining requirements. Zeolite 5A was also successfully synthesized using sodium feldspar and calcium carbonate, but further modifications need to be performed to enhance the products' particle size and crystallinity characteristics.

6.4 Conclusions

Zeolite 3A and zeolite 5A were successfully synthesized from locally available raw materials by using the one-pot fusion method for the first time. This method makes it possible to arrange the final product's K/Na and Ca/Na ratio by changing the fusion mixture's content. In this proof of concept study, the possibility of the developed methodology was implemented, and resulting particles were characterized according to the industrial specifications. Results obtained from the synthesized

zeolites were compared with the commercially available zeolites. Promising results were obtained within these studies, but further modifications on synthesis parameters such as seed addition to the reaction mixture before the aging step, improving the aging times, and reaction times are recommended for future studies. In this way, the performance of the synthesized zeolites can be further improved.

CHAPTER 7

SCALE UP STUDIES

Zeolite 4A and Zeolite 13X from various raw materials were successfully synthesized during this study. The synthesis was performed in HDPE bottles with closed caps with the help of magnetic stirrers, conventional ovens, and centrifuge systems. Due to the need for high quantity materials for industrial application trials, one aging tank, one reaction tank, and a filtration system were designed with 20 L volume. This amount allowed one to increase the yield almost 500 fold from one batch of synthesis.

7.1   Design of the Reactor and Filtration System

Commercial-grade high-density polyethylene bottles with closed caps were used in small-scale laboratory research studies. Scaling up the system to almost 500 fold with the same type of material is relatively high in cost, and experimental eruptions might occur after a couple of syntheses with the same HDPE bottle due to the increasing pressure in the bottle during the reaction.

304-grade stainless steel can be used instead of HDPE due to its strength over the alkali medium of the reaction mixture. Also, in small-scale laboratory-grade studies, a single HDPE bottle was transferred from a magnetic stirrer into a conventional oven for the reaction step. However, for scale-up studies, two different vessels were planned, one was for the aging step, and the next was for the reaction phase. The basic drawings and pictures of the aging and reaction vessels are shown in Figure 7.1 and Figure 7.2.
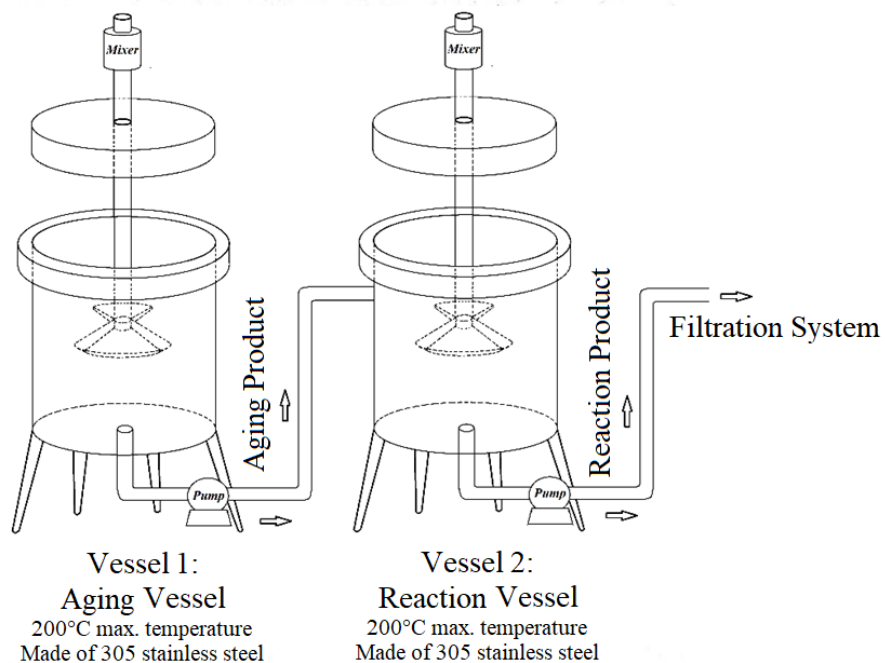
Figure 7.1. Schematic view of the aging and reaction vessels for the zeolite synthesis system.

Figure 7.2. Pictures of the zeolite synthesis system during aging and reaction steps.

Each vessel was 20 L with almost 1 kg of zeolite yield after each batch of zeolite synthesis. A filtration system was used to wash the samples after the reaction in the laboratory-scale synthesis route, and it was possible to use centrifugation to separate five micron-sized particles in a suspension with 50 ml volume. However, centrifugation was not possible for 20 liters of the reaction product due to economic concerns. Alternatively, a pressurized filtration system was developed with a metal sieve of 1-μm that was purchased from Pope Scientific Inc. Figure 7.3 shows the pictures of the developed filtration unit.
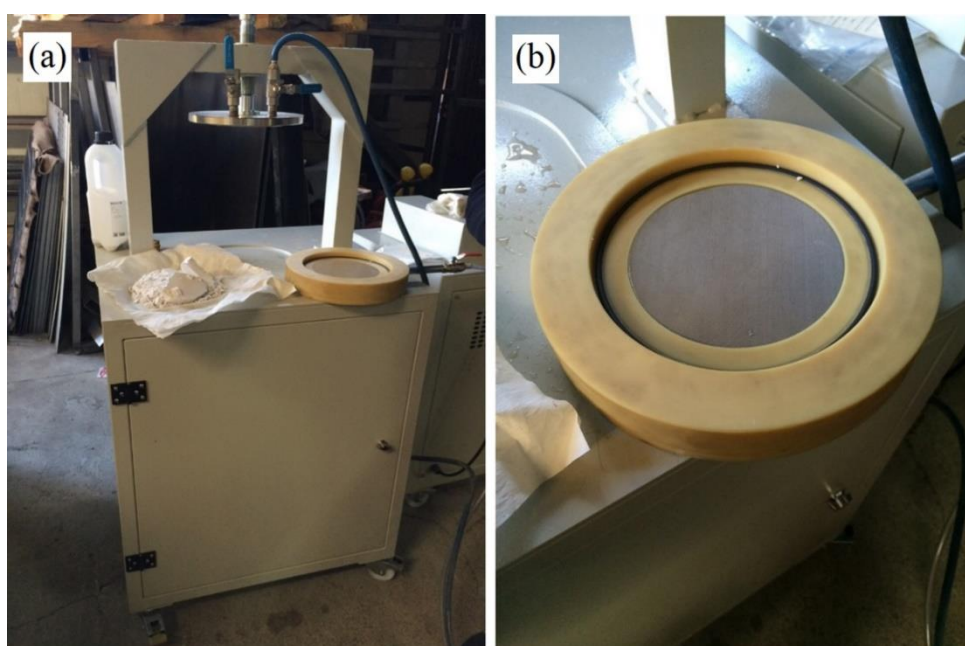
Figure 7.3. Pictures of the filtration system (a) with 1- μm mesh metal filter plate (b)

7.2   Synthesized Zeolites with Scale Up System

In this particular study, zeolite 4A was successfully synthesized from the calcination product of sodium feldspar, sodium carbonate, and aluminum hydroxide for the first time using the developed scale-up system. Sodium carbonate is a less hazardous chemical than sodium hydroxide with less cost. Optimized parameters of fusion,

aging, and reaction steps were used in this study. Almost 1 kg of synthesis product was obtained from every synthesis. Also, the reproducibility of this synthesis route was studied, and XRD patterns and the SEM images of the synthesized zeolites were shown in Figure 7.4 and Figure 7.5, respectively.
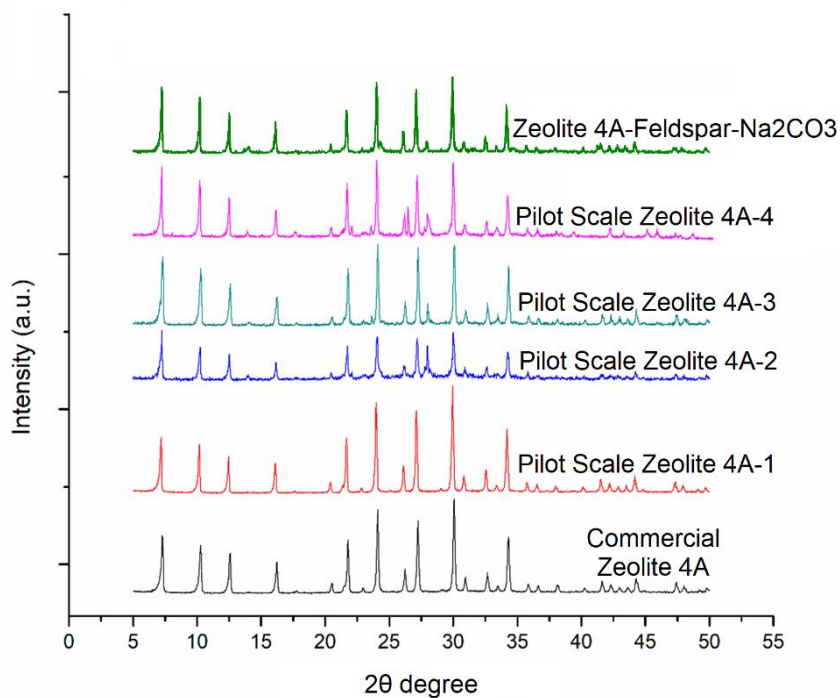
Figure 7.4. XRD pattern of zeolite 4A obtained from optimization studies, pilot-scale system, and commercial zeolite 4A.
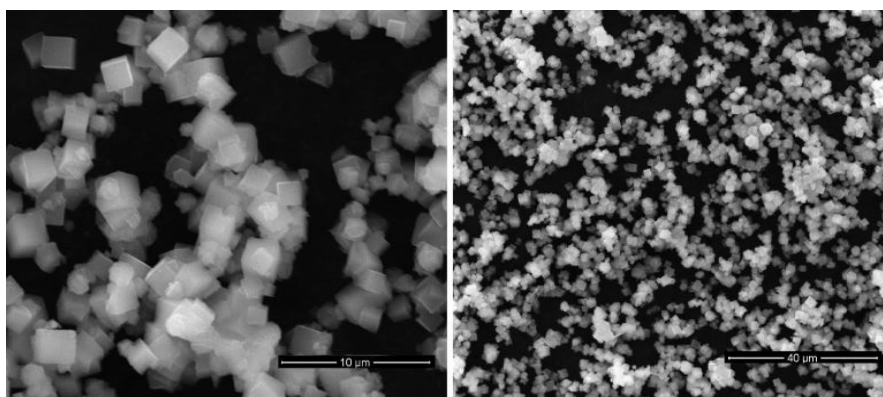
Figure 7.5. SEM images of zeolite 4A-1using using scale-up system zeolite 4A at different magnifications.

According to XRD patterns, zeolites with crystallinity values above 90% with respect to the commercial zeolite 4A were obtained can be synthesized with similar parameters with the laboratory-grade synthesis procedure. In this particular study, zeolites were aged at 60°C vessel for 4 h with continuous agitation while reaction took place at the second vessel at 100°C for 5 hours. Some agglomerations were observed in the SEM images given in Figure 7.5, which might be due to the uncontrolled stirring rate of the scale-up system. Particle size analyses were performed, and results obtained from 10 batch syntheses are summarized in Table 7.1.

Table 7.1 Average particle size analysis of zeolites obtained using the scale-up system and commercial zeolite 4A.

Zeolite Code	$d50$ (μm)	$d90$ (μm)
Commercial Zeolite 4A	3.06	5.90
Scale Up System Zeolite 4A-1	4.28	7.85
Scale Up System Zeolite 4A-2	4.65	8.79
Scale Up System Zeolite 4A-3	4.50	8.27
Scale Up System Zeolite 4A-4	4.48	8.30
Scale Up System Zeolite 4A-5	4.65	7.95
Scale Up System Zeolite 4A-6	3.98	6.25
Scale Up System Zeolite 4A-7	4.24	8.13
Scale Up System Zeolite 4A-8	4.88	9.12
Scale Up System Zeolite 4A-9	3.85	7.15
Scale Up System Zeolite 4A-10	4.05	8.42
Scale Up System Zeolite 4A-Average	4.24	7.83

The average particle size of products obtained from ten different batch syntheses runs was observed to be relatively higher with respect to the commercial zeolite 4A (4,24 μm for $d50$ and 7.83 for $d90$). These results may be related to the uncontrolled mixing rate in the aging tank, which could result in the lower dissolution of the

sodium aluminosilicates leading to the agglomeration of the crystals on top of the undissolved particles and acting as nuclei in zeolite formation.

Table 7.2 Water sorption capacities of scale-up system zeolites and commercial zeolite 4A

Zeolite Code	Weight Loss (wt. %)
Commercial Zeolite 4A	20.34
Scale Up System Zeolite 4A-1	19.25
Scale Up System Zeolite 4A-2	19.83
Scale Up System Zeolite 4A-3	20.08
Scale Up System Zeolite 4A-Average	19.72

The average water sorption capacity of the synthesized zeolites was 19.7 wt. % while commercial zeolite 4A was 20,3 wt. %. Although not very significant, the 0.6 wt. % difference might be caused by the larger average particle size of the agglomerated particles. It was observed that the scale-up system zeolites showed two peaks, while laboratory-scale synthesis showed one peak in particle size distribution analysis shown in Figure 7.6.
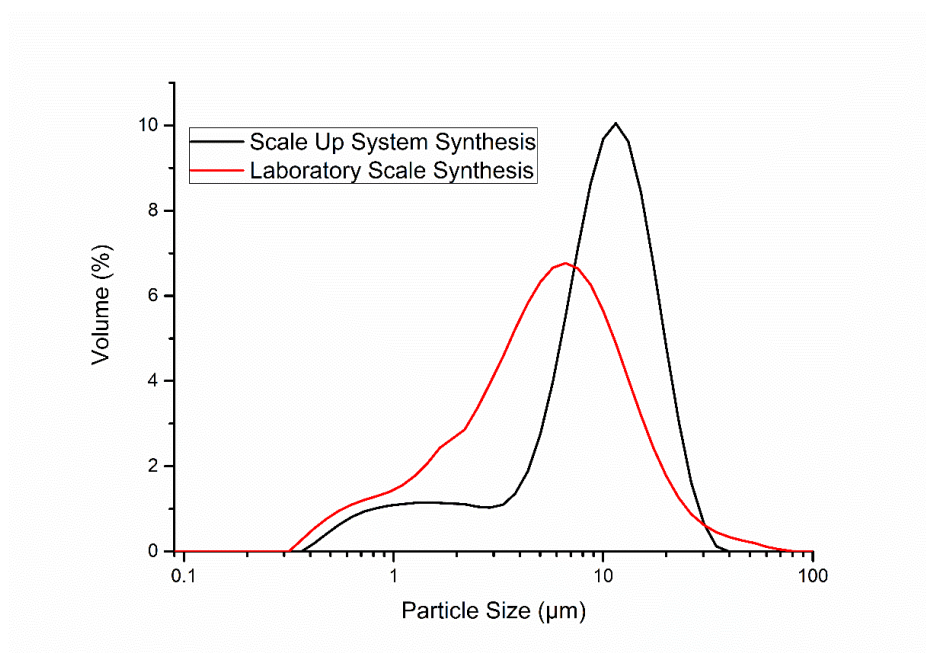
Figure 7.6. Particle size distributions of scale-up system zeolites and laboratory-scale zeolites.

The bigger average particle size of the scale-up system zeolites might be formed with agglomerations since no quenching was applied after the synthesis of the zeolites. After the reaction took place in the second vessel at 100°C, the resulting particles cooled down naturally for a more extended period of time. This natural cooling step could cause agglomerations and increase the product's average particle size.

Since the diffusion length of the water molecules is higher in average particle-sized zeolites, the adsorption and desorption mechanism could be acting slower in the products made using the scale-up system.

Also, applicational characterizations were performed with the synthesized zeolites as asphalt additives to form warm mix asphalts (WMA). Viscosity measurements were performed with scale-up system zeolite 4A added mixtures and compared with two commercial additives (Advera and Aspha-min). Results of these tests are given in Figure 7.7.
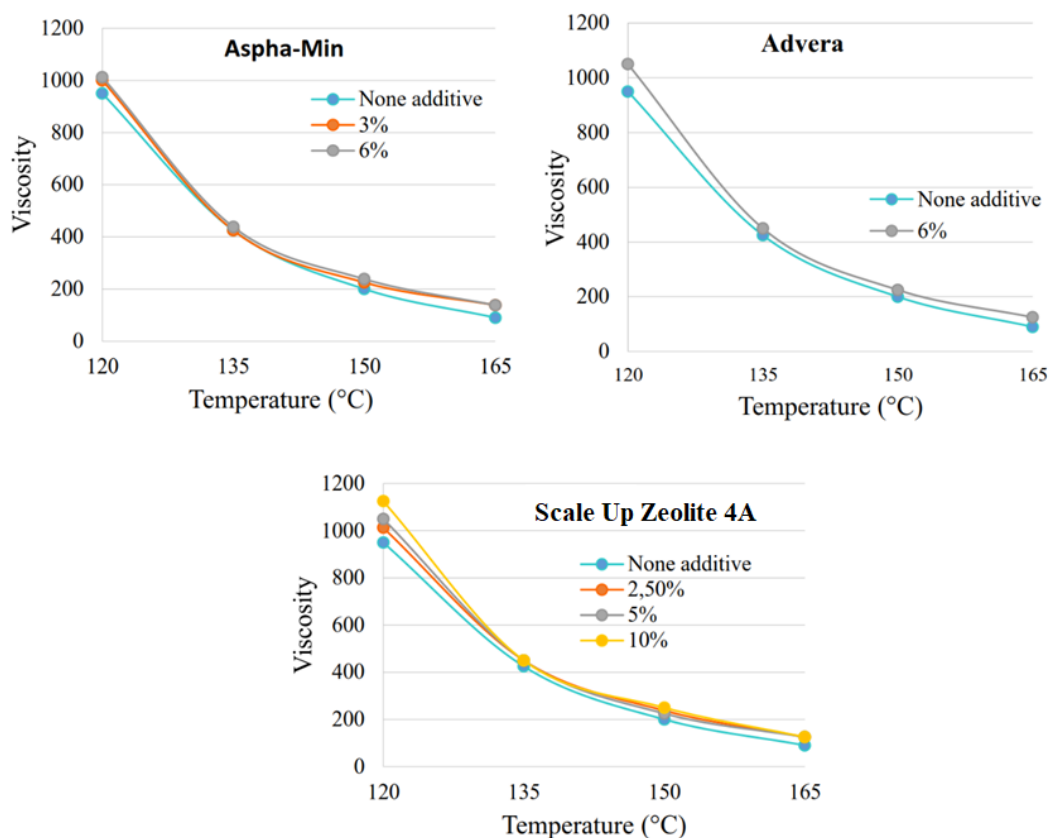
Figure 7.7. Viscosity results of WMA prepared with Advera, Aspha-min, and Scale-Up Zeolite 4A

According to the viscosity tests, it is clear that the viscosity increases with the addition of the additive. In addition, Scale Up Zeolite 4A is as effective as the commercial additives. It especially showed superior performance against commercial products at lower temperatures. However, it is also essential to analyze the effect on the asphalt mixtures. To be able to investigate the asphalts prepared with additives, compactability tests were performed, and results were shown in Figure 7.8.
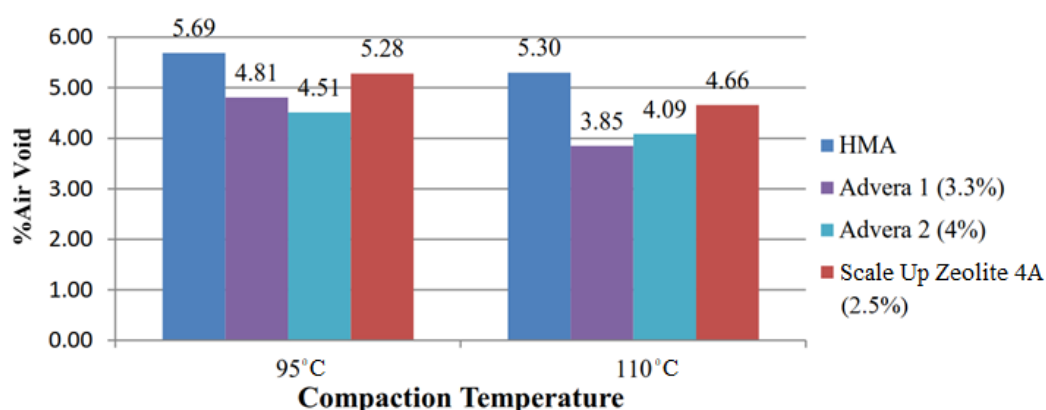
Figure 7.8. Air Voids of Asphalt Mixtures with respect to compaction temperatures

As shown in Figure 7.8, Scale Up Zeolite 4A improves the compaction at lower temperatures with respect to hot mix asphalt. Further studies with increasing dosages of zeolites for better understanding and comparison with commercial warm mix asphalt additives shall be performed.

7.3   Conclusion

Zeolite 4A crystals were successfully synthesized with the designed scale-up system composed of two heated and stirred reactors and a filtration system. The resulting zeolites were characterized with SEM, XRD, particle size analyzer, and TGA to better understand the characteristic properties of synthesized zeolites. Average particle sizes of the synthesized zeolites were relatively higher due to the agglomerated crystals on undissolved fusion products during the aging step. The larger average particle size of the synthesized zeolites showed slightly lower water sorption capacity over commercial zeolites due to the possible higher diffusion length for water molecules and the disordered nature of the agglomerated zeolite crystals.

Nevertheless, this system allowed the investigated proof-of-concept routes, i.e., one-pot-fusion, to be carried into industrial testing operations. The developed materials

were tested in many industrial partners, and several patent applications were made throughout the study. These industrial application areas can be summarized as antibacterial compounds, asphalt mixing industry, dry powder paint production, detergent producers, and desiccant industries. A summary of enhancements that could be made in order to take this work into the next step for successful national zeolite production in the future is given below.

CHAPTER 8

SUMMARY, CONCLUSIONS & FUTURE WORK

As the final chapter, raw material activation types, synthesis of zeolites from the activated semi-products, and applicational characterizations will be summarized and concluded.

8.1   Selection and Activation of Raw Materials

This thesis study aimed to evaluate the possibility of market-competitive, cost-effective zeolite synthesis by using locally available raw materials. For this purpose, two primary raw materials were used; kaolin and sodium feldspar.

It was found that zeolite 4A can be easily synthesized from kaolin by the metakaolinization method. Kaolin is one of the most suitable raw materials for zeolite 4A synthesis. It has a Si/Al ratio of 1, similar to zeolite 4A with a perfect match, and the metakaolinization process basically involves heating the raw material to temperatures higher than 600°C. However, the quality of the raw material itself is an important parameter that defines the specifications of the final product. The method developed needs to be adjusted for every application to be used in the industry. This adaptation usually needs more hard work using clays as raw materials rather than commercial products. Due to these drawbacks, the current study introduced two alternative approaches: alkali fusion and one-pot fusion of kaolin sources with additives [213]. These methods are beneficial due to the ease of control on the gel formulation in the primary step and converting quartz-like structures into water-soluble silicates.

On the other hand, zeolite 13X, which has a higher Si/Al ratio with respect to zeolite 4A, is more suitable for its synthesis from sodium feldspar sources. The only

disadvantage of feldspars, due to their tectosilicate structure, is the impossibility of generating an amorphous form of it by a simple heat treatment like kaolins. Thus, Sodium feldspars had to be subjected to alkaline fusion with sodium hydroxide and sodium carbonate to generate soluble aluminosilicates. Nevertheless, due to the chemical composition of sodium feldspars involving sodium in its chemical composition (rather than potassium), the required amount of sodium source used in the fusions was decreased up to 15 wt.%, which had a significant benefit in cost-reduction [214].

One-pot fusion was shown to be an innovative approach due to the total control on the gel formulation, which resulted in effortless conversion of fused product into zeolites by the simple addition of water, just like instant soup preparation. Also, this method enabled one to convert any kaolin source with a high amount of quartz impurity in the structure into a well crystalline zeolite with desired gel formulation adjustments without any pre and/or post-treatments.

Activated materials such as metakaolins of alkaline fused and one-pot fused products can be stored in closed containers allowing synthesis to be performed afterward using the stored semi-products. Since zeolite synthesis is mostly a batch synthesis process, it can be very advantageous to store the semi-products for further operations.

8.2   Zeolite 4A & Zeolite 13X Synthesis in Laboratory Scale

The methods for successfully synthesizing zeolite 4A and zeolite 13X crystals were developed from various kaolin [212] and sodium feldspar sources [214] in the current thesis study. Both activation and synthesis parameters were optimized on selected kaolin and sodium feldspar sources. Later, these methods were adopted to the other sources with varying chemical compositions [215]. The zeolites' production was performed using well-known hydrothermal synthesis methods with appropriate gel formulations for zeolite 4A and zeolite 13X. Since all the silica and alumina sources were placed in the vessel simultaneously, unlike laboratory-grade

144

chemicals used during standard synthesis, dissolution of silica and alumina species and formation of nuclei happens simultaneously. This was thought to be the main drawback of the methods developed since the sodium aluminosilicate species in the semi-product could act as a nucleation center and growth promoter. Accordingly, large agglomerations and intergrown crystals were observed in the synthesized products.

8.3   Direct Synthesis of Zeolite 3A & Zeolite 5A

Zeolite 3A and zeolite 5A are obtained by several process steps of subjecting zeolite 4A to ion-exchange step in the industry. In this study, zeolite 3A and zeolite 5A were directly synthesized from locally available raw materials by replacing the sodium-containing alkaline agents with locally available calcite or potash minerals possessing calcium or potassium for the first time [216].

In this way, it is possible to synthesize zeolite 3A and zeolite 5A with total control on the Ca/Na and K/Na ratio, which is very critical for their use in industry. One other superior property of the direct synthesis method is that it shortens the processing times by getting rid of the ion exchange procedure, which usually takes more than 24 h. The proposed mechanism is beneficial in several ways, such as shortening the production time, decreasing the energy and workforce used in the production, and cost-effectiveness by utilizing locally available raw materials such as calcite and potash instead of industrial-grade chemicals as calcium/potassium chlorides.

8.4   Synthesis of Zeolites in Scale-Up System

Zeolite 4A was successfully synthesized in the Scale-up system designed and built-in as a part of the San-Tez Project coded "0162.STZ.2013-01". Reproducibility studies were performed on the Scale-up system, and similar results were obtained in every batch operation. This particular study used gel formulations and synthesis

parameters for zeolite 4A, which was optimized in Chapter 4. Over 1 kg of the product was obtained from every batch synthesis from the Scale-Up System. The developed system can also be operated in a semi-batch mode where two tanks function for aging and reaction steps connected in series.

Synthesized zeolites were characterized with SEM, XRD, particle size analyzers, and TGA for water sorption capabilities. The synthesized zeolite crystals were shown to have competing performances compared to their industrial counterparts.

8.5   Suggestions and Future Work

This thesis deeply investigated zeolite synthesis from locally available raw materials such as kaolin and sodium feldspar with different activation methods. This study opened the gateway for extending the developed method to new locally available raw materials or waste products, such as natural zeolites (clinoptilolite), pyrophyllite, halloysite, and fly-ash.

Due to the nature of the one-pot fusion method, the dissolution of sodium aluminosilicate species and the formation of crystal nuclei co-occur, generating agglomerations in the final products. These agglomerations can be controlled by specific adjustments in the aging parameters, such as lowering the temperature and increasing time to allow the dissolution of sources before nucleation begins.

Zeolite 3A and Zeolite 5A were directly synthesized from sodium feldspar with calcite and potash as alkaline agents for the first time with the previously optimized parameters for zeolite 4A in Chapter 4. The ranges of Ca/Na and K/Na ratios and their constraints can be further studied. Also, another approach can be utilized to include metallic ions such as silver, zinc, and copper to synthesize antibacterial zeolites directly, eliminating the need for extra ion-exchange steps.

Fusion was shown to be an essentially critical step in the current thesis study, which was shown to generate the "semi-product" of sodium aluminosilicate species out of any raw material available in that particular local environment. This step was the

most energy-consuming part of the zeolite production process since high temperatures shall be achieved up to 900°C. Alternative activation studies can be performed to replace the alkaline fusion with mechanical systems such as ball milling. In this alternative, high energy in the colliding balls can generate the desired sodium aluminosilicates, and the most energy-consuming section of zeolite production can be eliminated.

REFERENCES

[1] C. Colella, W.S. Wise, The IZA Handbook of Natural Zeolites: A tool of knowledge on the most important family of porous minerals, Microporous Mesoporous Mater. 189 (2014) 4–10. https://doi.org/10.1016/j.micromeso.2013.08.028.

[2] E.M. Flanigen, Chapter 2 Zeolites and Molecular Sieves an Historical Perspective, Stud. Surf. Sci. Catal. 58 (1991) 13–34. https://doi.org/10.1016/S0167-2991(08)63599-5.

[3] T.B. Reed, D.W. Breck, Crystalline Zeolites. II. Crystal Structure of Synthetic Zeolite, Type A, J. Am. Chem. Soc. 78 (1956) 5972–5977. https://doi.org/10.1021/ja01604a002.

[4] D.W. Breck, Crystalline Zeolite Y, 3,130,007, 1964.

[5] R.M. Milton, Molecular Sieve Adsorbents, 2,882,244, 1959.

[6] I.M. Kalogeras, A.B. Vassilikou-Dova, Electrical Properties of Zeolitic Catalysts, Defect Diffus. Forum. 164 (1998) 1–36. https://doi.org/10.4028/www.scientific.net/DDF.164.1.

[7] D.W. Breck, Zeolite Molecular Sieves, John Wiley& Sons, New York, 1974. https://doi.org/https://doi.org/10.1093/chromsci/13.4.18A-c.

[8] D.H.O. C. Baerlocher, L.B. McCusker, Atlas of Zeolite Framework Types, 6th editio, Elsevier, 2007.

[9] Database of Zeolite Structures, (n.d.). https://europe.iza-structure.org/IZA-SC/ftc_table.php (accessed January 10, 2021).

[10] M. Moshoeshoe, M.S. Nadiye-Tabbiruka, V. Obuseng, A review of the Chemistry, Structure, Properties and Applications of Zeolites, Am. J. Mater. Sci. 7 (2017) 191–221. https://doi.org/10.5923/j.materials.20170705.12.

[11] E. Erdem, N. Karapinar, R. Donat, The removal of heavy metal cations by

natural zeolites, J. Colloid Interface Sci. 280 (2004) 309–314. https://doi.org/10.1016/j.jcis.2004.08.028.

[12] V. Berkgaut, A. Singer, High capacity cation exchanger by hydrothermal zeolitization of coal fly ash, Appl. Clay Sci. 10 (1996) 369–378. https://doi.org/10.1016/0169-1317(95)00033-X.

[13] A. Corma, M.E. Domine, S. Valencia, Water-resistant solid Lewis acid catalysts: Meerwein-Ponndorf-Verley and Oppenauer reactions catalyzed by tin-beta zeolite, J. Catal. 215 (2003) 294–304. https://doi.org/10.1016/S0021-9517(03)00014-9.

[14] A. Fritz, V. Pitchon, The current state of research on automotive lean NO(χ) catalysis, Appl. Catal. B Environ. 13 (1997) 1–25. https://doi.org/10.1016/S0926-3373(96)00102-6.

[15] S.M. Kuznicki, V.A. Bell, S. Nair, H.W. Hillhouse, R.M. Jacubinas, C.M. Braunbarth, B.H. Toby, M. Tsapatsis, A titanosilicate molecular sieve with adjustable pores for size-selective adsorption of molecules, Nature. 412 (2001) 720–724. https://doi.org/10.1038/35089052.

[16] Y. Yan, M.E. Davis, G.R. Gavalas, Preparation of Zeolite ZSM-5 Membranes by In-Situ Crystallization on Porous α-Al2O3, Ind. Eng. Chem. Res. 34 (1995) 1652–1661. https://doi.org/10.1021/ie00044a018.

[17] K.I. Okamoto, H. Kita, K. Horii, K. Tanaka, M. Kondo, Zeolite NaA membrane: Preparation, single-gas permeation, and pervaporation and vapor permeation of water/organic liquid mixtures, Ind. Eng. Chem. Res. 40 (2001) 163–175. https://doi.org/10.1021/ie0006007.

[18] L.C. Boudreau, J.A. Kuck, M. Tsapatsis, Deposition of oriented zeolite A films: In situ and secondary growth, J. Memb. Sci. 152 (1999) 41–59. https://doi.org/10.1016/S0376-7388(98)00166-5.

[19] A.R.R. Loiola, J.C.R.A.C.R.A. Andrade, J.M.M. Sasaki, L.R.D.R.D. da

Silva, Structural analysis of zeolite NaA synthesized by a cost-effective hydrothermal method using kaolin and its use as water softener, J. Colloid Interface Sci. 367 (2012) 34–39. https://doi.org/10.1016/j.jcis.2010.11.026.

[20]   L. Ayele, J. Pérez-Pariente, Y. Chebude, I. Diaz, Synthesis of zeolite A using kaolin from Ethiopia and its application in detergents, New J. Chem. 40 (2016) 3440–3446. https://doi.org/10.1039/c5nj03097h.

[21]   E. Costa, A. de Lucas, M.A. Uguina, J. Carlos Ruíz, Synthesis of 4A Zeolite from Calcined Kaolins for Use in Detergents, Ind. Eng. Chem. Res. 27 (1988) 1291–1296. https://doi.org/10.1021/ie00079a033.

[22]   R.P. Silverman, United States Patent (19), (1996).

[23]   Südchemie, Desiccant Performance Data, (2011) 1–2. http://www.agmcontainer.com/desiccantcity/pdfs/Desiccant performance.pdf.

[24]   Zeochem, Zeolites in Insulated Glass Healthier Living Spaces and Reducing Energy Costs, (n.d.). https://www.zeochem.com/news/zeolites-in-insulated-glass-healthier-living-spaces-and-reducing-energy-costs.

[25]   N. Zeolan, Teknik Bilgilendirme Zeolan / Nanomol Nem Alıcılar Teknik Bilgilendirme, (2020).

[26]   S. Kulprathipanja, Zeolites in Industrial Separation and Catalysis, Wiley-VCH Verlag GmbH & Co. KGaA, Great Britain, 2010. https://doi.org/10.1002/9783527629565.

[27]   N. Kosinov, J. Gascon, F. Kapteijn, E.J.M. Hensen, Recent developments in zeolite membranes for gas separation, J. Memb. Sci. 499 (2016) 65–79. https://doi.org/10.1016/j.memsci.2015.10.049.

[28]   X. Zou, G. Zhu, Gas Separations with Zeolite Membranes, Microporous Mater. Sep. Membr. (2019) 225–254. https://doi.org/10.1002/9783527343997.ch7.

[29] A. Palčić, V. Valtchev, Analysis and control of acid sites in zeolites, Appl. Catal. A Gen. 606 (2020) 117795. https://doi.org/10.1016/j.apcata.2020.117795.

[30] B. Xu, C. Sievers, S.B. Hong, R. Prins, J.A. van Bokhoven, Catalytic activity of Brønsted acid sites in zeolites: Intrinsic activity, rate-limiting step, and influence of the local structure of the acid sites, J. Catal. 244 (2006) 163–168. https://doi.org/10.1016/j.jcat.2006.08.022.

[31] W. Schirmer, Molecular Transport and Reaction in Zeolites — Design and Application of Shape Selective Catalysis, Zeitschrift Für Phys. Chemie. 191 (1995) 282–282. https://doi.org/10.1524/zpch.1995.191.part_2.282.

[32] S.M. Csicsery, Sigmund M. Csicsery, Shape-selective catalysis in zeolites.pdf, Zeolites. 4 (1984) 116–126.

[33] W. Vermeiren, J.P. Gilson, Impact of zeolites on the petroleum and petrochemical industry, Top. Catal. 52 (2009) 1131–1161. https://doi.org/10.1007/s11244-009-9271-8.

[34] P.T. Huong, J. Kim, B. Lee, Low - cost removal of polar aromatics pollutant by Using Nano Zeolite, (n.d.) 124–130.

[35] T. Sakano, H. Tamon, M. Miyahara, M. Okazaki, Adsorption Selectivity of Coffee Aroma Components on Zeolite 5A., Food Sci. Technol. Int. Tokyo. 2 (2009) 174–179. https://doi.org/10.3136/fsti9596t9798.2.174.

[36] M. Miyahara, H. Tamon, K. Yamakura, M. Okazaki, T. Sakano, Improvement of Coffee Aroma by Removal of Pungent Volatiles Using A-Type Zeolite, J. Food Sci. 61 (2006) 473–476. https://doi.org/10.1111/j.1365-2621.1996.tb14220.x.

[37] R. Tekin, N. Bac, J. Warzywoda, A. Sacco, Encapsulation of a fragrance molecule in zeolite X, Microporous Mesoporous Mater. 215 (2015) 51–57. https://doi.org/10.1016/j.micromeso.2015.05.020.

[38]   R. Tekin, H. Erdogmus, N. Bac, Assessment of Zeolites as Antimicrobial
        Fragrance Carriers Assessment of Zeolites as Antimicrobial Fragrance
        Carriers, Antimicrob. Res. Nov. Bioknowledge Educ. Programs (A.
        Mendez-Vilas, Ed.). (2017).

[39]   D.M. Ruthven, B.K. Kaul, Adsorption of Aromatic Hydrocarbons in NaX
        Zeolite. 2. Kinetics, Ind. Eng. Chem. Res. 32 (1993) 2053–2057.
        https://doi.org/10.1021/ie00021a029.

[40]   A. Helmut Jerg, G., Painter, (12) Patent Application Publication (10) Pub
        . No .: US 2010 / 0035098 A1 Patent Application Publication, US Pat.
        2010/0101613 A1. 1 (2010).
        https://patentimages.storage.googleapis.com/3b/c9/82/c283c7b24afe69/US2
        0100019677A1.pdf.

[41]   H.T. Johann Wienen, Marcel Neubert, Rainer Lang, Results from field trial
        with gas heat pump zeotherm by Vaillant, in: A. Kühn (Ed.), Therm. Driven
        Heat Pumps Heat. Cool., Berlin, 2013: pp. 27–37.

[42]   Alumina d.o.o. Products: Zeolite, (n.d.).
        https://www.aluminazv.ba/en/category-products/6.

[43]   SorbentSystem.com, Desiccant Chart Comparisons - SorbentSystems,
        (2015). https://www.sorbentsystems.com/desiccants_charts.html.

[44]   G. García, W. Aguilar-Mamani, I. Carabante, S. Cabrera, J. Hedlund, J.
        Mouzon, Preparation of zeolite A with excellent optical properties from
        clay, J. Alloys Compd. 619 (2015) 771–777.
        https://doi.org/10.1016/j.jallcom.2014.09.080.

[45]   C. Fruijtier-Pölloth, The safety of synthetic zeolites used in detergents,
        Arch. Toxicol. 83 (2009) 23–35. https://doi.org/10.1007/s00204-008-0327-
        5.

[46]   K.S. Hui, C.Y.H. Chao, Pure, single phase, high crystalline, chamfered-edge

zeolite 4A synthesized from coal fly ash for use as a builder in detergents, J. Hazard. Mater. 137 (2006) 401–409. https://doi.org/10.1016/j.jhazmat.2006.02.014.

[47] S.M. Al-Jubouri, H.A. Sabbar, H.A. Lafta, B.I. Waisi, Effect of synthesis parameters on the formation 4a zeolite crystals: Characterization analysis and heavy metals uptake performance study for water treatment, Desalin. Water Treat. 165 (2019) 290–300. https://doi.org/10.5004/dwt.2019.24566.

[48] P.Q. Corporation, Doucil 4A zeolite ®, (n.d.) 20–23. https://www.pqcorp.com/products/zeolites/doucil.

[49] A. Diab, Z. You, H. Wang, Rheological Evaluation of Foamed WMA Modified with Nano Hydrated Lime, Procedia - Soc. Behav. Sci. 96 (2013) 2858–2866. https://doi.org/10.1016/j.sbspro.2013.08.318.

[50] M. Marinković, T. Milović, B. Matić, Zeolit Kao Aditiv U Toplim Asfaltnim Mešavinama, Zb. Rad. Građevinskog Fak. 33 (2017) 483–490. https://doi.org/10.14415/konferencijagfs2017.051.

[51] D. Wen, Y.S. Ho, X. Tang, Comparative sorption kinetic studies of ammonium onto zeolite, J. Hazard. Mater. 133 (2006) 252–256. https://doi.org/10.1016/j.jhazmat.2005.10.020.

[52] Y. Adiguzel, H. Kulah, Biosensors and Bioelectronics Breath sensors for lung cancer diagnosis, Biosens. Bioelectron. 65 (2015) 121–138. https://doi.org/10.1016/j.bios.2014.10.023.

[53] O.O. Soldatkin, B.O. Kasap, S. V Dzyadevych, V.M. Arkhypova, B. Akata, M.K. Shelyakina, Study of zeolite influence on analytical characteristics of urea biosensor based on ion-selective field-effect transistors, Nanoscale Res. Lett. 9 (2014) 124. https://doi.org/10.1186/1556-276x-9-124.

[54] B. Ozansoy Kasap, S. V. Marchenko, O.O. Soldatkin, S. V. Dzyadevych, B. Akata Kurc, Biosensors Based on Nano-Gold/Zeolite-Modified Ion

Selective Field-Effect Transistors for Creatinine Detection, Nanoscale Res. Lett. 12 (2017). https://doi.org/10.1186/s11671-017-1943-x.

[55] J. Wang, A. Walcarius, Zeolite containing oxidase-based carbon paste biosensors, J. Electroanal. Chem. 404 (1996) 237–242. https://doi.org/10.1016/0022-0728(95)04357-8.

[56] A.T. Güntner, S. Abegg, K. Wegner, S.E. Pratsinis, Zeolite membranes for highly selective formaldehyde sensors, Sensors Actuators, B Chem. 257 (2018) 916–923. https://doi.org/10.1016/j.snb.2017.11.035.

[57] J. Santamaría, M. Vilaseca, A. Cirera, J.R. Morante, A. Cornet, J. Coronas, Use of zeolite films to improve the selectivity of reactive gas sensors, Catal. Today. 82 (2003) 179–185. https://doi.org/10.1016/s0920-5861(03)00230-x.

[58] G.P. Alcantara, L.E.B. Ribeiro, A.F. Alves, C.M.G. Andrade, F. Fruett, Humidity sensor based on zeolite for application under environmental conditions, Microporous Mesoporous Mater. 247 (2017) 38–45. https://doi.org/10.1016/j.micromeso.2017.03.042.

[59] S. Mintova, S. Mo, T. Bein, Humidity sensing with ultrathin LTA-type molecular sieve films grown on piezoelectric devices, Chem. Mater. 13 (2001) 901–905. https://doi.org/10.1021/cm000671w.

[60] Global Zeolite Industry, (n.d.). https://www.reportlinker.com/p05960558/Global-Zeolite-Industry.html (accessed January 10, 2021).

[61] T. Maesen, B. Marcus, Chapter 1 The zeolite scene—An overview, Stud. Surf. Sci. Catal. 137 (2001) 1–9. https://doi.org/10.1016/S0167-2991(01)80242-1.

[62] Synthetic Zeolites Market worth $5.9 billion by 2023, (n.d.). https://www.marketsandmarkets.com/PressReleases/synthetic-zeolite.asp (accessed January 10, 2021).

[63] J. Köhler, Detergent Phosphates : an EU Policy Assessment, Inst. Bus. Adm. 2 (2006) 15–30.

[64] T. Ogawa, K. Iyoki, T. Fukushima, Y. Kajikawa, Landscape of research areas for zeolites and metal-organic frameworks using computational classification based on citation networks, Materials (Basel). 10 (2017) 1–20. https://doi.org/10.3390/ma10121428.

[65] Z. Xue, Z. Li, J. Ma, X. Bai, Y. Kang, W. Hao, R. Li, Effective removal of Mg2+ and Ca2+ ions by mesoporous LTA zeolite, Desalination. 341 (2014) 10–18. https://doi.org/10.1016/j.desal.2014.02.025.

[66] R.M. Mohamed, A.A. Ismail, G. Kini, I.A. Ibrahim, B. Koopman, Synthesis of highly ordered cubic zeolite A and its ion-exchange behavior, Colloids Surfaces A Physicochem. Eng. Asp. 348 (2009) 87–92. https://doi.org/10.1016/j.colsurfa.2009.06.038.

[67] M. Maldonado, M.D. Oleksiak, S. Chinta, J.D. Rimer, Controlling crystal polymorphism in organic-free synthesis of na-zeolites, J. Am. Chem. Soc. 135 (2013) 2641–2652. https://doi.org/10.1021/ja3105939.

[68] J.M. Newsam, The zeolite cage structure, Science (80-.). 231 (1986) 1093–1099. https://doi.org/10.1126/science.231.4742.1093.

[69] B. Strzemiecka, M. Kasperkowiak, M. Łozyński, D. Paukszta, A. Voelkel, Examination of zeolites as fragrance carriers, Microporous Mesoporous Mater. 161 (2012) 106–114. https://doi.org/10.1016/j.micromeso.2012.05.024.

[70] E. Gabruś, J. Nastaj, P. Tabero, T. Aleksandrzak, Experimental studies on 3A and 4A zeolite molecular sieves regeneration in TSA process: Aliphatic alcohols dewatering-water desorption, Chem. Eng. J. 259 (2015) 232–242. https://doi.org/10.1016/j.cej.2014.07.108.

[71] R. Kusumastuti, Sriyono, M. Pancoko, S.L. Butar-Butar, G.E. Putra, H.

Tjahjono, Study on the Mechanism of CO2 Adsorption Process on zeolite
5A as a Molecular Sieve in RDE System: An Infrared Investigation, in: J.
Phys. Conf. Ser., IOP Publishing, 2019. https://doi.org/10.1088/1742-
6596/1198/3/032009.

[72]   J.C. Moreira, R.A.A.B. Santa, J. Nones, H.G. Riella, Synthesis of zeolite 4a
for obtaining zeolite 5A by ionic exchange for full utilization of waste from
paper industry, Brazilian J. Chem. Eng. 35 (2018) 623–630.
https://doi.org/10.1590/0104-6632.20180352s20160395.

[73]   L.V.C. Rees, Book Review, Zeolites. 1 (1981) 125.
https://doi.org/10.1016/S0144-2449(81)80027-9.

[74]   R.P. Townsend, Chapter 10 Ion Exchange in Zeolites, Stud. Surf. Sci. Catal.
58 (1991) 359–390. https://doi.org/10.1016/S0167-2991(08)63608-3.

[75]   B. Kadaifci, Multicomponent Ion Exchange on Zeolite 4A, Middle East
Technical University, 2011.

[76]   C.S. Cundy, P.A. Cox, The hydrothermal synthesis of zeolites: History and
development from the earliest days to the present time, Chem. Rev. 103
(2003) 663–701. https://doi.org/10.1021/cr020060i.

[77]   E.B.G. Johnson, S.E. Arshad, Hydrothermally synthesized zeolites based on
kaolinite: A review, Appl. Clay Sci. 97–98 (2014) 215–221.
https://doi.org/10.1016/j.clay.2014.06.005.

[78]   Database of Zeolite Structures, (n.d.). http://www.iza-
structure.org/databases/ (accessed September 2, 2019).

[79]   J. Yu, Synthesis of zeolites, Elsevier B.V., 2007.
https://doi.org/10.1016/S0167-2991(07)80791-9.

[80]   E.M. Flanigen, R.W. Broach, S.T. Wilson, Introduction, in: Zeolites Ind.
Sep. Catal., Wiley-VCH Verlag GmbH & Co. KGaA, Weinheim, Germany,
2010: pp. 1–26. https://doi.org/10.1002/9783527629565.ch1.

[81] J. Yu, Chapter 3 Synthesis of zeolites, Elsevier B.V., 2007.
      https://doi.org/10.1016/S0167-2991(07)80791-9.

[82] C. Du, H. Yang, Synthesis and characterization of zeolite 4A-type desiccant
      from kaolin, Am. Mineral. 95 (2010) 741–746.
      https://doi.org/10.2138/am.2010.3288.

[83] D.W. Breck, Crystalline Molecular Sieves, 41 (1964) 678–689.

[84] M. Zaarour, B. Dong, I. Naydenova, R. Retoux, S. Mintova, Progress in
      zeolite synthesis promotes advanced applications, Microporous Mesoporous
      Mater. 189 (2014) 11–21. https://doi.org/10.1016/j.micromeso.2013.08.014.

[85] F.E. Imbert, C. Moreno, A. Montero, B. Fontal, J. Lujano, Venezuelan
      natural alumosilicates as a feedstock in the synthesis of zeolite A, Zeolites.
      14 (1994) 374–378. https://doi.org/10.1016/0144-2449(94)90112-0.

[86] E.I. Basaldella, R.M.T. Sanchez, J.C. Tara, Iron influence in the
      aluminosilicate zeolites synthesis, 46 (1998) 481–486.
      https://doi.org/10.1346/CCMN.1998.0460501.

[87] M.A. Moneim, E.A. Ahmed, Synthesis of Faujasite from Egyptian Clays:
      Characterizations and Removal of Heavy Metals, Geomaterials. 05 (2015)
      68–76. https://doi.org/10.4236/gm.2015.52007.

[88] X. Bai, F., Hong-Wen M.A., Zhang, Experimental study on synthesis of
      13X zeolite molecular sieve from potassium feldspar powder by
      hydrothermal reaction, Bull. Mineral. Petrol. Geochemistry. 23 (2004) 10–
      14.

[89] S. Chandrasekhar, P.N. Pramada, Investigation on the synthesis of zeolite
      NaX from kerala kaolin, J. Porous Mater. 6 (1999) 283–297.
      https://doi.org/10.1023/A:1009632606671.

[90] I. Caballero, F.G. Colina, J. Costa, Synthesis of X-type zeolite from
      dealuminated kaolin by reaction with sulfuric acid at high temperature, Ind.

158

Eng. Chem. Res. 46 (2007) 1029–1038. https://doi.org/10.1021/ie060367y.

[91]   P. Wang, Q. Sun, Y. Zhang, J. Cao, Synthesis of zeolite 4A from kaolin and its adsorption equilibrium of carbon dioxide, Materials (Basel). 12 (2019) 1–12. https://doi.org/10.3390/ma12091536.

[92]   G. Garcia, E. Cardenas, S. Cabrera, J. Hedlund, J. Mouzon, Synthesis of zeolite y from diatomite as silica source, Microporous Mesoporous Mater. 219 (2016) 29–37. https://doi.org/10.1016/j.micromeso.2015.07.015.

[93]   A. Chaisena, K. Rangsriwatananon, Synthesis of sodium zeolites from natural and modified diatomite, Mater. Lett. 59 (2005) 1474–1479. https://doi.org/10.1016/j.matlet.2004.10.073.

[94]   T. Wajima, Y. Ikegami, Synthesis of crystalline zeolite-13X from waste porcelain using alkali fusion, Ceram. Int. 35 (2009) 2983–2986. https://doi.org/10.1016/j.ceramint.2009.03.014.

[95]   F. Querol, X., Moreno, N., Umana, J.C., Alastuey, A., Hernandez, E., Lopez-Soler, A., Plana, Synthesis of zeolites from coal fly ash: an overview, Int. J. Coal Geol. 50 (2002) 413–423. https://doi.org/10.1017/CBO9781107415324.004.

[96]   M. Inada, H. Tsujimoto, Y. Eguchi, N. Enomoto, J. Hojo, Microwave-assisted zeolite synthesis from coal fly ash in hydrothermal process, Fuel. 84 (2005) 1482–1486. https://doi.org/10.1016/j.fuel.2005.02.002.

[97]   M.A. Rahaman, M.A. Gafur, A.S.W. Kurny, Kinetics of Recovery of Alumina from Coal Fly Ash through Fusion with Sodium Hydroxide, Am. J. Mater. Eng. Technol. 1 (2013) 54–58. https://doi.org/10.12691/materials-1-3-6.

[98]   S.N. Ishmah, M.D. Permana, M.L. Firdaus, D.R. Eddy, Extraction of Silica from Bengkulu Beach Sand using Alkali Fusion Method, Pendipa J. Sci. Educ. 4 (2020) 1–5. https://doi.org/10.33369/pendipa.4.2.1-5.

[99] Handbook of Hydrothermal Technology - K. Byrappa, Masahiro
      Yoshimura, in: n.d.
      https://books.google.com.tr/books?hl=tr&lr=&id=vA5tXzLsHioC&oi=fnd
      &pg=PP1&ots=cyla5Vffhe&sig=guiIopV3PwjduGqa-
      zWeiNv9Jug&redir_esc=y#v=onepage&q&f=false (accessed January 10,
      2021).

[100] L. Ayele, J. Pérez-Pariente, Y. Chebude, I. Díaz, Conventional versus alkali
      fusion synthesis of zeolite A from low grade kaolin, Appl. Clay Sci. 132–
      133 (2016) 485–490. https://doi.org/10.1016/j.clay.2016.07.019.

[101] X.D. Liu, Y.P. Wang, X.M. Cui, Y. He, J. Mao, Influence of synthesis
      parameters on NaA zeolite crystals, Powder Technol. 243 (2013) 184–193.
      https://doi.org/10.1016/j.powtec.2013.03.048.

[102] W. Fan, S. Shirato, F. Gao, M. Ogura, T. Okubo, Phase selection of FAU
      and LTA zeolites by controlling synthesis parameters, Microporous
      Mesoporous Mater. 89 (2006) 227–234.
      https://doi.org/10.1016/j.micromeso.2005.11.001.

[103] S. Sivalingam, S. Sen, Optimization of synthesis parameters and
      characterization of coal fly ash derived microporous zeolite X, Appl. Surf.
      Sci. 455 (2018) 903–910. https://doi.org/10.1016/j.apsusc.2018.05.222.

[104] B. Bayati, A.A. Babaluo, R. Karimi, Hydrothermal synthesis of
      nanostructure NaA zeolite: The effect of synthesis parameters on zeolite
      seed size and crystallinity, J. Eur. Ceram. Soc. 28 (2008) 2653–2657.
      https://doi.org/10.1016/j.jeurceramsoc.2008.03.033.

[105] Hartati, D. Prasetyoko, M. Santoso, I. Qoniah, W.L. Leaw, P.B.D. Firda, H.
      Nur, A review on synthesis of kaolin-based zeolite and the effect of
      impurities, J. Chinese Chem. Soc. 67 (2020) 911–936.
      https://doi.org/10.1002/jccs.201900047.

[106] L. Ayele, J. Pérez-Pariente, Y. Chebude, I. Díaz, Synthesis of zeolite A

from Ethiopian kaolin, Microporous Mesoporous Mater. 215 (2015) 29–36. https://doi.org/10.1016/j.micromeso.2015.05.022.

[107] Y. Ma, C. Yan, A. Alshameri, X. Qiu, C. Zhou, D. Li, Synthesis and characterization of 13X zeolite from low-grade natural kaolin, Adv. Powder Technol. 25 (2014) 495–499. https://doi.org/10.1016/j.apt.2013.08.002.

[108] A.A.Y. Simanjuntak, E. Kusrini, Feasibility Study for Production of Zeolite A based on Kaolin, E3S Web Conf. 67 (2018) 1–5. https://doi.org/10.1051/e3sconf/20186702017.

[109] Jumaeri, S.J. Santosa, Sutarno, E.S. Kunarti, Synthesis of zeolite A from coal fly ash by alkali fusion and hydrothermal, Adv. Mater. Res. 1043 (2014) 198–203. https://doi.org/10.4028/www.scientific.net/AMR.1043.198.

[110] Y. Ma, C. Yan, A. Alshameri, X. Qiu, C. Zhou, D. Li, Synthesis and characterization of 13X zeolite from low-grade natural kaolin, Adv. Powder Technol. 25 (2014) 495–499. https://doi.org/10.1016/j.apt.2013.08.002.

[111] T. Abdullahi, Z. Harun, M.H.D. Othman, A review on sustainable synthesis of zeolite from kaolinite resources via hydrothermal process, Adv. Powder Technol. 28 (2017) 1827–1840. https://doi.org/10.1016/j.apt.2017.04.028.

[112] Chandrasekhar. S., Influence of metakaolinization temperature on the formation of zeolite 4A from kaolin, (1996) 253–261.

[113] L. Qiang, Z. Ying, C. Zhijun, G. Wei, C. Lishan, Influence of synthesis parameters on the crystallinity and Si/Al ratio of NaY zeolite synthesized from kaolin, Pet.Sci. 7 (2010) 403–409. https://doi.org/10.1007/s12182-010-0085-x.

[114] S.O. Otieno, F.O. Kengara, J.C. Kemmegne-Mbouguen, H.W. Langmi, C.B.O. Kowenje, R. Mokaya, The effects of metakaolinization and fused-metakaolinization on zeolites synthesized from quartz rich natural clays,

Microporous Mesoporous Mater. 290 (2019) 109668.
https://doi.org/10.1016/j.micromeso.2019.109668.

[115] M. Murat, A. Amokrane, J.P. Bastide, L. Montanaro, Synthesis of zeolites from thermally activated kaolinite. Some observations on nucleation and growth, Clay Miner. 27 (1992) 119–130.

[116] A.S. Kovo, S.M. Holmes, Effect of aging on the synthesis of kaolin-based zeolite Y from Ahoko Nigeria using a novel metakaolinization technique, J. Dispers. Sci. Technol. 31 (2010) 442–448. https://doi.org/10.1080/01932690903210218.

[117] A.S. Kovo, O. Hernandez, S.M. Holmes, Synthesis and characterization of zeolite y and ZSM-5 from Nigerian Ahoko Kaolin using a novel, lower temperature, metakaolinization technique, J. Mater. Chem. 19 (2009) 6207–6212. https://doi.org/10.1039/b907554b.

[118] M.A. Villaquirán-Caicedo, R.M. De Gutiérrez, M. Gordillo, N.C. Gallego, Synthesis of zeolites from a low-quality Colombian kaolin, Clays Clay Miner. 64 (2016) 75–85. https://doi.org/10.1346/CCMN.2016.0640201.

[119] J.A. González, M. del, Bleaching of kaolins and clays by chlorination of iron and titanium, Appl. Clay Sci. 33 (2006) 219–229. https://doi.org/10.1016/j.clay.2006.05.001.

[120] M. Chouafa, A. Idres, A. Bouhedja, K. Talhi, Chemical treatment of kaolin. case study of kaolin from the tamazert jijel mine, Min. Sci. 22 (2015) 171–180. https://doi.org/10.5277/msc152214.

[121] I. Lapides, L. Heller-Kallai, Reactions of metakaolinite with NaOH and colloidal silica - Comparison of different samples (part 2), Appl. Clay Sci. 35 (2007) 94–98. https://doi.org/10.1016/j.clay.2006.06.007.

[122] A.A. Mostafa, H.F. Youssef, A. Materials, Utilization of Egyptian kaolin for Zeolite-A Preparation and Performance Evaluation, Int. Conf. Environ. Sci.

Technol. 6 (2011) 43–48.

[123] H. Jülide Köroğlu, A. Sarioğlan, M. Tatlier, A. Erdem-Şenatalar, Ö. Tunç
Savaşçi, Effects of low-temperature gel aging on the synthesis of zeolite Y
at different alkalinities, J. Cryst. Growth. 241 (2002) 481–488.
https://doi.org/10.1016/S0022-0248(02)01321-0.

[124] H. Feng, C. Li, H. Shan, Effect of calcination temperature of kaolin
microspheres on the in situ synthesis of ZSM-5, Catal. Letters. 129 (2009)
71–78. https://doi.org/10.1007/s10562-008-9794-9.

[125] J. Zhang, X. Li, J. Liu, C. Wang, A comparative study of MFI zeolite
derived from different silica sources: Synthesis, characterization and
catalytic performance, Catalysts. 9 (2019).
https://doi.org/10.3390/catal9010013.

[126] F. Di Renzo, F. Remoué, P. Massiani, F. Fajula, F. Figueras, C. Thierry
Des, Crystallization kinetics of zeolite TON, Zeolites. 11 (1991) 539–548.
https://doi.org/10.1016/S0144-2449(05)80002-8.

[127] J. Ciric, Kinetics of zeolite A crystallization, J. Colloid Interface Sci. 28
(1968) 315–324. https://doi.org/10.1016/0021-9797(68)90135-5.

[128] A. Giaya, R.W. Thompson, Recovering the Crystal Size Distribution from
the Moment Equations, AIChE J. 50 (2004) 879–882.
https://doi.org/10.1002/aic.10084.

[129] S. Su, H. Ma, X. Chuan, Hydrothermal synthesis of zeolite A from K-
feldspar and its crystallization mechanism, Adv. Powder Technol. 27 (2016)
139–144. https://doi.org/10.1016/j.apt.2015.11.011.

[130] E.M. Flanigen, Zeolites and Molecular Sieves, Zeolites Mol. Sieves An
Hist. Perspect. 1862 (2003) 157–190.
https://doi.org/10.1002/047144409x.ch7.

[131] G.E. Christidis, H. Papantoni, Synthesis of FAU Type Zeolite Y from

Natural Raw Materials: Hydrothermal SiO2-Sinter and Perlite Glass, Open Mineral. J. 2 (2008) 1–5. https://doi.org/10.2174/1874456700802010001.

[132] H.M. Aly, M.E. Moustafa, E.A. Abdelrahman, Influence of Aluminum Source on the Synthesis of Nanosized ZSM-5 Zeolite, (n.d.). www.pelagiaresearchlibrary.com (accessed January 10, 2021).

[133] M.D. Oleksiak, J.D. Rimer, Synthesis of zeolites in the absence of organic structure-directing agents: Factors governing crystal selection and polymorphism, Rev. Chem. Eng. 30 (2014) 1–49. https://doi.org/10.1515/revce-2013-0020.

[134] C. Belviso, C. Cannas, N. Pinna, F. Cavalcante, A. Lettino, P. Lotti, G.D. Gatta, Effect of red mud added to zeolite LTA synthesis: Where is Fe in the newly-formed material?, Microporous Mesoporous Mater. 298 (2020) 110058. https://doi.org/10.1016/j.micromeso.2020.110058.

[135] Y.L. Zhu, Z.H. Chang, J. Pang, C.J. Xiong, Synthesis of Zeolite 4A from Kaolin and Bauxite by Alkaline Fusion at Low Temperature, Mater. Sci. Forum. 685 (2011) 298–306. https://doi.org/10.4028/www.scientific.net/MSF.685.298.

[136] K. Wruck, G.J. Millar, T. Wang, Transformation of heulandite type natural zeolites into synthetic zeolite LTA, Environ. Technol. Innov. 21 (2021) 101371. https://doi.org/10.1016/j.eti.2021.101371.

[137] Y. Wang, Transformation of natural clinoptilolite to high purity of synthetic zeolits, Appl. Mech. Mater. 466–467 (2012) 42–46. https://doi.org/10.4028/www.scientific.net/AMR.466-467.42.

[138] R.M. Barrer, Hydrothermal chemistry of zeolites, London : Academic press, 1982. http://lib.ugent.be/catalog/rug01:000907067.

[139] V.Y. Prokofév, N.E. Gordina, A.B. Zhidkova, A.M. Efremov, Mechanochemical synthesis of granulated LTA zeolite from metakaolin, J.

Mater. Sci. 47 (2012) 5385–5392. https://doi.org/10.1007/s10853-012-6421-3.

[140] T.A. Aragaw, A.A. Ayalew, Removal of water hardness using zeolite synthesized from Ethiopian kaolin by hydrothermal method, Water Pract. Technol. 14 (2019) 145–159. https://doi.org/10.2166/wpt.2018.116.

[141] Y. Bai, W. Wu, X. Bian, Dynamic synthesis route of zeolite y with kaolin to improve yield, Green Process. Synth. 7 (2018) 23–29. https://doi.org/10.1515/gps-2016-0172.

[142] D. Hartanto, A.B. Pambudi, D.N. Cahyanti, W.P. Utomo, On the Synthesis of ZSM-5 Directly from Kaolin Bangka with Aging Time, IOP Conf. Ser. Mater. Sci. Eng. 588 (2019). https://doi.org/10.1088/1757-899X/588/1/012039.

[143] Feldspar - Industrial Minerals Association Europe, (n.d.). https://ima-europe.eu/about-industrial-minerals/feldspar/.

[144] R.A. Howie, MINERALS / Feldspars, Encycl. Geol. 8 (2005) 534–539.

[145] M.K. Huang, P.M., Wang, MINERALS , PRIMARY, Encycl. Soils Environ. (2005) 500–510.

[146] A. Pakhomova, D. Simonova, I. Koemets, E. Koemets, G. Aprilis, M. Bykov, L. Gorelova, T. Fedotenko, V. Prakapenka, L. Dubrovinsky, Polymorphism of feldspars above 10 GPa, Nat. Commun. 11 (2020) 1–8. https://doi.org/10.1038/s41467-020-16547-4.

[147] B. Lothenbach, E. Bernard, U. Mäder, Zeolite formation in the presence of cement hydrates and albite, Phys. Chem. Earth. 99 (2017) 77–94. https://doi.org/10.1016/j.pce.2017.02.006.

[148] Y. Meng, B. Zhao, H. Zhang, X. Liu, J. Cao, Synthesis of Zeolite W from Potassic Rocks Activated by KOH Sub-molten Salt Method, Cryst. Res. Technol. 53 (2018) 1–10. https://doi.org/10.1002/crat.201700216.

[149] D. Feng, J.L. Provis, J.S.J. Van Deventer, Thermal activation of albite for the synthesis of one-part mix geopolymers, J. Am. Ceram. Soc. 95 (2012) 565–572. https://doi.org/10.1111/j.1551-2916.2011.04925.x.

[150] J. nan Liu, X. yi Shen, Y. Wu, J. Zhang, Y. chun Zhai, Preparation of ultrafine silica from potash feldspar using sodium carbonate roasting technology, Int. J. Miner. Metall. Mater. 23 (2016) 966–975. https://doi.org/10.1007/s12613-016-1313-1.

[151] W. Kim, W. Chae, S. Kwon, K. Kim, H. Lee, S. Kim, Effect of Dry Grinding of Pyrophyllite on the Hydrothermal Synthesis of Zeolite Na-X and Na-A, Mater. Trans. 55 (2014) 1488–1493. https://doi.org/10.2320/matertrans.M2014127.

[152] E. Polat, M. Karaca, H. Demir, a N. Onus, Use of natural zeolite (clinoptilolite) in agriculture, J. Fruit Ornam. Plant Reserarch. 12 (2004) 183–189.

[153] X. Qin, J. Zhao, J. Wang, M. He, Atomic structure, electronic, and mechanical properties of pyrophyllite under pressure: A first-principles study, Minerals. 10 (2020) 1–14. https://doi.org/10.3390/min10090778.

[154] A. De Lucas, A.M. Uguina, I. Covián, L. Rodríguez, Synthesis of 13X Zeolite from Calcined Kaolins and Sodium Silicate for Use in Detergents, Ind. Eng. Chem. Res. 31 (1992) 2134–2140. https://doi.org/10.1021/ie00009a010.

[155] A.F. Gualtieri, Synthesis of sodium zeolites from a natural halloysite, Phys. Chem. Miner. 28 (2001) 719–728. https://doi.org/10.1007/s002690100197.

[156] D. Novembre, B. Di Sabatino, D. Gimeno, Synthesis of Na-A zeolite from 10 Å halloysite and a new crystallization kinetic model for the transformation of Na-A into HS zeolite, Clays Clay Miner. 53 (2005) 28–36. https://doi.org/10.1346/CCMN.2005.0530104.

[157] D.C. Lin, X.W. Xu, F. Zuo, Y.C. Long, Crystallization of JBW, CAN, SOD and ABW type zeolite from transformation of meta-kaolin, Microporous Mesoporous Mater. 70 (2004) 63–70. https://doi.org/10.1016/j.micromeso.2004.03.003.

[158] T.H. Dang, B.H. Chen, D.J. Lee, Application of kaolin-based catalysts in biodiesel production via transesterification of vegetable oils in excess methanol, Bioresour. Technol. 145 (2013) 175–181. https://doi.org/10.1016/j.biortech.2012.12.024.

[159] M. Dondi, C. Iglesias, E. Dominguez, G. Guarini, M. Raimondo, The effect of kaolin properties on their behaviour in ceramic processing as illustrated by a range of kaolins from the Santa Cruz and Chubut Provinces, Patagonia (Argentina), Appl. Clay Sci. 40 (2008) 143–158. https://doi.org/10.1016/j.clay.2007.07.003.

[160] F. Bouzerara, A. Harabi, S. Achour, A. Larbot, Porous ceramic supports for membranes prepared from kaolin and doloma mixtures, J. Eur. Ceram. Soc. 26 (2006) 1663–1671. https://doi.org/10.1016/j.jeurceramsoc.2005.03.244.

[161] A. Kenzour, H. Belhouchet, M. Kolli, S. Djouallah, D. Kherifi, S. Ramesh, Sintering behavior of anorthite-based composite ceramics produced from natural phosphate and kaolin, Ceram. Int. 45 (2019) 20258–20265. https://doi.org/10.1016/j.ceramint.2019.06.299.

[162] P.S.C. Silva, S.M.B. Oliveira, L. Farias, D.I.T. Fávaro, B.P. Mazzilli, Chemical and radiological characterization of clay minerals used in pharmaceutics and cosmetics, Appl. Clay Sci. 52 (2011) 145–149. https://doi.org/10.1016/j.clay.2011.02.013.

[163] A. Panchal, G. Fakhrullina, R. Fakhrullin, Y. Lvov, Self-assembly of clay nanotubes on hair surface for medical and cosmetic formulations, Nanoscale. 10 (2018) 18205–18216. https://doi.org/10.1039/c8nr05949g.

[164] M.E. Awad, A. López-Galindo, M. Setti, M.M. El-Rahmany, C.V. Iborra,

Kaolinite in pharmaceutics and biomedicine, Int. J. Pharm. 533 (2017) 34–48. https://doi.org/10.1016/j.ijpharm.2017.09.056.

[165] J. Taboada, T. Rivas, M.A. Saavedra, M. Araújo, A. Argüelles, A fuzzy expert system application to the evaluation of ceramic- and paper-quality kaolin, Appl. Clay Sci. 33 (2006) 287–297. https://doi.org/10.1016/j.clay.2006.06.003.

[166] M.M. Ibrahim, W.K. El-Zawawy, G.A.M. Nawwar, Modified kaolin and polyacrylic acid-g-cellulosic fiber and microfiber as additives for paper properties improvements, Carbohydr. Polym. 88 (2012) 1009–1014. https://doi.org/10.1016/j.carbpol.2012.01.048.

[167] U. Clay minerals identification, USGS OFR01-041: Sample Preparation Procedures Table of Contents, (n.d.). https://pubs.usgs.gov/of/2001/of01-041/htmldocs/methods.htm.

[168] I. Daou, G.L. Lecomte-Nana, N. Tessier-Doyen, C. Peyratout, M.F. Gonon, R. Guinebretiere, Probing the dehydroxylation of kaolinite and halloysite by in situ high temperature x-ray diffraction, Minerals. 10 (2020). https://doi.org/10.3390/min10050480.

[169] S.I. Siafu, Material Science : An Indian Journal Kaolinite Intercalation Reactions Induced by Naturally Occurring Fe 3 +, 17 (2019) 1–11.

[170] K. Elaiopoulos, T. Perraki, E. Grigoropoulou, Monitoring the effect of hydrothermal treatments on the structure of a natural zeolite through a combined XRD, FTIR, XRF, SEM and N2-porosimetry analysis, Microporous Mesoporous Mater. 134 (2010) 29–43. https://doi.org/10.1016/j.micromeso.2010.05.004.

[171] M. Sakizci, L. Özgül Tanriverdi, Influence of acid and heavy metal cation exchange treatments on methane adsorption properties of mordenite, Turkish J. Chem. 39 (2015) 970–983. https://doi.org/10.3906/kim-1501-71.

[172] L. Dimowa, Y. Tzvetanova, O. Petrov, I. Piroeva, F. Ublekov, Powder xrd structural study of Ba2+ modified clinoptilolite at different stages of the ion exchange process conducted at two temperature regimes— room temperature and 90 °c, Minerals. 10 (2020) 1–16. https://doi.org/10.3390/min10110938.

[173] M. Sakızcı, Investigation of Thermal and Structural Properties of Natural and Ion-Exchanged Analcime, Anadolu Univ. J. Sci. Technol. A - Appl. Sci. Eng. 17 (2016) 724–724. https://doi.org/10.18038/aubtda.266863.

[174] M. Chirita, M.L. Kiss, A. Ieta, A. Ercuta, I. Grozescu, Synthesis of micrometric single crystalline magnetite with superparamagnetic properties for biomedical applications, Tech. Proc. 2013 NSTI Nanotechnol. Conf. Expo, NSTI-Nanotech 2013. 1 (2013) 378–381.

[175] P. Ambrozova, J. Kynicky, T. Urubek, V.D. Nguyen, Synthesis and modification of clinoptilolite, Molecules. 22 (2017) 1–13. https://doi.org/10.3390/molecules22071107.

[176] M.A. Klunk, M. Das, S. Dasgupta, Synthesis and characterization of mordenite-type zeolites with varying Si / Al ratio Corrigendum : Synthesis and characterization of mordenite-type zeolites with varying Si / Al ratio (2019 Mater . Res . Express 6, (2019).

[177] C. Du, H. Yang, Synthesis and characterization of zeolite 4A-type desiccant from kaolin, Am. Mineral. 95 (2010) 741–746. https://doi.org/10.2138/am.2010.3288.

[178] Q. Li, B. Mihailova, D. Creaser, J. Sterte, Aging effects on the nucleation and crystallization kinetics of colloidal TPA-silicalite-1, Microporous Mesoporous Mater. 43 (2001) 51–59. https://doi.org/10.1016/S1387-1811(00)00346-2.

[179] G. Sun, Y. Liu, J. Yang, J. Wang, Seeded synthesis of small polycrystalline NaY zeolite membrane using zeolite structure-directing agent and its

pervaporation performance, J. Porous Mater. 18 (2011) 465–473. https://doi.org/10.1007/s10934-010-9399-8.

[180] A.A. Ismail, R.M. Mohamed, I.A. Ibrahim, G. Kini, B. Koopman, Synthesis, optimization and characterization of zeolite A and its ion-exchange properties, Colloids Surfaces A Physicochem. Eng. Asp. 366 (2010) 80–87. https://doi.org/10.1016/j.colsurfa.2010.05.023.

[181] Q. Li, Y. Zhang, Z. Cao, W. Gao, L. Cui, Influence of synthesis parameters on the crystallinity and Si/Al ratio of NaY zeolite synthesized from kaolin, Pet. Sci. 7 (2010) 403–409. https://doi.org/10.1007/s12182-010-0085-x.

[182] X.S. Zhao, G.Q. Lu, H.Y. Zhu, Effects of Ageing and Seeding on the Formation of Zeolite Y from Coal Fly Ash, J. Porous Mater. 4 (1997) 245–251. https://doi.org/10.1023/A:1009669104923.

[183] A.R. García-Soto, G. Rodríguez-Niño, C.A. Trujillo, Zeolite LTA synthesis: Optimising synthesis conditions by using the modified sequential simplex method, Ing. e Investig. 33 (2013) 22–27.

[184] C. Du, H. Yang, Synthesis and characterization of zeolite 4A-type desiccant from kaolin, Am. Mineral. 95 (2010) 741–746. https://doi.org/10.2138/am.2010.3288.

[185] R.C. Andrades, R.F. Neves, F.R.V. Diaz, A.H.M. Júnior, Influence of alkalinity on the synthesis of zeolite A and hydroxysodalite from metakaolin, J. Nano Res. 61 (2020) 51–60. https://doi.org/10.4028/www.scientific.net/JNanoR.61.51.

[186] P. Galhotra, J.G. Navea, S.C. Larsen, V.H. Grassian, Carbon dioxide ($C16O2$ and $C18O 2$) adsorption in zeolite y materials: Effect of cation, adsorbed water and particle size, Energy Environ. Sci. 2 (2009) 401–409. https://doi.org/10.1039/b814908a.

[187] C.Y. Chang, W.T. Tsai, C.H. Ing, C.F. Chang, Adsorption of polyethylene

170

glycol (PEG) from aqueous solution onto hydrophobic zeolite, J. Colloid Interface Sci. 260 (2003) 273–279. https://doi.org/10.1016/S0021-9797(02)00174-1.

[188] C. Zhou, A. Alshameri, C. Yan, X. Qiu, H. Wang, Y. Ma, Characteristics and evaluation of synthetic 13X zeolite from Yunnan's natural halloysite, J. Porous Mater. 20 (2013) 587–594. https://doi.org/10.1007/s10934-012-9631-9.

[189] T.E. Purbaningtias, B. Wiyantoko, P. Kurniawati, D. Prasetyoko, Suprapto, The effect of aging temperature on natural zeolite modification, AIP Conf. Proc. 1911 (2017). https://doi.org/10.1063/1.5016006.

[190] R. Selvin, H.L. Hsu, L.S. Roselin, M. Bououdina, Effect of aging on the precursor sol for the synthesis of nanocrystalline ZSM-5, Synth. React. Inorganic, Met. Nano-Metal Chem. 41 (2011) 1028–1032. https://doi.org/10.1080/15533174.2011.591339.

[191] B. Adnadjević, J. Vukićević, Z. Filipović-Rojka, V. Marković, The influence of NaX zeolite particle size on crystallinity measured by the XRD method, Zeolites. 10 (1990) 699–702. https://doi.org/10.1016/0144-2449(90)90083-4.

[192] E.N. Coker, R.W. Thompson, A.G. Dixon, A. Sacco, S.S. Nam, S.L. Suib, Preparation of zeolite X with low levels of iron impurity from reaction mixtures containing triethanolamine, J. Phys. Chem. 97 (1993) 6465–6469. https://doi.org/10.1021/j100126a022.

[193] S. Su, H. Ma, Convenient Hydrothermal Synthesis of Zeolite A from Potassium-extracted Residue of Potassium Feldspar, 420 (2012) 297–302. https://doi.org/10.4028/www.scientific.net/AMR.418-420.297.

[194] M. Meftah, W. Oueslati, N. Chorfi, A. Ben Haj Amara, Effect of the raw material type and the reaction time on the synthesis of halloysite based Zeolite Na-P1, Results Phys. 7 (2017) 1475–1484.

https://doi.org/10.1016/j.rinp.2017.04.013.

[195]   Z. Sun, X. Feng, W. Hou, Morphology-controlled synthesis of α-FeOOH and its derivatives, Nanotechnology. 18 (2007) 455607. https://doi.org/10.1088/0957-4484/18/45/455607.

[196]   Q. Hao, S. Liu, X. Yin, Z. Du, M. Zhang, L. Li, Y. Wang, T. Wang, Q. Li, Flexible morphology-controlled synthesis of mesoporous hierarchical α-Fe2O3 architectures and their gas-sensing properties, CrystEngComm. 13 (2011) 806–812. https://doi.org/10.1039/c0ce00194e.

[197]   A. Fritz, V. Pitchon, The current state of research on automotive lean NOx catalysis, Appl. Catal. B Environ. 13 (1997) 1–25. https://doi.org/10.1016/S0926-3373(96)00102-6.

[198]   E. V. Alekseev, O. Felbinger, S. Wu, T. Malcherek, W. Depmeier, G. Modolo, T.M. Gesing, S. V. Krivovichev, E. V. Suleimanov, T.A. Gavrilova, L.D. Pokrovsky, A.M. Pugachev, N. V. Surovtsev, V. V. Atuchin, K[AsW2O9], the first member of the arsenate-tungsten bronze family: Synthesis, structure, spectroscopic and non-linear optical properties, J. Solid State Chem. 204 (2013) 59–63. https://doi.org/10.1016/j.jssc.2013.04.038.

[199]   V. V. Atuchin, N.F. Beisel, E.N. Galashov, E.M. Mandrik, M.S. Molokeev, A.P. Yelisseyev, A.A. Yusuf, Z. Xia, Pressure-Stimulated Synthesis and Luminescence Properties of Microcrystalline (Lu,Y)3Al5O12:Ce3+ Garnet Phosphors, ACS Appl. Mater. Interfaces. 7 (2015) 26235–26243. https://doi.org/10.1021/acsami.5b08411.

[200]   V. V. Atuchin, O.D. Chimitova, T.A. Gavrilova, M.S. Molokeev, S.J. Kim, N. V. Surovtsev, B.G. Bazarov, Synthesis, structural and vibrational properties of microcrystalline RbNd(MoO4)2, J. Cryst. Growth. 318 (2011) 683–686. https://doi.org/10.1016/j.jcrysgro.2010.09.076.

[201]   M. Raji, A.E.K. Qaiss, R. Bouhfid, Effects of bleaching and

functionalization of kaolinite on the mechanical and thermal properties of polyamide 6 nanocomposites, RSC Adv. 10 (2020) 4916–4926. https://doi.org/10.1039/c9ra10579d.

[202] J. Iannicelli, High extraction magnetic filtration of kaolin clay, Clays Clay Miner. 24 (1976) 64–68. https://doi.org/10.1346/ccmn.1976.0240203.

[203] J. Iannicelli, J. Pechin, Magnetic separation of kaolin clay using a high temperature superconducting magnet system, IEEE Trans. Appl. Supercond. 7 (1997) 1061–1064. https://doi.org/10.1109/77.614706.

[204] M.A. Tao, H., Hong-Wen, Experimental Research of the Synthesizing of 13X Molecular Sieves from Potash Feldspar Ores, J. Inorg. Mater. 16 (2001) 61–68.

[205] M. Mattioli, L. Giardini, C. Roselli, D. Desideri, Mineralogical characterization of commercial clays used in cosmetics and possible risk for health, Appl. Clay Sci. 119 (2016) 449–454. https://doi.org/10.1016/j.clay.2015.10.023.

[206] J. Tinschert, D. Zwez, R. Marx, K.J. Anusavice, Structural reliability of alumina-, feldspar-, leucite-, mica- and zirconia-based ceramics, J. Dent. 28 (2000) 529–535. https://doi.org/10.1016/S0300-5712(00)00030-0.

[207] R.P. Townsend, E.N. Coker, Chapter 11 Ion exchange in zeolites, Stud. Surf. Sci. Catal. 137 (2001) 467–524. https://www.sciencedirect.com/science/article/pii/S0167299101802536.

[208] H.S. Sherry, The ion-exchange properties of zeolites. I. Univalent ion exchange in synthetic faujasite, J. Phys. Chem. 70 (1966) 1158–1168. https://doi.org/10.1021/j100876a031.

[209] H. Lührs, J. Derr, R.X. Fischer, K and Ca exchange behavior of zeolite A, Microporous Mesoporous Mater. 151 (2012) 457–465. https://doi.org/10.1016/j.micromeso.2011.09.025.

[210] A.R. Sotiles, N.A.G. Gomez, S.C. Da Silva, F. Wypych, Layered double hydroxides with the composition Mn/Al-SO4-A (A = Li, Na, K; Mn:Al ca. 1:1) as Cation Exchangers, J. Braz. Chem. Soc. 30 (2019) 1807–1813. https://doi.org/10.21577/0103-5053.20190087.

[211] D.E.W. Vaughan, United States Patent (19), 1985.

[212] M.I. Binay, S.K. Kirdeciler, B. Akata, Development of antibacterial powder coatings using single and binary ion-exchanged zeolite A prepared from local kaolin, Appl. Clay Sci. 182 (2019) 105251. https://doi.org/10.1016/j.clay.2019.105251.

[213] S.K. Kirdeciler, B. Akata, One pot fusion route for the synthesis of zeolite 4A using kaolin, Adv. Powder Technol. 31 (2020) 4336–4343. https://doi.org/10.1016/j.apt.2020.09.012.

[214] S.K. Kirdeciler, B. Akata Kurc, A.D. Börekçi, Production of zeolite 4A and zeolite 13X from sodium feldspar and production methods thereof No : TR 2015 09919 B, 2017.

[215] S.Ş. Akın, S.K. Kirdeciler, F. Kazanç, B. Akata, Critical analysis of zeolite 4A synthesis through one-pot fusion hydrothermal treatment approach for class F fly ash, Microporous Mesoporous Mater. 325 (2021). https://doi.org/10.1016/j.micromeso.2021.111338.

[216] B. Akata Kurc, S.K. Kirdeciler, Doğal Aluminasilikat Kaynaklarına Ek Olarak Kalsit ve Potaş Kullanılarak Direkt Zeolit 3A ve Zeolit 5A Üretim Yöntemi, 2021.

APPENDICES

A. TDS of Kaolin B0 Extra

KAOLİN
ENDÜSTRİYEL MİNERALLER SAN.VE TİC.A.Ş.

TEKNİK VERİ KARTI

Kaolin B0 EXTRA

1. KİMYASAL ANALİZ, %

SiO_2	$49,00 \pm 2,00$
Al_2O_3	$36,50 \pm 0,50$
Fe_2O_3	$0,75 \pm 0,05$
TiO_2	$0,30 \pm 0,05$
CaO	$0,15 \pm 0,05$
MgO	$0,25 \pm 0,05$
Na_2O	$0,15 \pm 0,05$
K_2O	$0,60 \pm 0,20$
A.Z. (1050 ℃)	$12,50 \pm 0,60$

2. FİZİKSEL ÖZELLİKLER

Max.Katı Konsantrasyonu, 5 Ps (%)		$66,00 \pm 2,00$
Optimum Elektrolit Miktarı, 5 Ps (%)		$0,70 \pm 0,10$
Döküm Hızı (mm^2/dk)		$0,80 \pm 0,10$
Kuru Bağlama Dayanımı (kg/cm^2)		min. 7,50
-2 μm (%)		$67,00 \pm 3,00$
Toplu Küçülme	1180 ℃ (%)	$9,50 \pm 1,00$
	1200 ℃ (%)	$11,20 \pm 1,00$
Su Emme	1180 ℃ (%)	$22,00 \pm 1,00$
	1200 ℃ (%)	$17,00 \pm 1,00$
Beyazlık	1180 ℃ (%)	$89,80 \pm 1,50$
	1200 ℃ (%)	$90,40 \pm 1,50$

3. RUTUBET, %

$12,0 \pm 2,0$

4. PAKETLEME

Big-bag (~1,1 ton)

5. ÖNERİLEN UYGULAMALAR

Sır ve angop uygulamaları (Karo, Sıhhi Tesisat, Sofra-Süs Eşyası)
Bünye uygulamaları (Karo, Sofra-Süs Eşyası)

* Yukarıdaki değerler bilgilendirme amaçlıdır. Kaolin Endüstriyel,Mineraller San. ve Tic. A.Ş. veri kartı içeriğinde önceden haber vermeksizin değişiklik yapma hakkını saklı tutar.

Yenişehir Mah. Baraj Yolu Cd. Burak Sk.No.17 Darende İş Merkezi Kat:5 Daire:12 34779 ATAŞEHİR, İSTANBUL
Tel: +90 216 455 23 12 / Faks: +90 216 455 24 93
info@kaolin.com.tr

B. TDS of Feldspar Esan 5 Micron

İNCE FELDSPAT / ULTRA FINE FELDSPAR

Kimyasal Özellikler (Chemical Analysis)

KİMYASAL ANALİZ		Ultra İnce Feldspat
A.Z (Lol)	(%)	0,30
SiO_2	(%)	70,00
Al_2O_3	(%)	18,50
Fe_2O_3	(%)	0,02
TiO_2	(%)	0,02
CaO	(%)	0,70
MgO	(%)	0,20
Na_2O	(%)	10,50
K_2O	(%)	0,30

*KIZDIRMA KAYBI İÇİN: TM.LT.02 (TS.2980 ve TS.3245 e dayalı işletme içi metot) - (TS 2980:1978 ve TS 3245:1978'e Dayalı).
XRF İLE ANALİZ İÇİN: TM.LT.04 (EN 15039'a dayalı işletme içi metot)
Analiz metodu Türkak tarafından akreditedir.

Fiziksel Özellikler (Physical Properties)

TANE BOYUT DAĞILIMI		Ultra İnce Feldspat
d10	(μ)	1,809
d50	(μ)	3,140
d90	(μ)	5,706
d98	(μ)	7,670

*TANE İRİLİĞİ DAĞILIMI : Lazer yöntemi ile analiz; Uluslararası metod- ISO 13320-1 1999
Analiz Metodu Türkak tarafından akreditedir.

C. TDS of Feldspar Polat Madencilik Oğlankayası

ÜRÜN ADI *PRODUCT NAME*	KIRILMIŞ NA-FELDSPAT (-10mm) OGLANKAYASI CRUSHED NA-FELDSPAT (-10mm) OGLANKAYASI					
ÜRÜN KODU *PRODUCT CODE*	PM NA.KIR.OGLANKAYASI-10mm					
Kimyasal İçerik *Chemical Analys*	SiO$_2$ %	67,0 ± 1,5 %	K$_2$O %	0,6 ± 0,1 %	TiO$_2$ %	0,35 ± 0,05 %
	Na$_2$O %	10,0 ± 0,5 %	Fe$_2$O$_3$ %	0,25 ± 0,05 %	Al$_2$O$_3$ %	19,0 ± 1,0 %
Renk *Color*	L		a		b	

PARTICLE SIZE DISTRUBITION

Elek Analizi *Sieve Residue*			Malvern *Masterizer (2000)*	
Tolerans	Elek Boyutu			
%	Mesh	Mm		
1,0 max	2	+10		
Nem *Humidity*	5 % (Max) -Summer / 7 % (Max) -Winter			

D. TDS of Feldspar Polat Madencilik Gökbel

POLAT MADEN

Anasayfa / Kategoriler / Kırılmış Na-Feldspat

ÜRÜN ADI *PRODUCT NAME*	KIRILMIŞ NA-FELDSPAT (-10mm) GÖKBEL CRUSHED NA-FELDSPAT (-10mm) GOKBEL					
ÜRÜN KODU *PRODUCT CODE*	PM NA.KIR.GOKBEL-10mm					
Kimyasal İçerik *Chemical Analys*	SiO$_2$ %	65,0 ± 1,5 %	K$_2$O %	0,5 ± 0,1 %	TiO$_2$ %	0,35 ± 0,05 %
	Na$_2$O %	9,5 ± 0,5 %	Fe$_2$O$_3$ %	0,20 ± 0,05 %	Al$_2$O$_3$ %	21,0 ± 1,0 %
Renk *Color*	L		a		b	

PARTICLE SIZE DISTRUBITION

Elek Analizi *Sieve Residue*			**Malvern** *Masterizer (2000)*	
Tolerans	**Elek Boyutu**			
%	**Mesh**	**Mm**		
1,0 max	2	+10		
Nem *Humidity*	5 % (Max) -Summer / 7 % (Max) -Winter			

E. TDS of Kazan Soda Sodium Carbonate

AĞIR SODA KÜLÜ ÜRÜN ÖZELLİKLERİ
DENSE SODA ASH SPECIFICATION

Güncelleme Tarihi/ Update Date: 04.05.2020

Kimyasal Adı / Chemical Name	: Susuz Sodyum Karbonat / Sodium Carbonate Anhydrous
Formül / Formula	: Na_2CO_3
Mol. Ağırlığı / Molecular Weight	: 105,99
CAS No	: 497-19-8
EINECS No	: 207-838-8
Orijin / Origin	: Doğal Trona Cevheri / Natural Trona Ore
Diğer İsimler / Synonyms	: Soda Ash

Kimyasal Özellikler | Chemical Properties		
		Özellikler / Specification
Na_2CO_3	%	99.5 min
Na_2O	%	58.2 min
NaCl	%	0.1 max
Na_2SO_4	%	0.1 max
Fe (Toplam) | Fe (Total)	µg/g	10 max
Suda Çözünmeyen Madde | Water Insolubles	%	0.05 max
As	ppm	1 max
Pb	ppm	1 max
Hg	ppm	1 max
Çözünürlük | Solubility	g/100 ml su g/100 ml Water	45.5 (100°C) 49.5 (35.37 °C) 7 (0 °C)
pH	1 % çözelti	11.4
Sodyum Testi | Test for Sodium		Testi geçmektedir |Passes Test

PS.03.ŞT.50   YAYIN TARİHİ:05.09.2017   REV.NO/TARİHİ:01/03.05.2019

ciner KURULUŞUDUR | **KAZAN SODA ELEKTRİK ÜRETİM A.Ş** | Merkez: Söğütözü Cad. Sim Söğütözü İş Merkezi No: 14 / D Beştepeler Yenimahalle/ ANKARA | Tel : 0312 258 55 00 Fax: 0312 285 43 34

Sayfa 1/3

179

F. TDS of Koruma Sodium Hydroxide

KORUMA KLOR ALKALİ SAN. VE TİC. A.Ş.
Deniz mah. Petrol Ofisi cad. No:43 Derince/Kocaeli
Tel : 0262-2392270 (3 Hat)/ Fax : 0262-2392278

KOSFLAKE

(PAYET KOSTİK)

KİMYASAL ADI	SODYUM HİDROKSİT
TİCARİ ADI	KOSFLAKE
KİMYASAL FORMÜLÜ	NaOH
MOLEKÜL AĞIRLIĞI	40,01 gr / mol-gr

FİZİKSEL VE KİMYASAL ÖZELLİKLER

Parametre	Birim	Spesifikasyon
Görünüş	_	Beyaz renkli ,flake şeklinde
Sodyum Hidroksit (NaOH)	%	min. 98,0
Sodyumklorür (NaCl)	%	max. 0,10
Sodyum Karbonat (Na2CO3)	%	max. 0,4
Demir (Fe)	mg/kg	max.15
Arsenik (Ar)	mg/kg	< 2
Yoğunluk (20° C)	gr/m^3	2,13
Civa (Hg)	mg/kg	< 0,1
Nikel (Ni)	mg/kg	< 2
Krom (Cr)	mg/kg	< 1
Kurşun (Pb)	mg/kg	< 5
Antimon (Sb)	mg/kg	< 5
Selenyum (Se)	mg/kg	< 5
Kadmiyum (Cd)	mg/kg	< 1

Referans Standart TS EN 896 e göre düzenlenmiştir.

KULLANIM ALANLARI

Suni ipek , Kâğıt hamuru , Textil endüstrisi , Kauçuk ıslahı , Organik çözme ameliyesi ,

Revizyon tarihi : 20.05.2019

180

G. TDS of Eti Aluminyum Aluminum Hydroxide

TEKNİK BİLGİ FORMU / TECHNICAL DATA SHEET

ALÜMİNYUM HİDROKSİT / ALUMINUM HYDROXIDE - Al(OH)3

Kimyasal İçerik / Chemical Composition [%]		
	Nemli / Wet	Kuru / Dry
Kızdırma Kaybı / Loss on Ignition (1000 ºC)	~34.6	~34.6
Al2O3	>65.0	>65.0
SiO2	<0.015	<0.015
Fe2O3	<0.015	<0.015
Na2O	<0.20	<0.20
CaO	<0.030	<0.030
Fiziksel Özellik / Physical Properties		
Nem / Moisture [105 ºC, 2h]	2-7	0.1-0.3
Beyazlık / Whiteness, Ry 457 nm	>83	>83
Tane Boyut Dağılımı / Particle Size Distribution		
d 50 [μm]	85-125	85-125
< 45 μm[%]	<10	<12
Paketleme / Packaging	1.0 MT,1.1 MT,1.2 MT (PE-PP Bigbags) Dökme/Bulk	

Yukarıda verilen değerler ürün tolerans aralıklarına kaynak niteliğindedir. Gerçek değerler analiz sertifikasında verilmektedir.
All data listed above are reference to the product tolerances. The actual values are stated in the Certificate of Analysis.

Kimyasal Tescil Numaraları / Chemical Registration Numbers	G.T.İ.P. / H.S.CODE
CAS No: 21645-51-2 / Reach No : 01-2119529246-39	281830000000

K - Q TSE-ISO-EN 9000   C - E TSE-ISO-EN 14000   TS-ISO-45001   M - C TSE - ISO 10002   TSE TSE-ISO-EN 50001   REACH COMPLIANT

ETİ ALÜMİNYUM A. Ş. ————————————————— Bir CENGİZ HOLDİNG kuruluşudur.

Merkez Ofis: Altunizade Kısıklı Cd. No: 37 34662 Üsküdar/İSTANBUL

Tel: +90 216 554 53 00 (Pbx) Faks: +90 216 474 11 22

E-mail: mining@cengiz.com.tr

Fabrika: Atatürk Caddesi 42370 Seydişehir/KONYA

Tel: +90 332 582 30 30 (Pbx) Faks: +90 332 582 39 27

E-mail: pazarlama@etialuminyum.com   www.etialuminyum.com   Rev :09.02.2021

CURRICULUM VITAE

PERSONAL INFORMATION

Surname, Name: Kirdeciler, Salih Kaan

EDUCATION

Degree	Institution	Year of Graduation
MS	METU Micro and Nanotechnoloy Department	2012
BS	Gazi University, Chemical Engineering Department	2008
High School	Hacı Ömer Tarman Anatolian High School, Ankara	2004

WORK EXPERIENCE

Year	Place	Enrollment
2019-Present	Turkish Aerospace Inc.	Material Test & Characterization Engineer
2013-2018	METU Central Laboratory	Specialist
2011-2013	Nurol Ar-Ge	R&D Engineer
2008	AKUA Dış Tic. Ltd. Şti.	Sales Engineer

FOREIGN LANGUAGES

Advanced English

PUBLICATIONS

1. Akın, S.Ş., Kirdeciler, S.K., Kazanç, F., Akata, B., "Critical analysis of zeolite 4A synthesis through one-pot fusion hydrothermal treatment approach for class F fly ash", Microporous Mesoporous Materials, 325, 111338 (2021)

2. Kirdeciler, S.K., Akata B " One pot fusion route for the synthesis of zeolite 4A using kaolin ", Advanced Powder Technology, 31(10), 4336-4343 (2020)

3. Isler Binay, M., Kirdeciler, S.K., Akata, B. " Development of antibacterial powder coatings using single and binary ion-exchanged zeolite A prepared from local kaolin ", Applied Clay Science, 182, 105251 (2019)

4. Velychko, T.P., Soldatkin, O.O., Melnyk, V.G., Marchenko, S.V., Kirdeciler, S.K., Akata, B., Soldatkin, A.P., El'skaya, A.V., Dzyadevych, S.V., "A Novel Conductometric Urea Biosensor with Improved Analytical Characteristic Based on Recombinant Urease Adsorbed on Nanoparticle of Silicalite", Nanoscale Research Letters, 11, 106 (2016)

5. Kucherenko, I., Soldatkin, O., Kasap, B.O., Kirdeciler, S.K., Kurc, B.A., Jaffrezic-Renault, N., Soldatkin, A., Lagarde, F., Dzyadevych, S., "Nanosized zeolites as a perspective material for conductometric biosensors creation", Nanoscale Research Letters, 10, 209 (2015)

6. Soldatkin, O.O., Shelyakina, M.K., Arkhypova, V.N., Soy, E., Kirdeciler, S.K., Kasap, B.O., Lagarde, F., Jaffrezic-Renault, N., Kurc, B.A., Soldatkin, A.P., Dzyadevych, S.V., "Nano- and microsized zeolites as a perspective material for potentiometric biosensors creation", Nanoscale Research Letters, 10, 59 (2015)

7. Kirdeciler, S.K., Ozen, C., Akata, B., "Fabrication of nano- to micron-sized patterns using zeolites: Its application in BSA adsorption", Microporous and Mesoporous Materials, 191, 59-66 (2014)

8. Soldatkin, O.O., Kucherenko, I.S., Shelyakina, M.K., Soy, E., Kirdeciler, K., Ozturk, S., Jaffrezic-Renault, N., Akata, B., Dzyadevych, S.V., Soldatkin, A.P., "Application of Different Zeolites for Improvement of the Characteristics of a pH-FET Biosensor Based on Immobilized Urease", Electroanalysis, 25(2), 468-474 (2013)

9. Kucherenko, I.S., Soldatkin, O.O., Soy, E., Kirdeciler, K., Ozturk, S., Akata, B., Jaffrezic-Renault, N., Soldatkin, A.P., Dzyadevych, S.V., "Effect of different modifications of BEA-zeolites on operational characteristics of conductometric biosensor", Materials Science & Engineering C-Materials for Biological Applications, 32(6), 1648-1653 (2012)

10. Kirdeciler, S.K, Soy, E., Ozturk, S., Kucherenko, I., Soldatkin, O., Dzyadevych, S., Akata, B.," A novel urea conductometric biosensor based on zeolite immobilized urease", Talanta, 85(3), 1435-1441 (2011)